RHEOLOGY
AND STREAMING BIREFRINGENCE
OF AN
ANISOTROPIC FLUID

By

J. ERIC SCHONBLOM

A DISSERTATION PRESENTED TO THE GRADUATE COUNCIL OF THE
UNIVERSITY OF FLORIDA IN PARTIAL FULFILLMENT OF THE
REQUIREMENTS FOR THE DEGREE OF DOCTOR OF PHILOSOPHY

UNIVERSITY OF FLORIDA

1974

ACKNOWLEDGMENTS

To Dr. E. Rune Lindgren, for stimulating my interest in anisotropic liquids, for suggesting Milling Yellow as an experimental medium, for unstinting support and encouragement, and for unwillingness to accept facile explanations or unnecessary assumptions.

To Richard R. Johnson, for a hundred instances in which he interrupted work upon his own dissertation to provide practical suggestions or physical assistance.

To Dr. Ulrich H. Kurzweg, teacher, for assistance and advice in the mathematical formulation of the problem, for constant interest in day by day developments, and for exemplary performance as a lecturer.

To Dr. Martin A. Eisenberg, for serving on my advisory committee and for providing references concerning the torsion analogue of cylindrical fluid flow.

To Dr. Robert L. Sierakowski, for serving on my advisory committee, for useful comments concerning the organization of my dissertation, and for excellence as a lecturer.

To Dr. C. Michael Levy, for supervision of my Minor Program.

To Dr. Craig Hartley, for the loan of optical items.

To Dr. Gene Hemp, for the allocation of computer time.

To Frank Hearne, for microscopic examination of a Milling Yellow solution.

To John Tang, for the tedium of checking some trigonometric relationships.

To Max Suarez, for making the viscosity measurements which were necessary during my absence in July, 1972.

To Bill Wilson, for assistance in the preparation of the flow apparatus.

To Jerry Hornbuckle, for encouragement, for a useful discussion of variational solutions for the determination of shear-rate distributions, and for assistance in preparation for the qualifying examination.

To Carl Langner, for suggestions concerning numerical integrations.

To Edward Teska and William Lockhurst, for help in the shop.

To Dr. Donald E. Swarts, then President of the University of Pittsburgh Bradford Campus, for a grant of extended leave from my Assistant Professorship to enter doctoral studies and for acceptance, without predjudice, of my resignation when it was necessary for me to become a "permanent Florida resident."

To David Alford, for giving me something else to think about.

The research reported herein was supported in part by the National Science Foundation. At other times the author was supported by a National Science Foundation Traineeship. A portion of the computer cost was borne by the Department of Engineering Science, Mechanics, and Aerospace Engineering at the University of Florida

TABLE OF CONTENTS

LIST OF TABLES x
LIST OF FIGURES xii
KEY TO SYMBOLS xv
ABSTRACT xxii

CHAPTERS:

ONE INTRODUCTION 1
    Scope of Dissertation 2
TWO RESULTS OF PREVIOUS INVESTIGATIONS AND THEIR IMPLICATIONS 4
    Birefringent Flow Fields 5
    Physical Properties of Milling Yellow 10
        General Properties 10
        Optical Properties 13
            Theory of birefringence 14
            Experimental measurements of birefringence 15
        Rheological Properties 19
            Continuum mechanics 19
            Model construction 21
            Experimental measurements of rheology 24
    Velocity Distribution in Rectangular Conduits 29

CHAPTERS:

TWO (Continued)

Newtonian Flow in Cylinders 29

Non-Newtonian Fluids in Rectangular Conduits 31

THREE OPTICAL ANALYSIS 38

Two-Dimensional Flow 39

Three-Dimensional Flow 43

Assumptions 44

Definition of Effective Optical Properties 47

Analysis 48

Integration to Obtain Fringe Pattern 58

FOUR DETERMINATION OF OPTICAL PROPERTIES 62

Birefringence 62

Apparatus 63

Procedure 72

Prediction of Results 73

Experimental Data 75

Discussion of Results 88

Preliminary tests 88

Interpretation of data 89

Computation of optical coefficients 94

Orientation Angle 100

Assumption of Form 100

CHAPTERS:

FIVE DETERMINATION OF RHEOLOGICAL PROPERTIES 103

Empiricism in Rheological Formulations 103

Analysis of Sliding Ball Viscometer 110

Related Investigations 111

Analysis 116

Integration of viscometer equation 124

Experimental Results 130

Discussion of Results 140

Curve Fitting 140

Determination of $g(\tau)$ from Experimental Measurements 146

Range of Application 151

SIX DISTRIBUTION OF SHEAR RATES IN RECTANGULAR CONDUITS 156

Power-Law Fluids 156

Some Alternatives 161

SEVEN SUMMARY AND CONCLUSIONS 163

Optical Analysis of Birefringent Flow Fields 163

Optical Properties of Medium 164

Rheological Properties of Medium 165

Other Findings 166

APPENDICES:

A THE EFFECTIVE BIREFRINGENCE AND ORIENTATION ANGLE OF THE OPTICAL ELLIPSE FORMED BY THE INTERSECTION OF THE OPTICAL ELLIPSOID WITH THE PLANE ORTHOGONAL TO THE PATH OF LIGHT 167

B PREPARATION OF MILLING YELLOW SOLUTIONS 171

  Original Stock Solution 171

  Fresh Stock Solution 173

C VARIATION IN FLOW RATE AS AMOUNT OF LIQUID IN OVERHEAD TANK DECREASES 175

D ALIGNMENT OF POLARIZING ARRAYS 177

E CALIBRATION OF HÖPPLER RHEO-VISCOMETER 179

F BILINEAR MATERIALS 187

G SOME CHANNEL CONSTANTS 191

H VARIATIONS IN MILLING YELLOW SOLUTIONS WITH TIME 192

I VARIATIONS IN MILLING YELLOW APPARENT VISCOSITY WITH CONCENTRATION AND TEMPERATURE 195

  Apparatus 195

  Preparation of Samples 196

  Experimental Data 197

  Computation of Temperature Coefficients 197

J RESTRICTION OF VISCOMETER TO LIQUIDS HAVING VISCOSITY ABOVE 4 CENTIPOISE 205

K VISCOMETER RESPONSE AT VERY SLOW FALL TIMES 212

L DETERMINATION OF SAMPLE CONCENTRATIONS 218

BIBLIOGRAPHY 221

BIOGRAPHICAL SKETCH 229

LIST OF TABLES

I. INTERNAL DIMENSIONS OF CHANNELS 68

II. VALUES OF γ AND γ' FOR SUCCESSIVE ELEMENTS OF POLARIZING ARRAYS 71

III. FRINGE ORDER AT WALL - RUN 123 76

IV. FRINGE ORDER AT WALL - RUN 130 76

V. FRINGE ORDER AT WALL - RUN 131 77

VI. ORDER OF RED FRINGE AT WALL - RUN 218 77

VII. FRINGE ORDER AT WALL - RUN 42 78

VIII. FRINGE ORDER AT WALL - RUN 44 78

IX. FRINGE ORDER AT WALL - RUN 44A 79

X. FRINGE ORDER AT WALL - RUN 45 79

XI. FRINGE ORDER AT WALL - RUN 418 80

XII. FRINGE ORDER AT WALL - RUN 419 81

XIII. FRINGE ORDER AT WALL - RUN 420A 81

XIV. FRINGE ORDER AT WALL - RUN 420D 82

XV. FRINGE ORDER AT WALL - RUN 424 82

XVI. FRINGE ORDER AT WALL - RUN 425 83

XVII. BIREFRINGENT CONSTANTS FOR RUNS 42, 44, 44A, AND 45 (ORIGINAL STOCK SOLUTION) 96

XVIII. BIREFRINGENT CONSTANTS FOR RUNS 418, 419, 420A, 420D, 424, AND 425 (FRESH STOCK SOLUTION) 98

XIX. VISCOMETER MEASUREMENTS - RUN 42 131

XX. VISCOMETER MEASUREMENTS - RUN 44 132

LIST OF TABLES (Continued)

XXI. VISCOMETER MEASUREMENTS – RUN 418 133

XXII. VISCOMETER MEASUREMENTS – RUN 419 134

XXIII. VISCOMETER MEASUREMENTS – RUN 420 135

XXIV. VISCOMETER MEASUREMENTS – RUN 420B 136

XXV. VISCOMETER MEASUREMENTS – RUN 424 137

XXVI. VISCOMETER MEASUREMENTS – RUN 424B 138

XXVII. VISCOMETER MEASUREMENTS – RUN 425 139

XXVIII. RHEOLOGICAL CONSTANTS 145

XXIX. ESTIMATION OF APPARENT VISCOSITY 154

C-I CHANGE IN FLOW RATE AS OVERHEAD TANK EMPTIES 176

E-I CALIBRATION DATA 181

E-II CALIBRATION CHECK (WATER) 184

I-I TEMPERATURE COEFFICIENTS 203

K-I FALL TIMES FOR 1-MM INCREMENTS 214

K-II CORRECTED FALL TIMES FOR FIRST 10 MM OF FALL BY 1-MM INCREMENTS 217

L-I CONCENTRATIONS OF SAMPLES 219

LIST OF FIGURES

1. Dispersion in concentration data of Peebles, Prados, and Honeycutt (1965). 18

2. Unit vectors and angles relating to the flow. 40

3. Optical ellipsoid showing parameters θ, ψ, and Δn. 45

4. Poincaré sphere showing P, the condition of the polarized light beam, R, the principal (fast) optic axis of the medium, and ΔP, an arc on the surface representing the change in polarization which occurs. 49

5. Elliptically polarized light in the yz-plane. 52

6. Projection of $\overrightarrow{OP}$ on $\overrightarrow{OR}$ and definition of ϖ. 52

7. Definition of $\Delta\varpi$. 52

8. Schematic representation of successive determination of the variables. 59

9. Replot of data of Peebles, Prados, and Honeycutt (1965) to show linear relationship between square of fringe order and shear rate. 64

10. Schematic of experimental apparatus. 65

11. Cut-away view of rectangular conduit showing roughened walls, gaskets, and spacing wires. 67

12. Orientation of elements in polarizer and analyzer arrays. 70

13. Fringe order at wall as function of mass flow rate. Runs: 123; 131; 130; 218. 84

14. Fringe order at wall as function of mass flow rate. Runs: 42; 44; 44A; 45. 85

15. Fringe order at wall as function of mass flow rate. Runs: 418, 419; 420A. 86

LIST OF FIGURES (Continued)

16. Fringe order at wall as function of mass flow rate. Runs: 420D; 424; 425. 87

17. Birefringence of original stock solution compared with an extrapolation of the data of Peebles, Prados, and Honeycutt (1965). 95

18. Birefringence of fresh stock solution. 97

19. Extinction angles measured by Peebles, Prados, and Honeycutt (1965) replotted to obtain straight lines. 102

20. Data of Peebles, Prados, and Honeycutt (1965) replotted to obtain a linear relationship. 108

21. Höppler Rheo-Viscometer. 112

22. Geometry in annulus. 116

23. Response of viscometer, runs: 42; 420; 425. 141

24. Test of functional form: $Pt = \frac{k_1}{P} + k_2$. 143

25. Test of functional form: $P\left[Pt-(Pt)_{\infty}\right] = k_1 + \frac{k_2}{P}$. 144

26. Constructed relationship between shear stress and shear rate for Milling Yellow at 25° C. 149

27. Comparison of equations (5.6) and (5.7), run 424B, at 25° C. 150

28. Manometer readings compared with those expected for Newtonian fluid or a power-law fluid. 158

29. Schechter's (1961) coefficients plotted as function of power-law exponent. 160

E-1. Variation in calibration constant with load on ball. 182

F-1. Bi-functional material. 188

F-2. Flow field within viscometer showing boundary between regions obeying separate constitutive equations. 188

H-1. Variation in apparent viscosity with time. 194

LIST OF FIGURES (Continued)

I-1. Temperature variation of samples 103-30 and 1012-30. 198

I-2. Temperature variation of samples 107-25 and 1011-25. 198

I-3. Temperature variation of samples 103-20 and 109-20. 199

I-4. Temperature variation of samples 104-17 and 1011-17. 199

I-5. Temperature variation of sample 104-14. 200

I-6. Temperature variation of original stock solution. 200

J-1. Transition in measurement of apparent viscosity when P is too large. 206

J-2. Transition in measurement of apparent viscosity when temperature is too high. 206

TABLE OF SYMBOLS

a	Radius of viscometer ball
$a_0, a_1, \ldots a_n$	Coefficients of polynomial fit of $P^{-1}d(P^2/t)/dP$ as function of P
A	Cross-sectional area
A_p	Constant in Powell-Eyring equation
A_s	Amplitude of sinusoidal
$A_1, A_2, \ldots A_5$	Geometric factors relating ΔN and Ψ to Δn, ψ, and Θ (see Appendix A)
$b_0, b_1, \ldots b_n$	Coefficients of polynomial fit of $1/t$ as function of P
b_{st}	Coefficients of variational solution
B_s	Amplitude of sinusoidal
B_1, B_2, B_3	Geometric factors (see Appendix A)
c	Speed of light in vacuum
c_1	Speed of light when E is parallel to $\hat{n}_1$
c_2	Speed of light when E is parallel to $\hat{n}_2$
C_0, C_1, C_2	Experimental constants
$d_0, d_1, \ldots d_n$	Coefficients in curve-fitting
$\hat{d}$	Director - a unit vector characterizing directional property of anisotropic fluid
D	Diameter
$\frac{\mathcal{D}}{\mathcal{D}t}$	Jaumann derivative $-\ \mathcal{D}g_{ij}/\mathcal{D}t = \partial g_{ij}/\partial t + u_k \partial g_{ij}/\partial x_k - w_{ik}g_{kj} - w_{ki}g_{jk}$

$\hat{e}$	Unit vector characterizing principal direction of elliptically polarized light
E	Electric field vector
$\hat{E}$	Unit vector, E/E_0
E_a	Component of E parallel with $\hat{m}_a$
E_e	Electric field on emergence
E_{max}, E_{min}	Axes of elliptically polarized light
E_0	Amplitude of electric field entering flow
$\overline{E}_0$	Rms value of E_0
$F(x,y,z)$	$F(x,y,z) = 0$ is equation for surface of optical ellipsoid
g	Shear rate: in conduit, $\sqrt{(\partial u/\partial x)^2 + (\partial u/\partial y)^2}$; in viscometer, $\partial u/\partial \zeta$; in capillary, $\partial u/\partial r$
g_{ij}	Rate-of-deformation tensor
G	Mass flow rate
h	Manometer reading, difference in fluid levels
$\hat{i}$	Unit vector, x-direction (usually direction of the light path)
$\overline{I}$	Rms value, light intensity
I_0	Initial intensity of light
$\hat{j}$	Unit vector, y-direction (usually direction along which fringe pattern varies)
k, k_1, k_2, k_1', K..	Empirical constant, defined at point of use
$\hat{k}$	Unit vector, z-direction (flow direction is usually $-\hat{k}$)
ℓ	Fall distance: distance ball moves in viscometer during timed interval

L	Effective length of eccentric annulus in viscometer
L_c	Length of capillary
m	Power law exponent
m'	(1-m)/2m
M	(1+2m)/m
n	Exponent in power series
$\bar{n}$	Average refractive index
$\hat{n}_a$	Analyzer direction: direction of E for maximum transmission through analyzer
$\hat{n}_p$	Polarizer direction: direction of E for maximum transmission through polarizer
n_1	Index of refraction, c/c_1 $(c > c_1 > c_2)$
n_2	Index of refraction, c/c_2 $(c > c_1 > c_2)$
$\hat{n}_1$	Direction of major optic axis
$\hat{n}_2$	Direction of minor optic axis
Δn	Birefringence, $n_1 - n_2$
N	Integer, often the fringe order
N_p	Number of data pairs
N_s, N_s'	Integers tabulated by Schechter (1961)
N_w	Fringe order at the wall
N_1, N_2	Characteristic coordinates, optical ellipse (see Appendix A)
ΔN	Effective birefringence
ΔN_w	Effective birefringence at wall
p	Static pressure
P	Force on viscometer ball/area of ball, "average shearing stress" or "load on ball"

$P(\Omega,\Phi)$	Point on Poincaré sphere representing polarization of light
$\hat{\mathbb{P}}$	Position vector $\overrightarrow{\odot P}$, Poincaré sphere
P_1, P_2, P_3	Components of $\hat{\mathbb{P}}$
q	Concentration of Milling Yellow, weight percent
Q	Volumetric flow rate
r	Radial coordinate
$\mathbb{r}$	Radius for movement on Poincaré sphere
$\Delta\mathbb{r}$	Change in $\mathbb{r}$, chord of ΔP
R	Radius of capillary
$R_{equiv.}$	Equivalent radius of rectangular pipe, $2\delta_1\delta_2/(\delta_1+\delta_2)$
$R(\Omega,\Phi)$	Point on Poincaré sphere representing principal axis of medium
$\hat{\mathbb{R}}$	Position vector, $\overrightarrow{\odot\mathbb{R}}$, Poincaré sphere
Re	Reynolds number
s	Summation index
$s^2(X_s)$	Estimated variance of variable X_s
S_0	Constant: see Appendix G and the definition on page 74
t (as variable)	Time, especially fall time in viscometer
t (as integer)	Summation index
t_m	Experimental fall time, expressed in terms of τ_m
t_0	Initial time
t'	Time much greater than $\lambda\bar{n}/c$
T	Temperature

u	Velocity of fluid
$\bar{u}$	Mean velocity, $A^{-1}\int u\,dA$
u_1, u_2, u_3	Components of velocity
U	Speed of viscometer ball, ℓ/t
w_{ij}	Vorticity tensor
x	Spatial coordinate
x'	See Appendix A
x_1, x_2, x_3	Characteristic coordinates of Poincaré sphere; generalized coordinates
$\hat{x}_1$, $\hat{x}_2$, $\hat{x}_3$	Unit vectors associated with x_1, x_2, and x_3
X_s	Experimental variable
y	Spatial coordinate
y'	See Appendix A
z	Spatial coordinate
z'	See Appendix A
α	Half-angle of divergent channel
α_0, α_1, $..\alpha_n$	Coefficients of power law expansion of $g(\tau)$
β	Secondary normal stress function
β_0	$\delta_m/4L$
γ	Polarizer angle, measured from principal flow axis
γ'	Analyzer angle, measured from principal flow axis
$\bar{\gamma}$	Average field angle, $(\gamma+\gamma')/2$
$\Delta\gamma$	Field difference, $\gamma - \gamma'$
$\Gamma(M)$	Gamma function of M

δ	Width of viscometer annulus
$\bar{\delta}$	Thickness of optical field
δ_{ij}	Kronecker delta
δ_m	Maximum width of annulus
ϵ	Angle between $\hat{e}$ and principal flow axis
ζ	Spatial coordinate in viscometer, radial distance from surface of ball into fluid in plane of minimum clearance
η	Intrinsic viscosity, τ/g
η_0	$\zeta - \frac{\delta}{2}$
θ	Angular coordinate in viscometer, zero where ball contacts wall
θ_n	Primary normal stress function
Θ	Plane, Θ = constant, in which major axis of optical ellipsoid is inclined
λ	Wave length of incident light in vacuum
μ	Viscosity
μ_a	Apparent or average viscosity
μ_N	Newtonian viscosity
μ_0	Limiting value of viscosity as shear rate approaches zero
μ_∞	Limiting value of viscosity as shear rate increases without limit
ρ	Density
σ	Phase angle, elliptically polarized light
σ_0	$(\mu_\infty - \mu_0)/\mu_0\mu_\infty$
$\sigma^2(X_s)$	Variance of variable X_s

τ	Shearing stress
τ_c	Critical value of τ at which $g(\tau)$ changes its characteristics in a bi-functional constitutive relationship
τ_{ij}	Stress tensor
τ_m	Maximum shear stress in viscometer, $P\delta_m/2L$
τ_w	Shear stress at the wall
$\Upsilon(\tau_m)$, $\Upsilon'(\tau_m)$, $\Upsilon(0)$	Experimentally derived functions defined by equation (5.4)
φ	$\theta/2$
Φ	Coordinate of "latitude" on Poincaré sphere
χ	Extinction angle: angle between principal optic axis and principal direction of polarizer (or analyzer) when polarizer and analyzer are crossed. Of the four angles thus defined, the extinction angle is the only one which is less than $\pi/4$ and positive.
ψ	Orientation angle which $\hat{m}_1$ makes with principal flow axis
ψ_∞	Limiting value of orientation angle as shear rate increases without limit
Ψ	Effective orientation angle
Ψ_w	Effective orientation angle at wall
ω	Circular frequency of light
I, II, III	Invariants of g_{ij}

Abstract of Dissertation Presented to the
Graduate Council of the University of Florida in
Partial Fulfillment of the Requirements for
the Degree of Doctor of Philosophy

RHEOLOGY AND STREAMING BIREFRINGENCE OF AN ANISOTROPIC FLUID

By

J. Eric Schonblom

March, 1974

Chairman: Dr. E. Rune Lindgren
Major Department: Engineering Science, Mechanics, and
Aerospace Engineering

The intrinsic viscosity and birefringence of an aqueous solution of Milling Yellow NGS, a commercial organic dye, are obtained experimentally. Each property is measured in a flow where the velocity is dependent upon two spatial coordinates. It is shown that the rheological and optical properties thus obtained may be used to compare hypothetical velocity distributions in steady three-dimensional flows.

The rheological investigation employs a Höppler Rheo-Viscometer in which a ball slides without rotating through the fluid within a closely fitted cylinder. This instrument has previously been considered unsuited for the determination of basic rheological constants. By modeling the

flow past the ball on steady flow in an eccentric annulus, it is shown that the distribution of shear rates can be integrated to obtain a unique relationship between the shear rate and the shear stress for the fluid. The analysis is valid for all fluids and can be extended without difficulty to viscometers in which the tightly fitted ball is replaced by a cylinder.

Values for the birefringence (maximum difference in refractive index between the principal optic axes) of Milling Yellow have been previously reported. The present study shows that the previous data exhibit a linear relationship between the square of the birefringence and the shear rate. An analysis demonstrates that as a result, in a square pipe, the fringe order at the wall, squared, should vary linearly with the mass flow rate through the pipe. This expectation is confirmed experimentally, and the birefringence is calculated from the data.

When birefringent fluids are observed in flow between two polarizers a fringe pattern is seen. Such patterns have been used to obtain pressure and velocity distributions in two-dimensional flows and to estimate lift and drag coefficients. When conducted with Milling Yellow, such studies have been limited to the extremely low flow rates at which Milling Yellow's birefringence and shear stress vary linearly with the shear rate.

The results of the present study extend these methods to include steady three-dimensional flows in which velocity variations along the light paths are permissible. Further, shear rates for which the birefringence and shear stress vary non-linearly are no longer excluded. Although the direct determination of velocity distributions from fringe patterns remains impractical, the pattern which corresponds to any assumed velocity distribution may be computed and compared with the fringe pattern obtained experimentally. The method by which fringe patterns may be calculated once the velocity distribution has been assumed is outlined schematically.

A hypothetical distribution of shear rates for Milling Yellow flowing in a rectangular conduit has not been attempted for the rheological relationship obtained with the Höppler Rheo-Viscometer; however, the application of other constitutive relationships, notably that for a power-law fluid, is considered briefly.

CHAPTER ONE

INTRODUCTION

The velocity distribution of anisotropic liquids flowing steadily in rectangular pipes can be constructed in certain cases from a knowledge of the optical and rheological properties of the fluid. Specifically, if the material is birefringent, so that the refractive index bears a directional dependence upon the shear rate, then any hypothetical velocity distribution may be confirmed or denied by observing the fringe pattern which results when the flow is observed between crossed polarizers. The successive steps in such an evaluation are as follows:

Determination of constitutive relationships. -- Constitutive relationships must be provided which describe the optical and rheological properties of the material.

Determination of shear rate distribution. -- Based upon the rheological properties of the medium, a compatible distribution of shear rates for steady flow in rectangular pipes must be calculated. Depending upon the complexity of the rheological relationship, the mathematical solution of this boundary value problem may be exact or approximate.

Integration to obtain fringe patterns. – Once the distribution of shear rates is known, integration of the dependent optical properties along each light path will determine the relative intensity of the emergent light beam. Fringe patterns thus obtained may be compared with experimental data to evaluate the relationships derived in the previous steps.

Scope of Dissertation

This dissertation is concerned primarily with the first of the three steps just listed and with the properties of a single birefringent medium: an aqueous solution of a commercial organic dye, Milling Yellow NGS. In previous investigations the optical and rheological properties of Milling Yellow solutions (referred to hereafter as simply "Milling Yellow") have been measured in viscometric* flows using a concentric cylinder polariscope and a capillary viscometer respectively. The present study utilizes non-viscometric flows to measure the optical properties at the wall of a nearly square conduit and the rheological properties within the eccentric annulus of a sliding ball viscometer. Since neither of these measurements seem to have been employed previously, analyses are provided to support the present applications.

---

*A flow is viscometric for the purpose of this dissertation if the velocity field has the form $u_1 = 0$, $u_2 = 0$, $u_3 = u(x)$ where x is a single spatial coordinate. For a more general definition, see Coleman, Markovitz, and Noll (1966).

The determination of the distribution of shear rates for Milling Yellow flowing in a rectangular conduit has not been attempted for the measured rheological relationships; however, the application of other constitutive relationships, notably that of a so-called power-law fluid, is considered briefly.

An optical analysis is performed to demonstrate the means by which the resultant fringe pattern may be obtained once the preceding steps have been accomplished. It is shown that if the optical properties do not change along a given light path through the flowing medium the optical relationship simplifies to a familiar result from two-dimensional optical stress analysis.

CHAPTER TWO

RESULTS OF PREVIOUS INVESTIGATIONS AND THEIR IMPLICATIONS

This assessment of the present state-of-the-art is in three parts. The first is devoted to studies in which birefringent liquids have been used to obtain information concerning velocity fields. Emphasis is laid upon those studies in which Milling Yellow was the birefringent medium. The second part is concerned with the physical properties of Milling Yellow and includes a discussion of continuum mechanics and model construction as they relate to Milling Yellow's rheology. The final part describes previous investigations of velocity distributions in rectangular pipes.

In Chapter Five, preceding the analysis of the Höppler Rheo-Viscometer, is a review of the rolling ball viscometer, the falling cylinder viscometer, and the ball and tube flow meter, subjects too specific for inclusion in this more general chapter.

Birefringent Flow Fields

The first reports of streaming birefringence are those of Mach (1873) and Maxwell (1873) a century ago. Said Maxwell (1873, p. 46):

> I am not aware that this method of rendering visible the state of strain of a viscous liquid has been hitherto employed.

Although many theories have arisen from this humble beginning, the employment of birefringence for the quantitative investigation of flow fields has remained scant to the present day.

The most popular media for these studies have been suspensions of colloidal bentonite and solutions of organic dyes, notably Milling Yellow. Dewey (1941) observed two-dimensional flow patterns with bentonite and concluded that quantitative velocity gradients could be obtained from such data. Similar studies by Weller (1947) were hampered by the high viscosity of the polymeric medium which he used. Vinogradov's (1950) work with colloids provided pictures of two-dimensional flows around circular obstacles and suggested applications for lubrication theory. Rosenberg (1952), another user of bentonite, described the optical properties of his medium, recommended suitable concentrations and colloidal dimensions, and suggested methods of using two-dimensional models to calculate pressure distributions, lift and drag coefficients, velocity distributions and streamlines. He concluded that applications to turbulence would remain qualitative reflecting Binnie's (1945) experience with dilute solutions of benzopurpurin. Later Lindgren (1953 et seq.) and Wayland (1955) used bentonite to visualize turbulence but not for the purpose of computing the velocity field.

All of the early quantitative studies were hampered either by high viscosities (as in Weller's case) or by marginal birefringence (with bentonite). These considerations prompted Jury in 1950 to suggest to Fields the investigation of various organic dyes for their feasibility as birefringent media. Fields (1952) concluded that the most likely candidate for such use was an aqueous solution of commercial Milling Yellow. A preliminary study of its usage by Peebles, Garber, and Jury (1953) ratified this conclusion and sparked some independent studies by other investigators. Although the 1953 report did not attempt a quantitative evaluation of the flow fields which it investigated, it did include photographs of the two-dimensional flow patterns, details for the preparation of the dye solution, determination of the density (1.005 gm/cm^3) and a plot of apparent viscosity versus temperature for four different dye concentrations. The latter information is discussed in more detail in the next section.

The first of the independent studies using Milling Yellow was completed by Hargrove and Thurstone (1957) who observed flow through an orifice. Although this study was not quantitative, the usefulness of the medium prompted its further use by Thurstone for the investigation of wave propagation: Thurstone (1961); Thurstone and Schrag (1962, 1964); Cerf and Thurstone (1964). From these studies emerged numerical values for the viscoelastic properties of Milling Yellow which correlated well with the measured wavelengths and propagation velocities of small amplitude waves. Thurstone (1961) also replicated the earlier density measurement.

Other independent studies were conducted by Swanson, Scheuner, and Ousterhout (1965) and Swanson and Ousterhout (1965). They assumed a linear relationship between birefringence and shear rate and demonstrated the means by which a two-dimensional flow field could be calculated from such data. They also described a flow tunnel built for this purpose.

While these independent studies were under way, Peebles and his students, particularly Prados, continued the original work at the University of Tennessee. Prados (1957) and Prados and Peebles (1959) obtained velocity profiles for two-dimensional flow in straight channels, in converging and diverging channels, and in a straight channel around a cylinder. Bogue and Peebles (1962) suggested a technique for obtaining velocity profiles from isochromatic* fringes only. Their technique was applied to data obtained in a converging channel by Liu. Liu and Peebles (1963) indicated that Milling Yellow can be used to describe two-dimensional flows in converging and diverging channels, in free jets, and in wall jets. Building upon work by Bogue and Peebles (1962) and Hirsch (1964), Peebles and Liu (1965) describe in detail the numerical technique by which two-dimensional velocity profiles may be obtained from an isochromatic pattern using a laminar expanding jet as the experimental configuration.

---

*Isochromatic: optical response (colored in white light) which depends only upon the birefringence, Δn.

An important restriction upon this research was that quantitative evaluation of flow fields using Milling Yellow appeared possible only at extremely low flow rates where the optical and rheological properties vary linearly with the shear rate as predicted by the theories described later in this chapter. Further, only two-dimensional configurations, in which the variation in fluid velocity along a given light path can be neglected, were considered tractable for analysis. When these restrictions were observed, velocity fields could be calculated with an average error of about 13 percent according to Peebles and Liu (1965).

It should be mentioned that most of the flow field investigations were accompanied by concurrent examinations of the optical and rheological properties of the medium. Those findings which relate to Milling Yellow are reviewed in the section which follows.

Excluding polymeric media in which elastic properties predominate (extruded polyethylene was observed by Wales, 1969, through windows set in the long walls of a capillary slit, for example) one three-dimensional flow field has been examined quantitatively. Durelli and Norgard (1972) photographed flow around a cylinder in a rectangular channel with an aspect ratio of 0.75; that is, the light path was actually shorter than the channel width. This arrangement violated the requirement set by the Tennessee studies for two-dimensional flows based on Purday's (1949) estimate that the light path must be 5 to 10 times the width of the channel. Durelli and Norgard chose to treat the flow as two-dimensional and calculated average velocities along each light path. This assumption yielded good agreement with local velocities obtained by averaging speeds measured from streak photographs of hydrogen bubbles at three locations in the same channel.

From this review of flow analyses using birefringent media it is evident that there is a need for a technique by which three-dimensional flows can be considered. It would be helpful if the restriction to extremely low flow rates could be relaxed or eliminated.

Physical Properties of Milling Yellow

General Properties

The medium for the present investigation was obtained by dissolving in water a commercial dye designated by the Society of Dyers and Colourists (1971) as Colour Index Acid Yellow 44. The common name is Milling Yellow. The trade name for the commercial product supplied by the Keystone Aniline and Chemical Company, Incorporated, Chicago, is Milling Yellow NGS. It is this product which was used in the current investigations and unless otherwise indicated, the term Milling Yellow in this dissertation will refer to solutions of this commercial product rather than the pure dyestuff.

Swanson and Green (1969) provide a number of details concerning the physical chemistry of Milling Yellow. They give the structural formula as

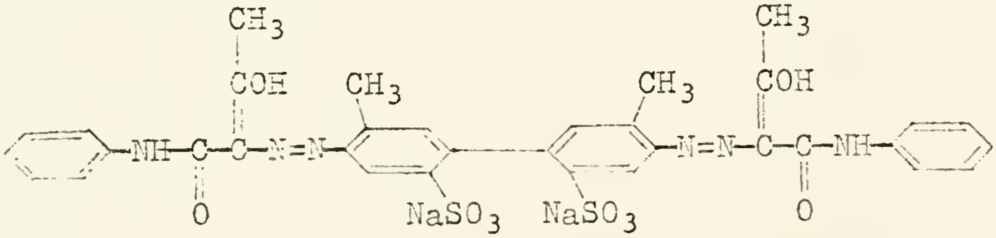

and state that the birefringence is due to a solid phase precipitated from solution. They describe this solid phase as consisting of transparent, rhombic crystals with an aspect ratio of 5.7 and "strong inherent polarization."

Swanson and Green state, and the supplier confirms, that the presence of impurities, notably NaCl and Na_2SO_4 with some sodium acetate, may constitute more than 30 percent of the commercial product.

In dilute solution (less than 1 percent) Milling Yellow is lemon yellow and highly transparent. Swanson and Green obtained birefringence with pure dye solutions having concentrations as low as 0.1 percent by salting the solution with electrolytes, but such solutions were highly unstable.

At higher concentrations Milling Yellow is orange and deeply colored. The preparation of the medium used in this dissertation was basically that described by Peebles, Garber, and Jury (1953). The dye was mixed with water at a weight concentration below that desired and heated to just under 100° C. At this temperature water was evaporated until the desired concentration was obtained. Further details are provided in Appendix B.

Although earlier investigators follow Peebles, Garber, and Jury in suggesting dilution of the concentrated medium to obtain the desired level of birefringence for a given experiment, this dissertation concurs with Swanson who cautioned against dilution since the equilibrium of the medium is disturbed when distilled water is added, and, on occasion, sedimentation may result.

It was observed that when Milling Yellow is suddenly diluted to about 1 percent there is a short period during which significant birefringence remains in the dispersed mixture, but the viscosity approaches that of water. Investigators who are willing to tolerate rapid changes in the optical properties of the medium may find this unstable dispersion a useful medium for the observation of qualitative phenomena. Although the birefringence soon disappears, the color remains the deep orange which characterizes solutions concentrated by heating.

There is disagreement concerning the stability of Milling Yellow preparations. Peebles, Garber, and Jury (1953) detected no qualitative differences in the observed optical properties of their 1.5 to 1.8 percent medium over a period of 10 months, nor was there a perceptible darkening after more than a week's continuous contact with iron pipe, steel, copper, brass, or rubber. Prados and Peebles (1959) did report darkening of their 1.3 percent solution within two weeks of preparation except for small samples stored in glass bottles which remained unchanged after three months. Peebles, Prados, and Honeycutt (1965) emphasized that small changes in concentration due to evaporation have a marked influence upon both the optical and rheological properties of the medium.

During the current investigation it was found that a significant concentration gradient may develop between the surface and the bottom of the storage container due to evaporation within the container followed by draining of condensate from the lid. The refluxing action, unless controlled by floating plastic sheeting on the fluid surface, seems to lead to sedimentation.

From the preceding paragraphs it is clear that the preparation of standardized birefringent media having specified properties is not practical due to variability in the commercial dyestuff, apparent instability, and marked variation in properties arising from evaporation. The recommended procedure is to measure all significant properties at the time of each use. This has been done in the present study and in every previous quantitative investigation using Milling Yellow.

Optical Properties

In non-steady shearing flow the optical properties of Milling Yellow have both in-phase and out-of-phase components which have been studied by Thurstone and Schrag (1962, 1964) and Cerf and Thurstone (1964). They found that the birefringence is highly dependent upon strain as well as strain rate particularly below room temperature at oscillatory rates less than 1 Hz. Thus, as Harris (1970) concludes, the analysis of unsteady flows is not possible in the general case. In the present study only steady state conditions are considered in the measurement of the optical properties and the out-of-phase components are neglected.

Two in-phase optical characteristics, the birefringence and the extinction angle, serve to define streaming birefringence in steady flow. Besides Harris (1970), Jerrard (1959) and Peterlin (1956) have described these characteristics in useful review articles.

Theory of birefringence

Based upon earlier work by Jeffery (1922), Boeder (1932), Peterlin and Stuart (1939), and Snellman and Bjornstahl (1941), the birefringence of a suspension of rigid non-interacting ellipsoids has been calculated by Scheraga, Edsall, and Gadd (1951). This body of theory, which predicts a linear dependence of birefringence upon shear rate at low flow rates, has been applied to Milling Yellow by Cerf and Thurstone (1964) for the assessment of small amplitude oscillations and by Peebles, Prados, and Honeycutt (1965) and Swanson and Green (1969) to estimate particle size. The theory fails when there are interactions between particles or when the particle dimensions exceed the upper limit of 10^{-6} meters set by Peterlin and Stuart (1939) and Snellman and Bjornstahl (1941). Little is known about the microstructure of birefringent solutions of Milling Yellow. Cerf and Thurstone (1964) observed crystals between 1 and 2 microns in length under the electron microscope but do not report how the solution was prepared for viewing in a vacuum.* Recent descriptions of lyotropic mesophases, such as those given by Hartshorne and Stuart (1970) suggest a viable alternative to the usual assumption that the properties of Milling Yellow are due to a crystalline precipitate of the type described by Swanson and Green (1969). The hydrodynamics of such mesophases requires further investigation before the applicability of suspension theory can be assessed.

---

*At my request Mr. Frank Hearne made a microscopic observation of a 2.8 percent Milling Yellow solution under an oil-immersion magnification of X1000. He observed no crystals but did obtain stress birefringence in the clear medium by pressing upon the cover glass.

Experimental measurement of birefringence

The introductory studies of Fields (1952) and Peebles, Garber, and Jury (1953) provided qualitative information about the optical properties of Milling Yellow. The first quantitative evaluation was reported by Prados (1957) and Peebles and Prados (1959) who calibrated their solution (roughly 1.3 percent dye) in simple shearing flow using a concentric cylinder polariscope. They also verified that the measurement of the distance between fringes in parallel channel flow could be used as an alternative method of calibration. The latter method is still in use (*e.g.* Durelli and Norgard, 1972). Peebles and Prados obtained a nearly linear relationship between birefringence and rate of deformation for rates up to 19 sec^{-1}. A marked temperature dependence was observed. The birefringence at 24.75° C was 11 percent higher than at 24.95° C and 36 percent higher than at 25.20° C. The extinction angle was measured only at 25° C and dropped monotonically from

45° at negligible rates of shear to about 28° at 20 sec^{-1}.

The data of Thurstone and Schrag (1962) are of limited usefulness to the present study since they considered oscillatory, rather than steady shear flows. Their 1.72 percent solution showed a progressive, 20-fold reduction in the optical coefficient (loosely, the birefringence) as the temperature was raised from 12° C to 42° C. When the temperature was held constant at 23° C, the coefficient showed little change as oscillatory frequencies increased from 10^{-2} to 1 Hz, but dropped rapidly with further increases.

The range of dependence of birefringence upon shear rates was extended by Hirsch (1964) in his study of diverging ducts, but the most extensive study was reported by Peebles, Prados, and Honeycutt (1965) who again used a concentric cylinder polariscope for their measurements. For shear rates ranging up to 2500 sec^{-1} and concentrations between 1.248 and 1.455 percent by weight, they found increasing non-linearity as shear rates increased, although they identify a possible "second range of linearity" at the highest shear rates. All of their data were taken at 25° C. Although the concentrations, which were measured very accurately by evaporating samples to dryness, are reported to four significant figures, dispersion results when a correlation is attempted between concentration and the shear rate required to obtain a given fringe order in the polariscope. Figure 1 shows this dispersion, some of which may be due to inaccuracies in replotting. The remaining variability can be attributed to the use of the commercial dyestuff and to the difficulty of preparing a standardized medium as alluded to earlier. In any case it is clear that birefringence increases markedly with dye concentration.

Peebles, Prados, and Honeycutt also measured extinction angles over the same range of concentrations. They found that the more concentrated solutions exhibit asymptotic values for the extinction angle in the vicinity of 20° as the shear rate increases above 40 sec^{-1}. At lower concentrations a similar asymptote is reached, but at higher shear rates.

No expressions for either the birefringence or the extinction angle are advanced by the authors to represent their findings. Consequently, for the purpose of the present study it has been necessary to construct empirical relationships which describe the data of Peebles, Prados, and Honeycutt. This has been done in Chapter Four.

Swanson and Green (1969) were concerned only with the minimum concentration at which birefringence could be observed and not with its magnitude. They hypothesize that the variability of Milling Yellow preparations is due to a small fraction of the dissolved material, as little as 0.04 percent, which exists in suspension. Their hypothesis is not evaluated in this dissertation.

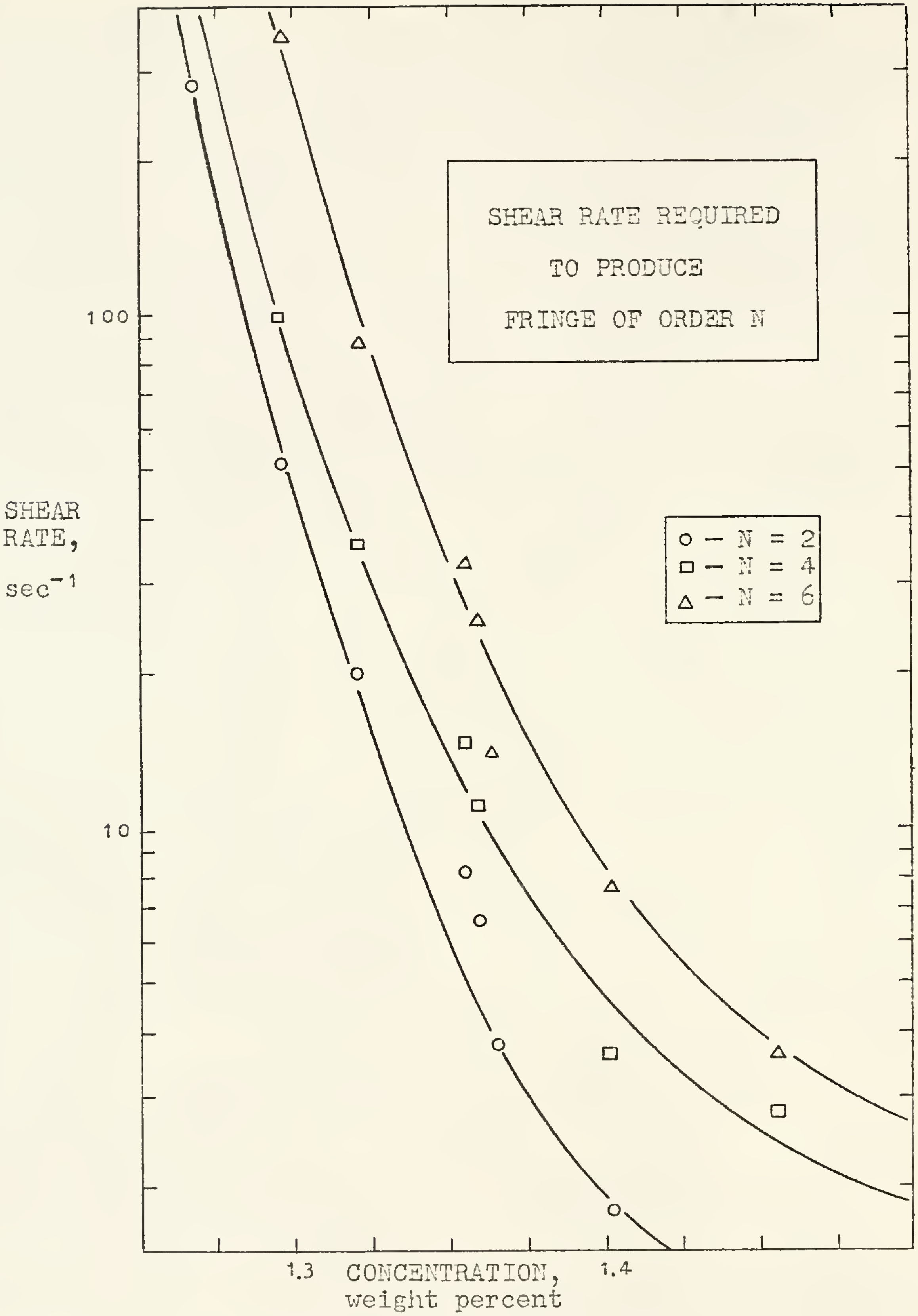

FIGURE 1. Dispersion in concentration data of Peebles, Prados, and Honeycutt (1965)

Rheological Properties

The rheological behavior of media such as Milling Yellow may be described rigorously in terms of continuum mechanics, theoretically, but with less rigor in terms of hydrodynamic models, or empirically, based upon experimental evidence. Each of these methods is discussed in turn.

Continuum mechanics

With the advent of liquid crystals as a practical media for electronic display devices (Caulfield and Soref, 1971, is one report among many), there has been a great increase in publications relating to the constitutive behavior of anisotropic materials. Not all such reports have been useful. One reviewer, Kisiel (1968, p. 1043) spoke for many when commenting upon a study which shall remain nameless:

> This investigation belongs to a class, abundant at present, of papers dealing with very general problems with limited applicability to the solving of practical questions.

An overview of the current state of the art indicates that rigorous application of the continuum mechanics of anisotropic media is limited to viscometric flows of the simple type in which the velocity components are given by

$$u_1 = 0; \quad u_2 = 0; \quad u_3 = u(x)$$

where x is a single spatial coordinate. Further, numerical solutions are possible only for the very small class of substances, notably p-azoxyanisole, for which some, at least, of the necessary constitutive constants have been measured and published. Neither of these conditions is satisfied in the present dissertation; hence, the discussion of anisotropic continuum mechanics which follows is succinct and selective.

Oldroyd (1950) established the general procedure by which constitutive equations must be constructed if the necessary conditions for tensor invariance were to be preserved. Noll (1958) introduced the concept of a "simple fluid": one in which the properties are completely defined by the temperature and the strain history. The viscometry of simple, non-Newtonian* fluids was examined by Coleman, Markovitz, and Noll (1966) in a general treatise which includes a bibliography of over 350 references spanning the period from 1687 to 1965.

Specific constitutive relationships for anisotropic fluids were formulated by Ericksen (1960a _et seq._) and Leslie (1966 _et seq._) who postulate that at each point in the continuum there is a preferred direction characterized by a unit vector, or "director," $\hat{d}$. On the basis of this hypothesis it was found that, in general, the constitutive stress tensor is non-symmetric, and seven or more constitutive constants are required. The theory has been applied with some success by Atkin and Leslie (1970) and Tseng,

---

*Non-Newtonian: a substance is Newtonian if and only if the shear stress is directly proportional to the shear rate.

Silver, and Finlayson (1972) to certain specialized flows.

A more general and even less tractable theory has been developed by Eringen (1964 et seq.) who postulates a micromotion of the material points which define the continuum. Associated with this micromotion are corresponding micromoments and microinertia. A linear constitutive relationship is obtained at the price of additional unknown constitutive constants. The current literature is replete with argument concerning the existence of the various constants, with their signs, and with the relationships, frequently in the form of inequalities, among them. Truesdell (1965) has pointed out that the complexity of modern continuum mechanics is a reflection of nature and requires no apology, but a hopeful reading of the most recent review of anisotropic continuum mechanics by Ariman, Turk, and Sylvester (1973) leads only to the conclusion that the theory is not yet useful.

Model construction

As an alternative to the utilization of rigorous, but complex constitutive relationships for a continuum, many authors have elected to model anisotropic behavior in terms of the effect which the presence of microscopic particles in a Newtonian medium has upon the macroscopic properties of the mixture. The success of such theories, of which Einstein's (1906) calculation of the intrinsic viscosity of a suspension of rigid spheres is the classic example, has led not only to the analysis of particles whose shape is less well defined, as in colloidal suspensions, but also to inferences about the microstructure when an ill-defined or poorly understood medium is found to obey the predictions of a particular theory.

The most influential body of analysis has grown from Jeffery's (1922) solution for the periodic motion of rigid ellipsoids suspended in a viscous fluid undergoing uniform shearing motion. Jeffery's solution was open-ended, consisting of an infinite set of permissible orbits. Other authors, notably Peterlin (1938), calculated the distribution of orbits which would result from perturbations of the particles due to Brownian motion as expressed by the rotational diffusivity constant. Integration of such distributions leads to an estimate of the viscosity. Kuhn and Kuhn (1945), Scheraga (1955), and Leal and Hinch (1971) are among those who have performed this integration.

Cylindrical particles have been treated by Boeder (1932), who replaced the cylinders by ellipsoids of high axial ratio, Burgers (1938), who obtained the torques due to shears for true cylinders, and Broersma (1960), who included end effects. Still later Bretherton (1962) demonstrated that any rigid particle having an axis of revolution can be replaced by an ellipsoid of appropriate dimensions and incorporated into the general theory.

A common assumption of these theories is that there is no interaction between the particles. When interaction is permitted, as in Ziegel (1970) or Batchelor (1971), the analysis is greatly complicated.

Although rigid spheres, ellipsoids, and rods have served as the primary models for the analysis of non-linear rheological behavior, other shapes also play an important role. A sampling of investigations which have served as alternate models might include the work of Taylor (1934) on drops, Debye (1946) on swarms and porous spheres, Kuhn and Kuhn (1943) and Kirkwood and Riseman (1948, 1949) on chains and necklaces, Simha (1950) on dumbbells, and Frohlich and Sack (1946) on elastic spheres.

The practical value of these theories is that they permit the replacement of a complex constitutive relationship with many unknown constants by a relatively simple constitutive equation; however, the coefficients of this equation will exhibit an involved (though theoretically explicit) dependence upon the various material parameters, and these parameters may prove as difficult to measure as the constitutive constants which they replace. An example is the rigorous, three-constant constitutive equation

$$\tau_{ij} = -p\delta_{ij} - \eta g_{ij} - \frac{1}{2}(\theta_n+\beta)g_{ik}g_{kj} + \frac{1}{2}\theta_n \frac{\partial g_{ij}}{\partial t}$$

where the constants are the intrinsic viscosity η, and the primary and secondary normal stress functions θ_n and β.

For the model of rigid ellipsoidal particles in suspension, η has been calculated by Saito (1951) and Scheraga (1955), and the stress functions have been obtained by Giesekus (1962). The study by Scheraga tabulates its results in terms of the rotational diffusivity constant and the ratio of the lengths of the major and minor axes of the ellipsoid. In practice it has been commoner to infer these properties from the macroscopic properties rather than the reverse. Thus the model, even when it is valid, may not be predictive.

Experimental measurements of rheology

Amenemhet's (1540 B.C.) boastful account of his water-clock, which was capable of compensating for seasonal variations in viscosity (due to temperature changes), begins the written record of rheology. It is clear that Amenemhet did his work without the benefit of continuum mechanics.

The present knowledge of the rheology of Milling Yellow is also founded upon experiment. Although the empirical relationships which describe these data may violate conditions of invariance prescribed by continuum mechanics and include constants which cannot be obtained from model construction, they may be employed with care provided that the flows to which they are applied do not differ too greatly from those in which the experimental data were obtained. A more lengthy discussion of the feasibility of employing empirical relationships to describe the rheology of Milling Yellow will be found at the beginning of Chapter Five.

When the feasibility of Milling Yellow as a birefringent medium was established by Peebles, Garber, and Jury (1953), measurements of the apparent viscosity were made in a rolling ball viscometer at various temperatures. For solutions varying in concentration from 1.46 to 2.02 percent, a sharp exponential rise in viscosity was observed as the temperature decreased. In the 2 percent solution, the viscosity doubled as the result of a two-degree temperature drop. Above a certain critical temperature the optical activity of the solution ceased and the viscosity approached that of water. It was recognized that the apparent viscosity had a shear rate dependence which was not obtained from the measurements.

Prados (1957) and Peebles and Prados (1959) measured the viscosity of a 1.3 percent solution but did not report the results. For shear stresses less than 5 dyne/cm^2, Prados assumed that the viscosity was constant, citing Honeycutt and Peebles (1955) as his authority that Milling Yellow solutions:

> ...exhibit marked non-Newtonian behavior when subjected to shearing stresses greater than five to ten dynes per square centimeter. (Prados, 1957, pp. 55-56)

Thurstone (1961) measured the acoustic impedance of a 1.39 percent solution in a circular tube whose base was excited by low-amplitude, axial, oscillatory vibrations. At an uncontrolled temperature between 22° and 26° C, he found that Milling Yellow exhibited viscoelastic properties. That is, the local stresses were a function of both the shear and the shear rate. As the frequency increased from 10 to 300 Hz, the viscous term of the complex viscosity coefficient dropped from 66 to 13 centipoise, the elastic component having about the same magnitude as the viscous component over this range.

Thurstone and Schrag (1964) and Cerf and Thurstone (1964) did not report the viscous and elastic terms separately. Thurstone and Schrag found that the complex viscosity coefficient is approximately the same for both axial and transverse oscillations of the medium. Cerf and Thurstone found that elastic forces predominate at frequencies below 0.3 Hz, but that viscous forces are dominant above 10 Hz for oscillatory shear waves. At very high frequencies a limiting viscosity of 45 centipoise was obtained for their 1.73 percent solution at 25° C.

In steady flows the most extensive examination of Milling Yellow rheology is Peebles, Prados, and Honeycutt (1965) who measured apparent viscosities with a capillary viscometer at 25° C over a concentration range of 1.25 to 1.50 percent. For each sample they obtained smooth monotonic curves for calculated values of wall shear stress versus shear rate with linear responses when the shear rate exceeded about 2500 sec^{-1}. When the wall shear stress corresponding to a given shear rate is replotted versus concentration, there is a significant scatter of the data, just as a similar replotting of the optical data (Figure 1) also resulted in dispersion. This confirms a difficulty experienced in all investigations including the current one: specification of the commercial dye concentration is insufficient to define the properties of the medium even at a fixed temperature.

An important result of the investigation of Peebles, Prados, and Honeycutt was the demonstration that plots of apparent viscosity versus wall shear stress are independent of the diameter (and L_c/D ratio) of the capillary in which the measurement is made. As Skelland (1967, pp. 32-39), among others, has pointed out, this coincidence of curves indicates the absence of inlet effects of the type described by Maude and Whitmore (1956) or of wall effects such as slippage or the radial migration of microscopic elements as measured by Goldsmith and Mason (1961, 1962, 1964) and Gauthier, Goldsmith, and Mason (1971). In the absence of a reliable explanation of Milling Yellow's exceptional properties, the elimination of such effects from consideration is welcome.

Peebles, Prados, and Honeycutt (1965) conclude that Milling Yellow is well represented, though not uniquely, by the Powell-Eyring equation:

$$\mu = \mu_{\infty} + \frac{A_p}{g}(\mu_0 - \mu_{\infty}) \sinh^{-1}(g/A_p)$$

where μ is the viscosity at shear rate g, and μ_0, μ_{∞}, and A_p are constants. The authors provide straight-line plots of these constants versus concentration, and for the four concentrations plotted the agreement is excellent. Based upon these plots, the following numerical relations can be obtained:

$$\log_{10} \mu_o = 10.72\, q - 12.92,$$

$$\log_{10} \mu_{oo} = 1.38\, q - 1.63,$$

$$\log_{10} A_p = -10.87\, q + 16.16.$$

The units of μ, μ_o, and μ_{oo} are centipoise, shear rates g and A_p are in $\sec^{-1}$, and q is the weight percent of Milling Yellow in the solution.

The data of Peebles, Prados, and Honeycutt are not compelling with regard to the prediction of the Powell-Eyring equation that the viscosity will approach a constant value at low shear rates. Since most of the quantitative studies reported in the literature were conducted at very low shear rates, the absence of conclusive data in this range is of major concern. Fortunately, Peebles and Liu (1965) have provided a plot from Hirsch's (1964) dissertation which indicates clearly that the viscosity does approach a constant value for shear rates below about 5 $\sec^{-1}$. These data were obtained in a capillary viscometer and replicate closely data from a "Rotovisco" instrument when the two methods are compared at shear rates around 50 $\sec^{-1}$. The latter instrument shows the upper range of linear responses. It should be recalled that Prados (1957) measured, though he did not report, constant viscosities at lower shear rates.

Velocity Distribution in Rectangular Conduits

Whenever a differentiable expression for the velocity distribution is known, the shear-rate distribution is defined by direct differentiation. Once the shear-rate distribution is known, the birefringence and orientation angle (or extinction angle) can be calculated. In the present dissertation the shear-rate distribution is required in a rectangular conduit. This distribution has not been calculated for a fluid with Milling Yellow's rheological properties. The review which follows includes those studies which show a potential usefulness in the development of such a distribution.

Newtonian Flow in Cylinders

The determination of velocity distributions in pipes dates from the experimental studies of Hagen (1839) and Poiseuille (1840). In modern derivations the equation which bears their names

$$u(r) = -\frac{1}{4\mu_N}(R^2 - r^2)\frac{dp}{dz},$$

where u(r) is the speed at a distance r from the center-line, R is the pipe radius, μ_N is the viscosity, and dp/dZ is the pressure gradient, is obtained directly from the Navier-Stokes equation for incompressible fluids,

$$-\nabla p + \mu_N \nabla^2 u + \rho F = \rho\, du/dt,$$

by recognizing that

$$u_r = 0, \quad u_\theta = 0, \quad u_z = u(r),$$

and integrating. The density ρ is implicit in the dp/dz term which, in gravitational fields, is simply

$$dp/dz = -\rho g_c$$

where g_c is the gravitational constant.

For a pipe which is not circular in cross-section, the assumption

$$u_1 = 0, \quad u_2 = 0, \quad u_3 = u(x_1, x_2), \tag{2.1}$$

yields

$$\mu_N \nabla^2 u = dp/dz. \tag{2.2}$$

Exact solutions for this equation have been obtained for cross-sections in the shape of concentric circles, ellipses, and equilateral triangles. Lamb (1945), in reviewing these solutions, points out that the analysis of laminar flow in a cylindrical conduit is identical in mathematical form to the analysis of torsion in a uniform cylindrical bar and of fluid motion in a rotating cylindrical case, the cylinders in each case having the same cross-section. Tiedt (1969) adds the reminder that the analog is valid without modification only if the boundary of the cylinder is simply connected.

Davies and White (1928) obtained the relationship between the pressure gradient dp/dz along a rectangular duct and the Reynolds number

$$Re = \frac{\rho u \delta_1 \delta_2}{\mu_N(\delta_1 + \delta_2)}$$

where δ_1 and δ_2 are the half-width and half-depth of the duct.

In the same year Cornish (1928) published the solution to equation (2.2) in a rectangular conduit in the form of a Fourier series:

$$u = -\frac{1}{2\mu_N}\frac{dp}{dz}\left\{(\delta_1{}^2 - x^2) + \frac{32\delta_1{}^2}{\pi^3}\sum_{S=1,3..}^{\infty}\frac{(-1)^{\frac{S+1}{2}}}{s^3}\cos\left[\frac{s\pi x}{2\delta_1}\right]\frac{\cosh(s\pi y/2\delta_1)}{\cosh(s\pi\delta_2/2\delta_1)}\right\}. \tag{2.3}$$

Cornish successfully related the corresponding volumetric flow rate to experimental pressure gradients. Further data which support this relationship are those of Nikuradse (1930) and Lea and Tadros (1931), which also show the predicted dependence of pressure gradient upon average flow rate. The accuracy of the velocity profile must be inferred from Eckert and Irvine (1956) who obtained excellent agreement between local velocity measurements and the Fourier series solution to equation (2.2) for triangular cross-sections. The Cornish solution is clearly inaccurate when violations of equation (2.1) occur due to secondary flows arising from convective effects. Such flows are common even in circular pipes as demonstrated most recently by Johnson (1974).

Non-Newtonian Fluids in Rectangular Conduits

Of the various forms of the rheological equation which have been or will be suggested for Milling Yellow in this dissertation, only one has been investigated in pipes. Christiansen, Ryan, and Stevens (1955) related pressure gradients to average flow rates for a Powell-

Eyring fluid, but their analysis was limited to circular pipes.

It will be shown in Chapter Five that at low flow rates two of the empirical expressions for Milling Yellow reduce to the form

$$\tau = K g^{1/3}$$

which is the one-dimensional form of a power-law fluid. Power-law fluids are defined by

$$\tau_{ij} = k_p \, II^{\frac{m-1}{2}} g_{ij}$$

where τ_{ij} is the stress tensor, g_{ij} is the rate-of-deformation tensor, II is the second invariant of g_{ij}, and k_p and m are constants. For the limited range over which the power law applies to Milling Yellow, $m = 1/3$. Power-law fluids have been investigated in rectangular pipes by several authors.

Schechter (1961) used variational methods to obtain the pressure drop along rectangular pipes for power-law fluids having $m = 0.5$, 0.75, and 1.0 when the pipe aspect ratio δ_1/δ_2 was 0.25, 0.5, 0.75, and 1. He tabulates the coefficients to be used in the series solution

$$u = \bar{u} \sum_{s=1}^{6} A_s \sin(N_s \pi x/2\delta_1) \sin(N_s' \pi y/2\delta_2) \qquad (2.4)$$

to obtain local velocity values.

Wheeler and Wissler (1965) elected to solve the same problem by finite difference methods. Taking the solution for a Newtonian fluid ($m = 1$) as a starting point, successive approximations for the velocity distribution were obtained for values of m between 0.4 and 1. Both the stability of the solution and the rate of convergence decreased with m. Below m = 0.5 stability was a serious problem, and several hundred iterations were required for convergence at the lowest value of m. For square pipes it was found that:

$$-dp/dz = 7.4942\ (1.7330\ m^{-1} + 5.8606)^m K\ \bar{u}^m / 2\delta^{1+m}\ . \qquad (2.5)$$

For $0.4 < m < 1.0$, the constants in this relationship were accurate to four significant figures. Velocity profiles obtained by this method were not published, but Wheeler and Wissler state that the profiles obtained by their method could be differentiated numerically several times. In contrast, differentiation of Schechter's profiles led to erratic results. The empirical expression given above was verified experimentally using power-law constants obtained for their medium (sodium carboxymethylcellulose solutions of various concentrations) by averaging the measurements made in a circular pipe and a Couette viscometer. For Reynolds numbers less than 2000 there was excellent agreement between the predicted pressure drop and the corresponding Reynolds number.

Arai and Toyoda (1968) considered short rectangular conduits with power-law fluids having values of m from 0.3 to 1. They provide average wall shear rates in terms of an effective radius:

$$R_{equiv.} = 2\delta_1\delta_2/(\delta_1+\delta_2).$$

The velocity distribution obtained for $m = 0.4$, $\delta_1/\delta_2 = 2$, is also provided together with the corresponding shear-rate distribution.

A return to variational methods was provided by Röthemeyer (1970) who obtained a series of non-linear equations for the coefficients b_{st} of the polynomial

$$u = \sum_{s=0}^{s} \sum_{t=0}^{t} b_{st}\, x^{2s}\, y^{2t} \tag{2.6}$$

by substitution into the non-linear partial differential equation governing power-law substances in pipe flow:

$$\begin{aligned} \frac{\partial p}{\partial z} = \frac{1}{2}\left(\frac{2}{K}\right)^{\frac{1}{m'}}\left(\frac{1}{4}\right)^{m'} \Bigg\{ & \left[\left(\frac{\partial u}{\partial x}\right)^2 + \left(\frac{\partial u}{\partial y}\right)^2\right]^{m'} \left[\frac{\partial^2 u}{\partial x^2} + \frac{\partial^2 u}{\partial y^2}\right] \\ & + 2m'\left[\left(\frac{\partial u}{\partial x}\right)^2 + \left(\frac{\partial u}{\partial y}\right)^2\right]^{m'-1} \left[\left(\frac{\partial u}{\partial x}\right)^2 \frac{\partial^2 u}{\partial x^2} \right. \\ & \left. + 2\,\frac{\partial u}{\partial x}\,\frac{\partial u}{\partial y}\,\frac{\partial^2 u}{\partial x \partial y} + \left(\frac{\partial u}{\partial y}\right)^2 \frac{\partial^2 u}{\partial y^2}\right]\Bigg\}, \end{aligned}$$

where $m' = (1-m)/2m$. The substitution was made at each point (x,y) of a lattice distributed across one quadrant of the cross-section. This set of equations was linearized by substituting into the non-linear terms the values of b_{st} obtained in the previous iteration. For the first iteration the Navier-Stokes solution obtained by Cornish (1928) was used. The boundary condition was met by setting $u = 0$ in equation (2.6) for lattice points along the wall and adding the resultant set of linear equations to the linearized set obtained by substitution. The decision not to write equation (2.6) in a form which satisfied the boundary conditions, as was done by Schechter (1961), was dictated by Röthemeyer's intent to provide a method which was appropriate for cylinders of arbitrary cross-section. In general the number of lattice points (x,y) was greater than the number of b_{st} so that the system of linearized equations was overdetermined. The extra degrees of freedom were used to minimize the error due to the b_{st} estimate, a least squares fit being employed. The iterative process ended when the computed flow rate through the cross-section differed by less than 1 percent from the previous iteration.

Substances other than Newtonian fluids and power-law substances have received little attention in flows through rectangular conduits. Sokolovskii (1966) considered a dilatant material with the response:

$$g \begin{cases} \tau/\mu_0 & \tau < \tau_c \\ \tau_c/\mu_0 & \tau \geqslant \tau_c \end{cases} .$$

For rectangular pipes he considered only freely dilantant movement ($\tau_c \rightarrow 0$) for which the lines of constant velocity form a set of rectangles, one inside the next.

Greenberg, Dorn, and Wetherell (1960) solved by finite difference methods the torsion problem for a square cylinder composed of a material obeying the Ramberg-Osgood stress-strain law. The fluid analog of a Ramberg-Osgood solid is a DeHaven fluid, defined by the relationship:

$$\tau = \mu_0 \, g/(1 + k\tau^n).$$

The values of n for which DeHaven (1959a, 1959b) employed this relationship were much smaller than the values preferred by Greenberg, Dorn, and Wetherell (1960).

Hanzawa and Ishikawa (1970) investigated the problem of Greenberg et al. after greatly simplifying the boundary conditions by replacing the straight walls by concave surfaces. Comparable results were obtained where the stresses were highest.

Litvinov (1968) used variation methods upon empirical rheological data for polypropylene. After expressing τ and g in the form

$$\tau = \begin{cases} d_1 g + d_2 g^2 + d_3 g^3 & g < g_c \\ d_4 g + d_5 & g \geqslant g_c \end{cases},$$

where $\tau(g)$ was determined in one-dimensional flow, he assumed that

$$u = (\delta_1{}^2 - x^2)(\delta_2{}^2 - y^2) \sum_{s=0}^{s} \sum_{t=0}^{t} b_{st} \, x^{2s} \, y^{2t}$$

and minimized the error introduced by the coefficients over the cross-section of his flow.

In a follow-up of their 1965 study, Wheeler and Wissler (1966) measured the velocity distribution of a 0.9 percent solution of sodium carboxymethylcellulose flowing in a square pipe. By observing the movement of suspended particles at 12 locations in and surrounding one quadrant of the cross-section, they found deviations of up to 7 percent from the velocity profile obtained by Wheeler and Wissler (1965). The direction of the variations was consistent with the hypothesis that there was secondary flow within the cross-section. To test this hypothesis, the authors chose to model the liquid as a

Stokesian fluid* with a constant, but non-zero, normal stress function. The velocity distributions thus obtained gave qualitative support to the hypothesis that secondary flows were present. The method by which the distribution was calculated is stated in general terms and the constants which were obtained for the Stokes equation were not published.

---

*Stokesian fluids are discussed at considerable length in Chapter Five.

CHAPTER THREE

OPTICAL ANALYSIS

As stated in the Introduction, when a birefringent liquid flows between two polarizers, a pattern of fringes is observed. The purpose of this chapter is to derive a method for determining the amount of light which emerges from a given location on the second polarizer (hereafter called the analyzer). The form of the resultant relationships will determine the parameters and functions which are necessary to compute the location of fringes for a given flow field.

The discussion is in three parts. The first considers flows in which the velocity may be regarded as constant along any given light path. Such flows will be designated as two-dimensional and have a direct parallel in the two-dimensional models analyzed by the traditional methods of photoelasticity. The second part of the discussion will consider steady flows in which the velocity varies along the light paths. It will be shown that the results of this three-dimensional analysis reduce to those of the two-dimensional case when the limiting case of negligible variation along each light path is considered. The final part of this chapter lists the successive steps to be carried out in turn to obtain the fringe pattern from a hypothetical velocity distribution in the cross-section.

Two-Dimensional Flow

The analysis of two-dimensional flows of birefringent fluids occurs in many places. An example is Thurstone and Schrag (1962). Consider Figure 2 in which a two-dimensional flow field in the yz-plane is observed by polarized light moving through the flow field in the positive x-direction. Neglecting attenuation, the electric field* has the form

$$\mathbf{E} = E_0 \cos(2\pi x/\lambda) \, (-\sin\gamma \, \hat{\mathbf{j}} + \cos\gamma \, \hat{\mathbf{k}})$$

where E_0 is the amplitude of the wave, λ is the wavelength, and γ is the angle which the polarizer makes with $\hat{\mathbf{k}}$.

The propagation of the vector $\mathbf{E}$ is a function of its direction in the birefringent medium. Specifying the $\mathbf{E}$ directions for maximum and minimum propagation speeds by $\hat{\mathbf{n}}_1$ and $\hat{\mathbf{n}}_2$ respectively and assuming that $\hat{\mathbf{n}}_1 \cdot \hat{\mathbf{n}}_2 = 0$, the vector $\mathbf{E}$ can be resolved into components parallel with $\hat{\mathbf{n}}_1$ and $\hat{\mathbf{n}}_2$:

$$\mathbf{E} = E_0 \left[\cos(2\pi n_1 x/\lambda) \cos(\gamma-\psi) \, \hat{\mathbf{n}}_1 - \cos(2\pi n_2 x/\lambda) \sin(\gamma-\psi) \, \hat{\mathbf{n}}_2 \right] .$$

Here ψ is the orientation angle shown in Figure 2, and n_1 and n_2 are the refractive indices of the medium when $\mathbf{E}$ is parallel with $\hat{\mathbf{n}}_1$ and $\hat{\mathbf{n}}_2$ respectively.

When the light emerges from the flow field at $x = \overline{\delta}$ the only light which will pass through the analyzer is

---

*In this dissertation vectors are designated by boldface ($\mathbf{E}$) and unit vectors are denoted by a circumflex ($\hat{\mathbf{n}}_1$).

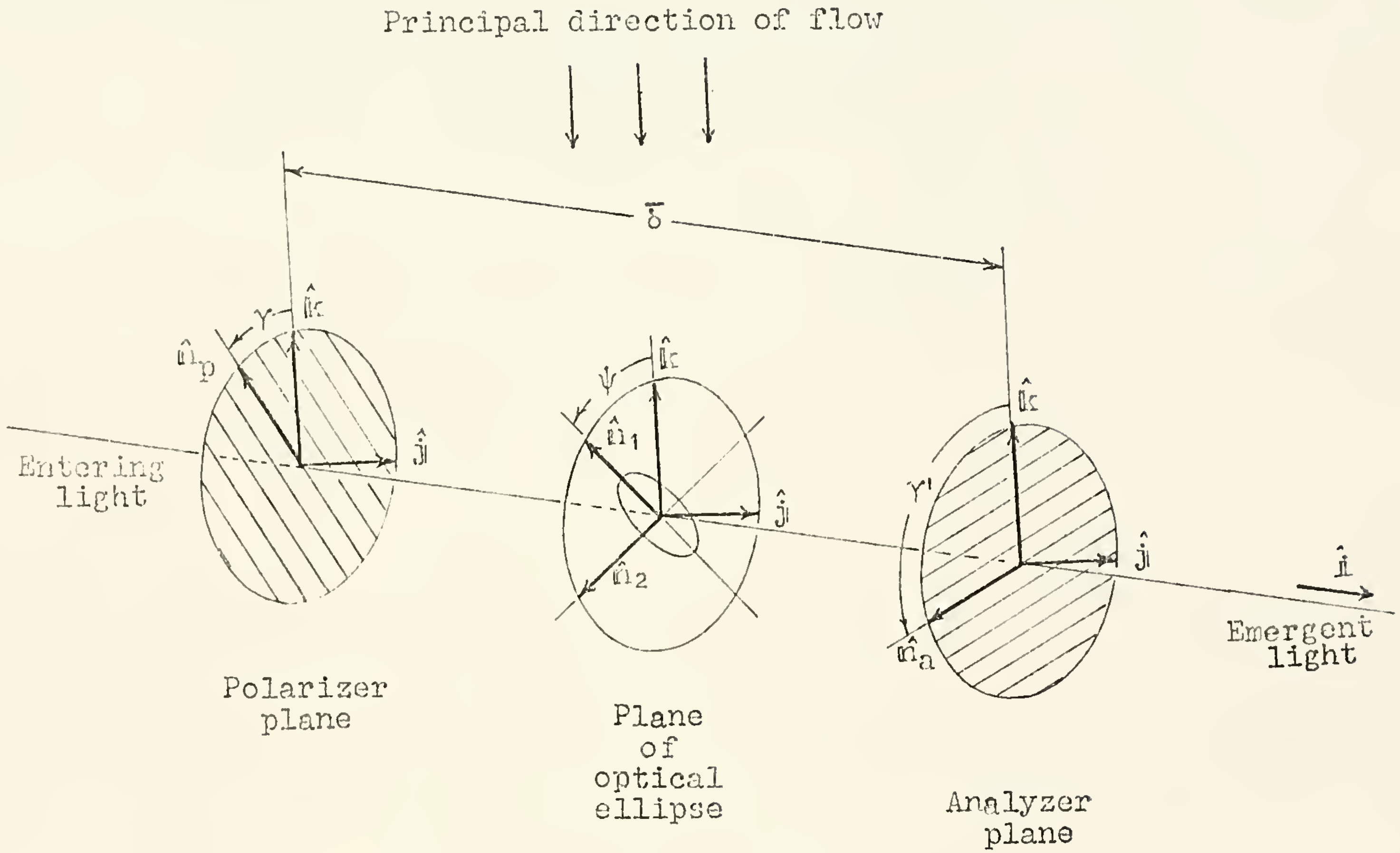

FIGURE 2. Unit vectors and angles relating to the flow. The total light path $\bar{\delta}$ is also indicated.

that component which is parallel with $\hat{\mathbf{n}}_a$ where

$$\hat{\mathbf{n}}_1 \cdot \hat{\mathbf{n}}_a = \cos(\gamma' - \psi),$$

$$\hat{\mathbf{n}}_2 \cdot \hat{\mathbf{n}}_a = \sin(\gamma' - \psi).$$

In that case the emergent amplitude is

$$E_e = \mathbf{E} \cdot \hat{\mathbf{n}}_a$$

or

$$E_e = E_0 \left[\cos(2\pi n_1 \bar{\delta}/\lambda) \cos(\gamma - \psi) \cos(\gamma' - \psi) + \cos(2\pi n_2 \bar{\delta}/\lambda) \sin(\gamma - \psi) \sin(\gamma' - \psi) \right] .$$

Setting

$$\bar{n} = (n_1 + n_2)/2$$

$$\Delta n = n_2 - n_1$$

and expanding the cosines yields

$$E_e = E_0 \left\{ \left[\cos(2\pi\bar{\delta}\bar{n}/\lambda) \cos(\pi\bar{\delta}\Delta n/\lambda) + \sin(2\pi\bar{\delta}\bar{n}/\lambda) \sin(\pi\bar{\delta}\Delta n/\lambda) \right] \cos(\gamma - \psi) \cos(\gamma' - \psi) + \left[\cos(2\pi\bar{\delta}\bar{n}/\lambda) \cos(\pi\bar{\delta}\Delta n/\lambda) - \sin(2\pi\bar{\delta}\bar{n}/\lambda) \sin(\pi\bar{\delta}\Delta n/\lambda) \right] \sin(\gamma - \psi) \sin(\gamma' - \psi) \right\} .$$

This simplifies to

$$E_e = E_0 \left[\cos(2\pi\bar{\delta}\bar{n}/\lambda) \cos(\pi\bar{\delta}\Delta n/\lambda) \cos(\gamma - \gamma') + \sin(2\pi\bar{\delta}\bar{n}/\lambda) \sin(\pi\bar{\delta}\Delta n/\lambda) \cos(\gamma + \gamma' - 2\psi) \right] .$$

For a dark polarizing field, $\gamma - \gamma' = \pi/2$ with the familiar result upon substitution,

$$E_e = E_0 \sin(2\pi\bar{\delta}\bar{n}/\lambda) \sin(\pi\bar{\delta}\Delta n/\lambda) \sin 2(\gamma - \psi),$$

which is used in two-dimensional optical stress analysis of solids (e.g. Dally and Riley, 1965, p. 171).

For a fringe to be observed it is necessary and sufficient that any of the sine factors in this equation equals zero. Each of these conditions will be discussed individually.

The first factor reflects the periodic variation in E_e due to the wave nature of light. The associated frequency, about 10^{14} Hz, is too rapid for eye or camera. For this reason the constant amplitude is usually replaced by $\bar{E}_0$, where

$$\bar{E}_0 = E_0 \sin(2\pi\delta\bar{n}/\lambda).$$

The middle factor is responsible for the colored fringes known as isochromatics which are seen when the flow field is illuminated with white light. In monochromatic light the same name is retained for those fringes resulting from the condition

$$\Delta n\bar{\delta}/\lambda = N$$

where N is an integer known as the fringe order.

The final factor is responsible for the black fringes known as isoclinics along which the principal optical axes are parallel with the polarizers. This condition is known as extinction and the so-called extinction angle is defined by

$$\chi = \begin{cases} |\gamma - \psi| & |\gamma - \psi| < \frac{\pi}{4} \\ \frac{\pi}{2} - |\gamma - \psi| & |\gamma - \psi| \geq \frac{\pi}{4} \end{cases} .$$

In monochromatic light it is difficult to distinguish isochromatics from isoclinics. This difficulty may be avoided by using circularly polarized light for which

$$E_e = \bar{E}_0 \sin(\pi\Delta n\bar{\delta}/\lambda).$$

The derivation of this expression is straightforward, but tedious, and it may be found in many references including Dally and Riley (1965, pp. 174-179).

Three-Dimensional Flow

The experimental stress analysis of three-dimensional solids is accomplished by locking the deformation in place and then cutting the model into slices for two-dimensional analysis. The availability of this technique, which provides local stress distributions along any desired path, has inhibited interest in the study of three-dimensional fringe patterns as such. Some studies have been carried out using scattered light polariscopes which have the effect of placing a temporary analyzer or polarizer at a selected plane within the three-dimensional model. This technique is described by Van Daele-Dossche and Van Geen (1969).

In liquids the direct three-dimensional analysis of birefringent patterns to obtain velocity fields is not feasible due to the variety of conditions which, in principle, could lead to the same fringe configuration. On the other hand, there seems no theoretical objection to the inverse method: assuming a flow distribution and determining the resultant fringe pattern. The corresponding analysis follows.

In three-dimensional flows, even if the streamlines are parallel, the principal optic axes will be oriented in three-dimensional space. As a result, the directions $\hat{n}_1$ and $\hat{n}_2$ must be recognized as lying parallel to the principal axes of the ellipse formed by the intersection of a three-dimensional ellipsoid with the plane orthogonal to the light path at the point of interest (Sommerfeld, 1964, pp. 139-147). Care must be taken not to confuse the directions $\hat{n}_1$ and $\hat{n}_2$ with the projected axes of the ellipsoid. The former are orthogonal; the latter, in general, are not. In three-dimensional flows the directions $\hat{n}_1$ and $\hat{n}_2$ will vary along the light paths as will n_1 and n_2, the magnitudes of their respective refractive indices.

Assumptions

In the analysis which follows three assumptions are made regarding the optical ellipsoid. These are discussed separately.

Assumption 1. – The properties of the optical ellipsoid are completely defined by three characteristics: the difference between the length of the longest axis and the two shorter axes (assumed equal), the magnitude of the inclination of the longest axis to the principal flow direction, and the direction of that inclination. These variables are shown in Figure 3 and are denoted by Δn, ψ, and Θ respectively. The first two are easily identified with the birefringence and the orientation angle of the previous section. The third parameter, Θ, will be identified as the rotation

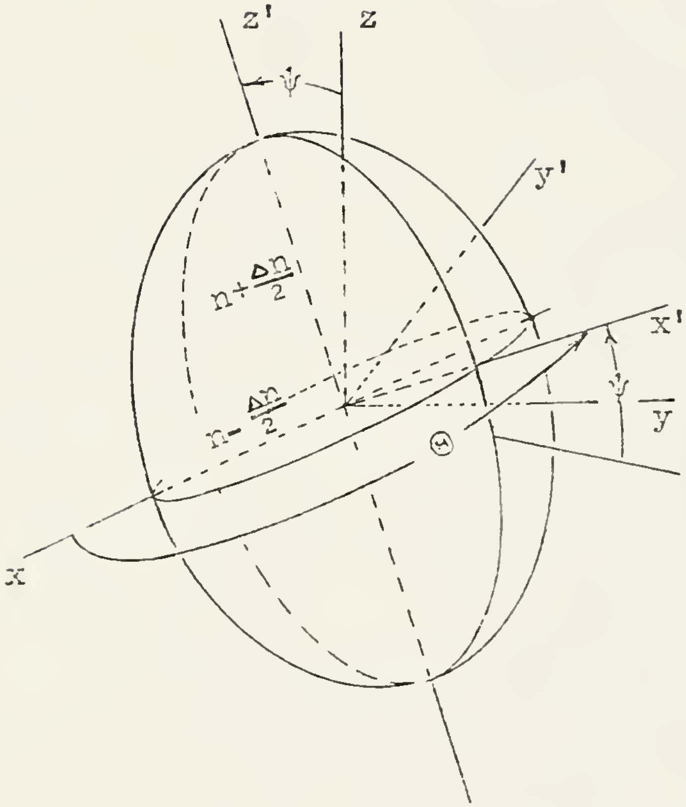

FIGURE 3. Optical ellipsoid, showing parameters θ, ψ, and Δn.

angle and is necessary to describe variation of the optical properties as the direction of the flow changes along the light path. The magnitudes of the ellipsoidal axes vary so little, $\Delta n \ll \bar{n}$, that it can be assumed, as usual, that the mean value of the refractive index is constant. The previous assumption that the two shorter optical axes are equal in length has been made principally in the interest of economy since it reduces the number of optical parameters to a manageable number.

Assumption 2. - The optical properties are uniquely defined by the local shear rate. Numerous authors, among them Truesdell and Noll (1965), have pointed out the critical importance of history in the description of the properties of a material. In the present case the flow is steady. If a fading memory is assumed for the material, then after a short time the history of the flow may be neglected. The neglect of strain in the definition of the optical properties follows from experimental work with the medium which indicates that the elastic properties are negligible except at very low rates of shear. Work in this area, principally by Thurstone and his associates (e.g. Thurstone and Schrag, 1962), was discussed in the previous chapter. A unique dependence of the optical properties upon the shear rate is consistent with those theories which explain birefringence in terms of the continuous rotation of microelements within the fluid as described by, say, Boeder (1932) and Kuhn and Kuhn (1943). Acceptance of these theories is not necessary for acceptance of Assumption 2 which is not contradicted by any experimental evidence.

Assumption 3. – The inclination of the longest axis of the ellipsoid occurs in the direction of the local velocity gradient. That is, the rotation angle is given by

$$\Theta = \tan^{-1}\left|\frac{\partial g/\partial y}{\partial g/\partial x}\right|$$

where g is the magnitude of the shear rate. The coincidence of principal directions for certain optical and rheological properties has been suggested by Lodge (1956) and has strong heuristic appeal.

Definition of Effective Optical Properties

The properties of the optical ellipse at any point on a light path within the three-dimensional flow field follow immediately from the assumptions. As shown in Appendix A, the effective birefringence will be

$$\begin{aligned}\Delta N = {} & \left[(A_1{}^2+A_2{}^2+A_3{}^2)\cos^2\Psi - 2(A_1A_4+A_3A_5)\sin\Psi\cos\Psi \right.\\ & \left. + (A_4{}^2+A_5{}^2)\sin^2\Psi\right]^{-1/2} \\ & - \left[(A_1{}^2+A_2{}^2+A_3{}^2)\sin^2\Psi + 2(A_1A_4+A_3A_5)\sin\Psi\cos\Psi \right.\\ & \left. + (A_4{}^2+A_5{}^2)\cos^2\Psi\right]^{-1/2}\end{aligned}$$

where Ψ is the effective orientation angle,

$$\Psi = \frac{1}{2}\tan^{-1}\left[\frac{2\ (A_1A_4+A_3A_5)}{A_1{}^2+A_2{}^2+A_3{}^2-A_4{}^2-A_5{}^2}\right]$$

and the variables A_1 through A_5 are defined in terms of the optical parameters Δn, ψ, and Θ. For example,

$$A_1 = \cos\psi \sin\theta / (\bar{n} - \frac{\Delta n}{2}).$$

Values for A_2 through A_5 are given in Appendix A.

It is appropriate to consider conditions for light paths parallel with and close to the side walls where Θ has a limiting value of $\pi/2$. Substitution of this result leads after considerable manipulation to the result

$$\Psi_w = \psi,$$

$$\Delta N_w = \Delta n \sin^2 2\psi.$$

At low flow rates, when ψ approaches $\pi/4$,

$$\Delta N_w = \Delta n.$$

Analysis

To analyze flows in which ΔN and Ψ vary along each light path, it is convenient to employ the Poincaré (1889) model in which any change in the condition of a polarized light beam may be represented by the movement of a point on the surface of a unit sphere. Procedures for use of the Poincaré sphere are found in many texts. The present sign convention follows Hartshorne and Stuart (1970) and is illustrated in Figure 4. Each point on the sphere is expressed in terms of angular coordinates Φ and Ω which correspond respectively to latitude and longitude in terrestrial navigation, "West" and "North" being the positive directions.

Two points are designated on the Poincare sphere: P, which represents the condition of the polarized light, and R, which represents the principal optic axis of the medium. These points are determined as follows.

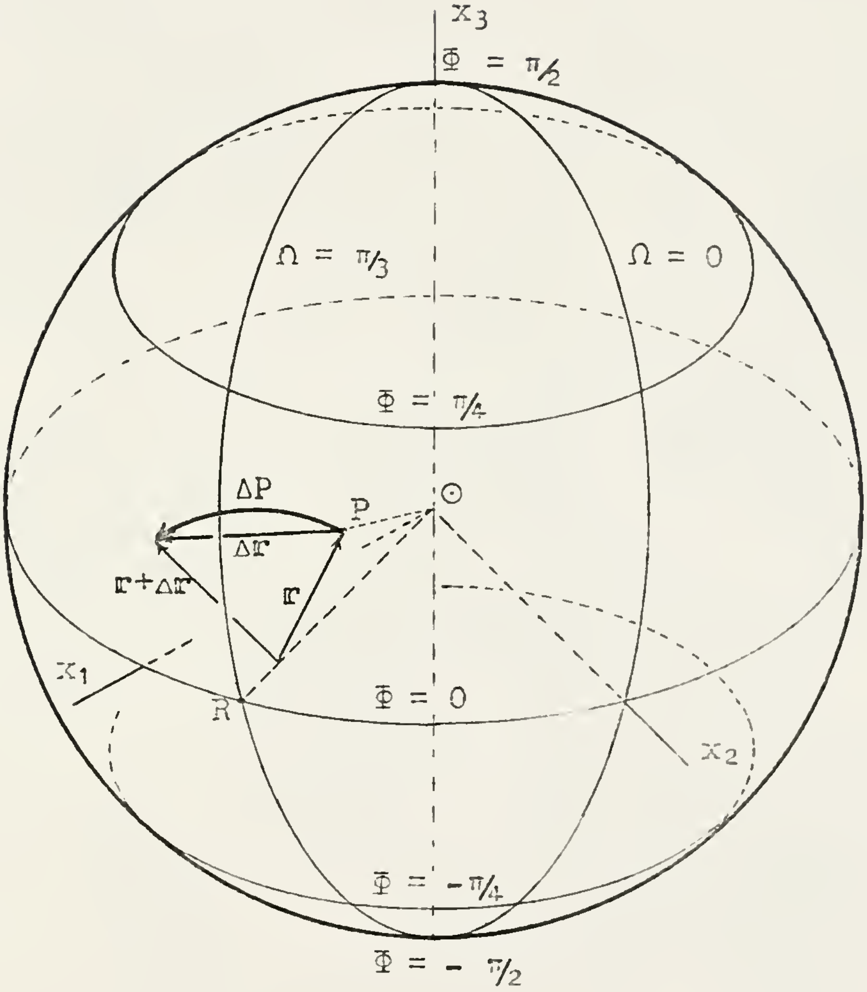

FIGURE 4. Poincaré sphere showing P, the condition of the polarized light beam, R, the principal (fast) optic axis of the medium, and ΔP, an arc on the surface representing the change in polarization which occurs.

Point P. — In the general case polarized light is elliptically polarized having the general form (for propagation along the x-axis):

$$\mathbb{E} = A_s \cos(\omega t + \tfrac{\sigma'}{2})\, \hat{\mathbb{X}}_1 + B_s \cos(\omega t + \tfrac{\sigma''}{2})\, \hat{\mathbb{X}}_2,$$

where σ', σ'', A_s, and B_s are constants, only two of which are independent, and $\hat{\mathbb{X}}_1$ and $\hat{\mathbb{X}}_2$ are orthogonal cartesian unit vectors in the yz-plane. In the present case the form selected is

$$\mathbb{E} = \frac{E_0}{\sqrt{2}}\left[\hat{\mathbb{X}}_1 \cos(\omega t - \tfrac{\sigma}{2}) + \hat{\mathbb{X}}_2 \cos(\omega t + \tfrac{\sigma}{2})\right],$$

which yields on rotation through the angle $(\epsilon - \pi/4)$:

$$\begin{aligned}\mathbb{E} = \frac{E_0}{\sqrt{2}} \Big\{ -\Big[\sin(\epsilon - \tfrac{\pi}{4}) \cos(\omega t - \tfrac{\sigma}{2}) - {} \\ \cos(\epsilon - \tfrac{\pi}{4}) \cos(\omega t + \tfrac{\sigma}{2})\Big]\, \hat{\mathbb{j}} \\ + \Big[\cos(\epsilon - \tfrac{\pi}{4}) \cos(\omega t - \tfrac{\sigma}{2}) + {} \\ \sin(\epsilon - \tfrac{\pi}{4}) \sin(\omega t + \tfrac{\sigma}{2})\Big]\, \hat{\mathbb{k}} \Big\}.\end{aligned}$$

Further trigonometric manipulation yields:

$$\begin{aligned}\mathbb{E} = E_0 \Big[-(\sin\epsilon \cos\tfrac{\sigma}{2} \cos\omega t + \cos\epsilon \sin\tfrac{\sigma}{2} \sin\omega t)\, \hat{\mathbb{j}} \\ + (\cos\epsilon \cos\tfrac{\sigma}{2} \cos\omega t - \sin\epsilon \sin\tfrac{\sigma}{2} \sin\omega t)\, \hat{\mathbb{k}} \Big].\end{aligned}$$

This form of representing $\mathbb{E}$ has two useful properties (Figure 5). The variable ϵ can be identified with the angle which the principal axis of the elliptically polarized light makes with the principal flow direction $\hat{\mathbb{k}}$. The variable σ reflects the eccentricity of the ellipse for which the major and minor axes have magnitudes:

$$E_{max} = E_0 \cos \frac{\sigma}{2} ,$$

$$E_{min} = E_0 \sin \frac{\sigma}{2} .$$

Further, the variables ϵ and σ are simply related to the coordinates of the Poincaré sphere. Specifically,

$$P(\Omega,\Phi) = P(2\epsilon,\sigma).$$

The dependence of the electric field vector upon time is usually neglected in studies utilizing polarized light, and texts such as Hartshorne and Stuart (1970) utilize the parameters ϵ and σ directly without stating $E(t)$ explicitly.

Point R. — Point R on the Poincaré sphere represents the optical properties of the medium. If, as has been assumed in all previous studies using Milling Yellow as the birefringent medium, the solution acts as a linear wave plate, then the point R is located on the "equator" of the Poincaré sphere at

$$R(\Omega,\Phi) = R(2\Psi,0)$$

where Ψ is the effective orientation angle. In this case point R represents the location of the "fast" optical axis parallel to $\hat{n}_1$. If there were evidence of isomerism or helicity in the molecular structure of Milling Yellow, or if a degree of circular polarization were observed under conditions of zero shear, then these effects would require redesignation of point R at that value of Φ corresponding to the eccentricity of the elliptical wave plate (see, for example, Shurcliff and Ballard, 1964).

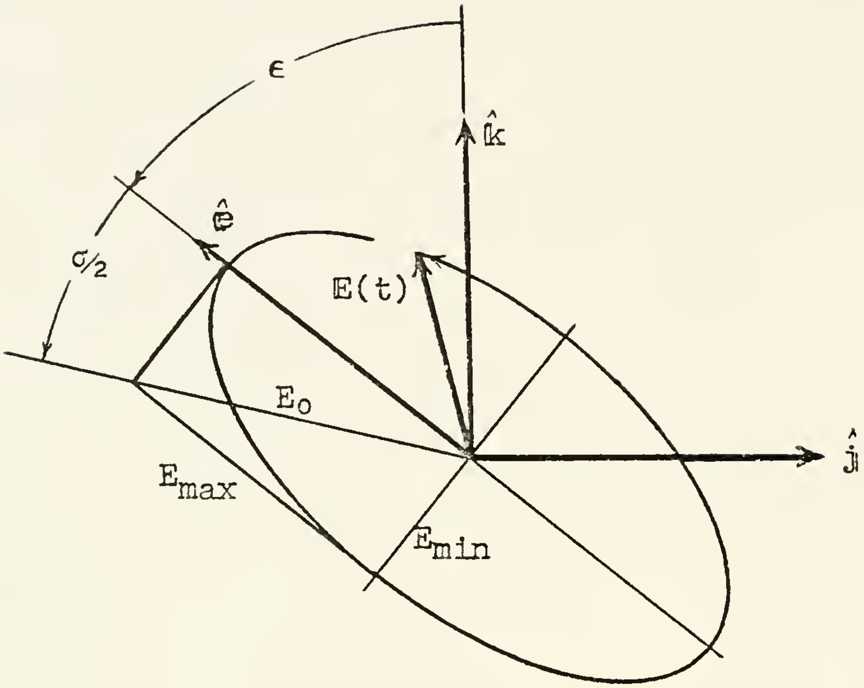

FIGURE 5. Elliptically polarized light in the yz-plane.

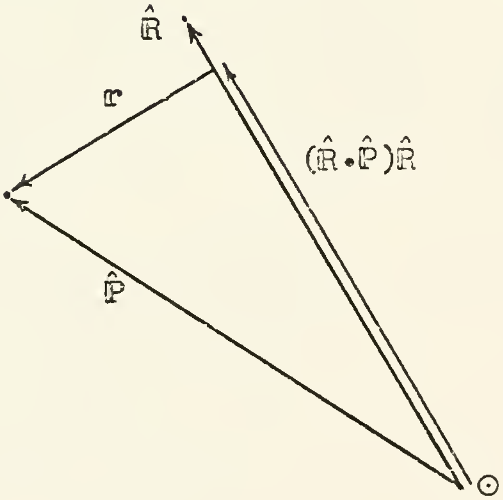

FIGURE 6. Projection of $\overline{OP}$ on $\overline{OR}$ and definition of r.

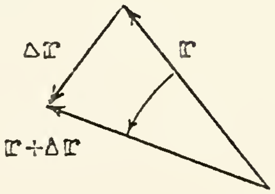

FIGURE 7. Definition of Δr. Angle is $2\pi\Delta N\Delta x/\lambda$.

Once points P and R have been designated the change in polarization follows directly. The Poincaré sphere is constructed such that the change in P due to a medium with properties represented by R follows a counter-clockwise circular path about the axis $\overline{OR}$ with an included angle of $2\pi\Delta N\Delta x/\lambda$ relative to this axis.

To obtain the associated vector equations, designate the cartesian coordinates of the sphere by x_1, x_2, and x_3 with corresponding unit vectors $\hat{x}_1$, $\hat{x}_2$, and $\hat{x}_3$. Locate P and R by the unit vectors $\hat{\mathbb{P}}$ and $\hat{\mathbb{R}}$ where

$$\hat{\mathbb{R}} = \overrightarrow{OR} = \hat{x}_1 \sin 2\Psi + \hat{x}_2 \cos 2\Psi$$

and

$$\hat{\mathbb{P}} = \overrightarrow{OP} = \hat{x}_1 \cos\sigma \sin 2\epsilon + \hat{x}_2 \cos\sigma \cos 2\epsilon + \hat{x}_3 \sin\sigma . \qquad (3.1)$$

Referring to Figure 6, the projection of $\overrightarrow{OP}$ on $\overrightarrow{OR}$ is $(\hat{\mathbb{P}}\cdot\hat{\mathbb{R}})\hat{\mathbb{R}}$ and the radius of the path is

$$\mathbb{r} = \hat{\mathbb{P}} - (\hat{\mathbb{P}}\cdot\hat{\mathbb{R}})\,\hat{\mathbb{R}}.$$

The change in P is ΔP, a circular arc with chord $\Delta\mathbb{r}$, where

$$\Delta\mathbb{r} = \hat{\mathbb{P}} - \hat{\mathbb{P}}_0 .$$

Since the chord subtends an angle of $2\pi\Delta N\Delta x/\lambda$, it follows from Figure 7 that the length of $\Delta\mathbb{r}$ is

$$\Delta r = 2r \sin(\pi\Delta N\Delta x/\lambda)$$

and its direction is determined by the conditions:

$$\hat{\mathbb{R}}\cdot\Delta\mathbb{r} = 0,$$

$$\mathbb{r}\cdot\Delta\mathbb{r} = -r\,\Delta r \sin(\pi\Delta N\Delta x/\lambda),$$

$$(\hat{\mathbb{P}}\times\mathbb{r})\cdot\Delta\mathbb{r} = (\hat{\mathbb{P}}\cdot\hat{\mathbb{R}})\, r\,\Delta r \cos(\pi\Delta N\Delta x/\lambda).$$

When the indicated vector operations are carried out, three simultaneous equations result from which the components of Δr are found to be: (3.2)

$$\Delta r_1 = 2 \sin(\pi \Delta N \Delta x/\lambda) \cos 2\Psi \left[\sin \sigma \cos(\pi \Delta N \Delta x/\lambda) - \cos \sigma \sin(\pi \Delta N \Delta x/\lambda) \sin 2(\epsilon - \Psi)\right];$$

$$\Delta r_2 = -2 \sin(\pi \Delta N \Delta x/\lambda) \sin 2\Psi \left[\sin \sigma \cos(\pi \Delta N \Delta x/\lambda) - \cos \sigma \sin(\pi \Delta N \Delta x/\lambda) \sin 2(\epsilon - \Psi)\right];$$

$$\Delta r_3 = -2 \sin(\pi \Delta N \Delta x/\lambda) \left[\sin \sigma \sin(\pi \Delta N \Delta x/\lambda) + \cos \sigma \cos(\pi \Delta N \Delta x/\lambda) \sin 2(\epsilon - \Psi)\right].$$

Consider a homogeneous flow of thickness $\Delta x = \bar{\delta}$ having optical properties $\Delta N = \Delta n$ and $\Psi = \psi$ which are constant along any given light path. Upon this two-dimensional flow let light fall which is plane-polarized ($\sigma = 0$) by passage through a polarizer oriented such that $\gamma = \epsilon$. If

$$\Delta n \bar{\delta}/\lambda = N$$

where N is an integer, or

$$\gamma = \psi \pm \frac{\pi}{2}$$

it can be seen that

$$\Delta r_1 = \Delta r_2 = \Delta r_3 = 0$$

and the polarization of the light is the same when it leaves the flow as when it enters. In a "dark polarizing field" the analyzer is oriented at right angles to the polarizer, and for such a field, if $\Delta r = 0$, a fringe will result. Necessarily the conditions for which $\Delta r = 0$ are identical with those for isochromatics and isoclinics in the previous section on two-dimensional flow.

For more general two-dimensional conditions it must be recognized that there will occur two types of fringes: those due to total extinction of plane-polarized light and those due to partial extinction of elliptically polarized light. Besides the cases already considered, there exists only one other condition for which the light is plane-polarized and completely extinguished as it leaves the flow. This occurs when

$$\Delta n\bar{\delta}/\lambda = N + \tfrac{1}{2}$$

where N is an integer, and simultaneously

$$\psi = \tfrac{1}{2}(\Delta\gamma \pm \tfrac{N\pi}{2})$$

where N is again an integer and $\Delta\gamma$ is the angle between the principal directions of the polarizer and analyzer. Note that both conditions must be satisfied for a fringe to be observed.

In general, light emerging from a flow field will be elliptically polarized. In the discussion of how point P is determined on the Poincaré sphere, the electric field vector was expressed in the form:

$$E = E_0 \Big[-(\sin\epsilon \cos\tfrac{\sigma}{2} \cos\omega t + \cos\epsilon \sin\tfrac{\sigma}{2} \sin\omega t)\hat{j}$$
$$+ (\cos\epsilon \cos\tfrac{\sigma}{2} \cos\omega t - \sin\epsilon \sin\tfrac{\sigma}{2} \sin\omega t)\hat{k}\Big].$$

Upon passage through an analyzer, the emergent amplitude of such light would be $E_e = \hat{E}\cdot\hat{n}_a$, where

$$\hat{n}_a = -\hat{j} \sin\gamma' + \hat{k} \cos\gamma',$$

or

$$E_e = E_0 \left[\cos(\epsilon - \gamma') \cos \omega t \cos \frac{\sigma}{2} - \sin(\epsilon - \gamma') \sin \omega t \sin \frac{\sigma}{2}\right].$$

The intensity of the light varies with the square of the electric field (see, for example, Feynman, Leighton, and Sands, 1963, p. 31-10):

$$I = kE_e{}^2,$$

and the average value of the intensity for periods of time much larger than the period of the light waves will be:

$$\begin{aligned}\overline{I} &= \lim_{t' \to \infty} \frac{k}{t'} \int_0^{t'} I \, dt \\ &= \frac{kE_0{}^2}{2} \left[\cos^2(\epsilon - \gamma') \cos^2 \frac{\sigma}{2} + \sin^2(\epsilon - \gamma') \sin^2 \frac{\sigma}{2}\right].\end{aligned}$$

The conditions for a fringe when the light is plane-polarized ($\sigma = 0$) have already been discussed. If the light is circularly polarized ($\sigma = \pm \frac{\pi}{2}$), then

$$\overline{I} = kE_0{}^2/2,$$

a result which, predictably, does not depend upon the characteristic direction $\hat{m}_a$ of the analyzer. For any other condition of light leaving the fluid there will be some analyzer angle γ' which will minimize $\overline{I}$. This condition may be obtained formally by differentiating $\overline{I}(\gamma')$ with respect to γ' and setting the result equal to zero. The result,

$$\epsilon - \gamma' = \frac{\pi}{2},$$

is consistent with what would be predicted from looking at Figure 5 and can be used to determine the necessary condition for a fringe to occur when the emergent light is elliptically polarized.

For two-dimensional flows, since the entrance conditions are $\sigma = 0$, $\epsilon = \gamma$, the initial polarization is given by substitution into equation (3.1) to obtain

$$\hat{\mathbb{P}}_0 = \hat{x}_1 \sin 2\gamma + \hat{x}_2 \cos 2\gamma.$$

The change in $\hat{\mathbb{P}}$ is $\Delta\mathbb{r}$, for which when $\sigma = 0$, $\epsilon = \gamma$, $\Delta N = \Delta n$, $\Psi = \psi$, and $\Delta x = \bar{\delta}$:

$$\Delta r_1 = -2 \sin^2(\pi\Delta n\bar{\delta}/\lambda) \cos 2\psi \sin 2(\gamma-\psi),$$

$$\Delta r_2 = 2 \sin^2(\pi\Delta n\bar{\delta}/\lambda) \sin 2\psi \sin 2(\gamma-\psi),$$

$$\Delta r_3 = -2 \sin(\pi\Delta n\bar{\delta}/\lambda) \cos(\pi\Delta n\bar{\delta}/\lambda) \sin 2(\gamma-\psi).$$

On emergence the condition for a fringe requires that

$$\hat{\mathbb{P}}(\epsilon,\sigma) = \hat{\mathbb{P}}(\tfrac{\pi}{2} + \gamma',\sigma).$$

Setting

$$\hat{\mathbb{P}}(\tfrac{\pi}{2} + \gamma',\sigma) = \hat{\mathbb{P}}(\gamma,0) + \Delta\mathbb{r}$$

and solving for σ yields

$$\sigma = \sin^{-1} \left[-\sin(2\pi\Delta n\bar{\delta}/\lambda) \sin 2(\gamma-\psi)\right],$$

which defines the ellipticity of the emergent light, and

$$\tan^2(\pi\Delta n\bar{\delta}/\lambda) = \frac{-\sin 2(\gamma'-\gamma)}{\sin 2(\gamma'+\gamma-2\psi)}$$

which is the condition for a minimum to occur when the light is elliptically polarized.

It has been shown in the previous paragraph that the Poincaré sphere can be used to obtain a complete description of the polarization of light passing through a two-dimensional flow. These relationships will now be used in an iterative scheme to determine the polarization of a light beam passing along a path for which the effective optical properties are known explicitly but are no longer constant.

Integration to Obtain Fringe Patterns

The polarization of a light beam moving through a birefringent medium has been obtained in terms of a position vector $\hat{\mathbb{P}}$ which designates a point on the surface of the Poincaré sphere. The incremental change in $\hat{\mathbb{P}}$ may be expressed in terms of the chord $\Delta\mathbf{r}$:

$$\hat{\mathbb{P}}(x+\Delta x;\epsilon+\Delta\epsilon,\sigma+\Delta\sigma;\Delta N,\Psi) = \hat{\mathbb{P}}(x;\epsilon,\sigma;\Delta N,\Psi) + \Delta\mathbf{r}(\Delta x;\epsilon,\sigma;\Delta N,\Psi).$$

By choosing values of Δx small enough so that ΔN and Ψ may be regarded as constant for the increment, the change in $\hat{\mathbb{P}}$ along the entire light path may be obtained by summation:

$$\hat{\mathbb{P}}(x=\delta_1) = \hat{\mathbb{P}}(x=-\delta_1) + \sum_{s=0}^{S}\Delta\mathbf{r}_S.$$

The effective parameters ΔN and Ψ are functions of Δn, ψ, and Θ which vary in turn with the local shear rate $g(x,y)$, itself a function of the spatial coordinates x and y. Figure 8 provides a schematic representation of the means by which the summation is to be performed. The corresponding steps are tabulated below:

1. — Choose the y-coordinate of the light beam. Set $x = -\delta_1$.

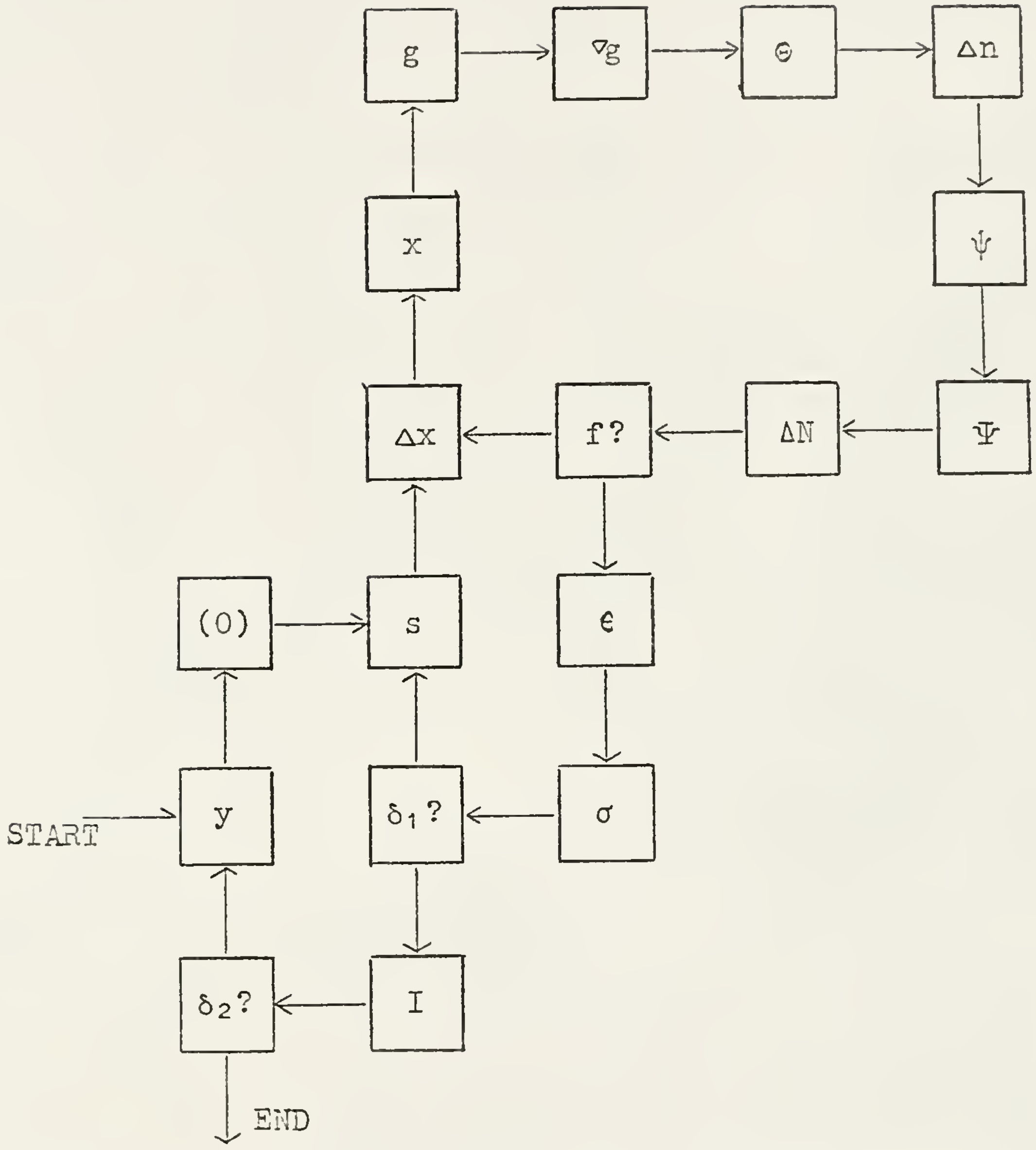

FIGURE 8. Schematic representation of successive determinations of the variables. The subscript s has been omitted from the variable names. The notation (0) indicates that all variables except y are reset at their initial ($x = -\delta_1$) values. Question marks indicate decisions.

2. – Determine the polarization $\hat{P}$ as the light beam enters the flow by setting $\epsilon = \gamma$ and $\sigma = 0$ in equation (3.1).

3. – Obtain the shear rate $g_s(x_s,y)$ from a distribution calculated from those in Chapter Six or elsewhere. The subscript indicates that this is the s^{th} iteration.

4. – It has been assumed that the rotation angle Θ_s is defined by

$$\Theta_s = \tan^{-1}\left|\frac{\partial g_s/\partial y}{\partial g_s/\partial x}\right| .$$

Obtain $\Theta_s(g_s)$.

5. – Obtain $\Delta n_s(g_s)$ from the optical relationships of Chapter Four or elsewhere. Obtain $\psi_s(g_s)$ in a similar manner.

6. – $\Psi_s(\Delta n_s,\psi_s,\Theta_s)$ and $\Delta N_s(\Delta n_s,\psi_s,\Theta_s)$ are defined in Appendix A. Obtain Ψ_s and ΔN_s.

7. – Choose a trial value for Δx_s.

8. – Repeat steps 3 through 7 with $x_{s+1} = x_s + \Delta x_s$ to obtain the corresponding terms with subscripts $s+1$.

9. – Set $\Psi = (\Psi_{s+1} + \Psi_s)/2$.

10. – Set $\Delta N = (\Delta N_{s+1} + \Delta N_s)/2$.

11. – Determine the fractional variations, $(\Psi-\Psi_s)/\Psi$ and $(\Delta N-\Delta N_s)/\Delta N$, of the optical coefficients for the interval Δx_s. If either variation exceeds a prescribed level, say $f = 0.01$, reduce the value of Δx_s and repeat steps 8 through 11. Omit this step if ΔN or $\Psi = 0$.

12. – Obtain Δr_s from equation (3.2).

13. – Set $\hat{P}_{s+1} = \hat{P}_s + \Delta r_s$.

14. – From the definition of $\hat{P}$ the $\hat{x}_3$-component is

$$P_3 = \sin\sigma .$$

Hence,

$$\sigma_{s+1} = \sin^{-1}\left[(P_3)_{s+1}\right] .$$

Obtain σ_{s+1}.

15. – From the definition of $\hat{P}$ it is also clear that

$$\epsilon_{s+1} = \frac{1}{2}\tan^{-1}(P_1/P_2)_{s+1} .$$

Obtain ϵ_{s+1}.

16. – If $\Delta x_s + x_{s+1} < \delta_1$, repeat steps 8 through 15. If $\Delta x_s + x_{s+1} \geqslant \delta_1$, set $\Delta x_s = \delta_1 - x_{s+1}$ and repeat steps 8 through 15. If $\Delta x_s = 0$, go on to step 17.

17. – Calculate the relative intensity of the light emerging from the flow field and analyzer at coordinate y. Recall that:

$$\frac{I}{I_0} = \cos^2(\epsilon-\gamma')\cos^2(\sigma/2) + \sin^2(\epsilon-\gamma')\sin^2(\sigma/2).$$

18. – Choose a new y-coordinate and repeat steps 2 through 17.

19. – When the final y-coordinate has been chosen ($y = \delta_2$) and the final relative intensity has been calculated, plot I/I_0 as a function of y to obtain the fringe pattern predicted by the relationships chosen in steps 3 and 5.

CHAPTER FOUR

DETERMINATION OF OPTICAL PROPERTIES

This chapter discusses the determination of two optical properties of Milling Yellow: the birefringence, Δn, and the orientation angle ψ. Both of these quantities have been defined in Chapter Three. They will be discussed separately, the orientation angle only briefly at the end.

Birefringence

The birefringence is that property of an optically active fluid which is responsible for that part of the fringe pattern known as isochromatics. The necessary condition for these fringes is that

$$\Delta n \bar{\delta} / \lambda = N$$

where Δn is the birefringence, $\bar{\delta}$ is the thickness of the flow field through which the light passes, λ is the wavelength of the incident light, and N is an integer known as the fringe order. It is clear that, except for a constant of proportionality, the birefringence and the fringe order may be used interchangeably for a given experimental arrangement.

The data of Peebles, Prados, and Honeycutt (1965) indicate that at a given concentration and temperature Milling Yellow has a birefringence (fringe order) which shows a progressive non-linear increase with shear rate. This increase suggested that the data be replotted with the square of the fringe order as the dependent variable. Figure 9 shows the result when this is done for the four most concentrated solutions reported by Peebles, Prados, and Honeycutt. The hypothetical relationship

$$N^2 = k_1 g + k_2$$

appears adequate for the range of shear rates shown.

An experimental verification of this form was carried out with the Milling Yellow used in the present dissertation. In contrast to the data of Peebles, Prados, and Honeycutt, which were measured in a concentric cylinder polariscope at nearly constant shear rates, the data for the present study were obtained near the wall of a nearly square rectangular conduit which is described in the next section. In the succeeding sections will be found an analysis of Milling Yellow's optical response when flowing slowly through such a channel, some experimental data, and a discussion thereof.

Apparatus

The Milling Yellow solution was prepared as described in Appendix B. The nearly square conduits used in these experiments have been described previously by Lindgren (1962, 1963) who constructed them to observe the transition between laminar and turbulent flows in bentonite suspensions. A schematic of the apparatus is shown in Figure 10.

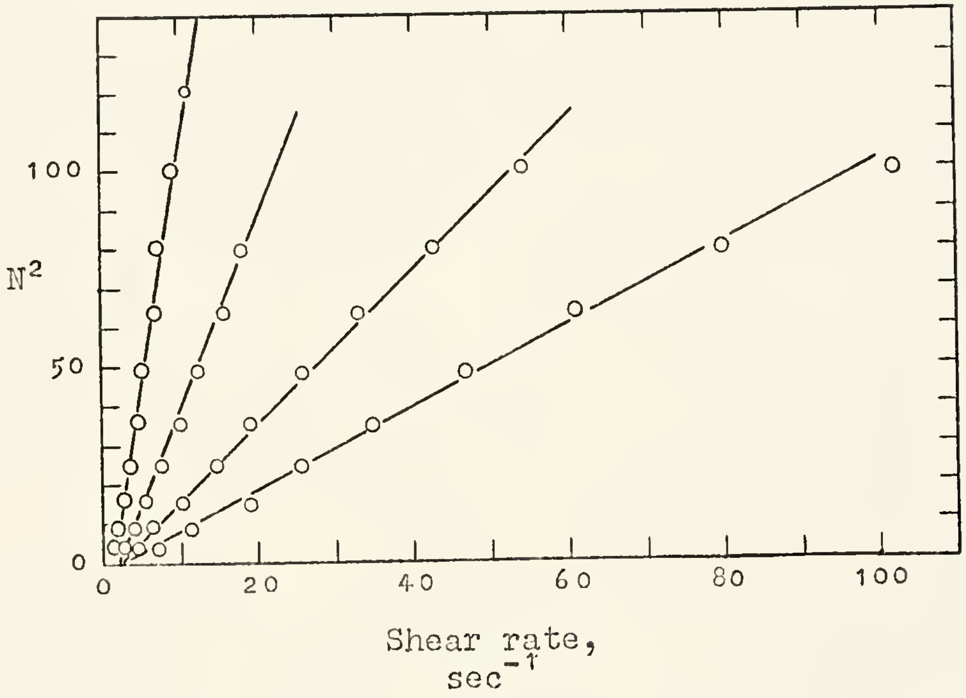

FIGURE 9. Replot of data of Peebles, Prados, and Honeycutt (1965) to show linear relationship between square of fringe order and shear rate. From left to right the concentrations are (weight percent): 1.455, 1.401, 1.363, and 1.358.

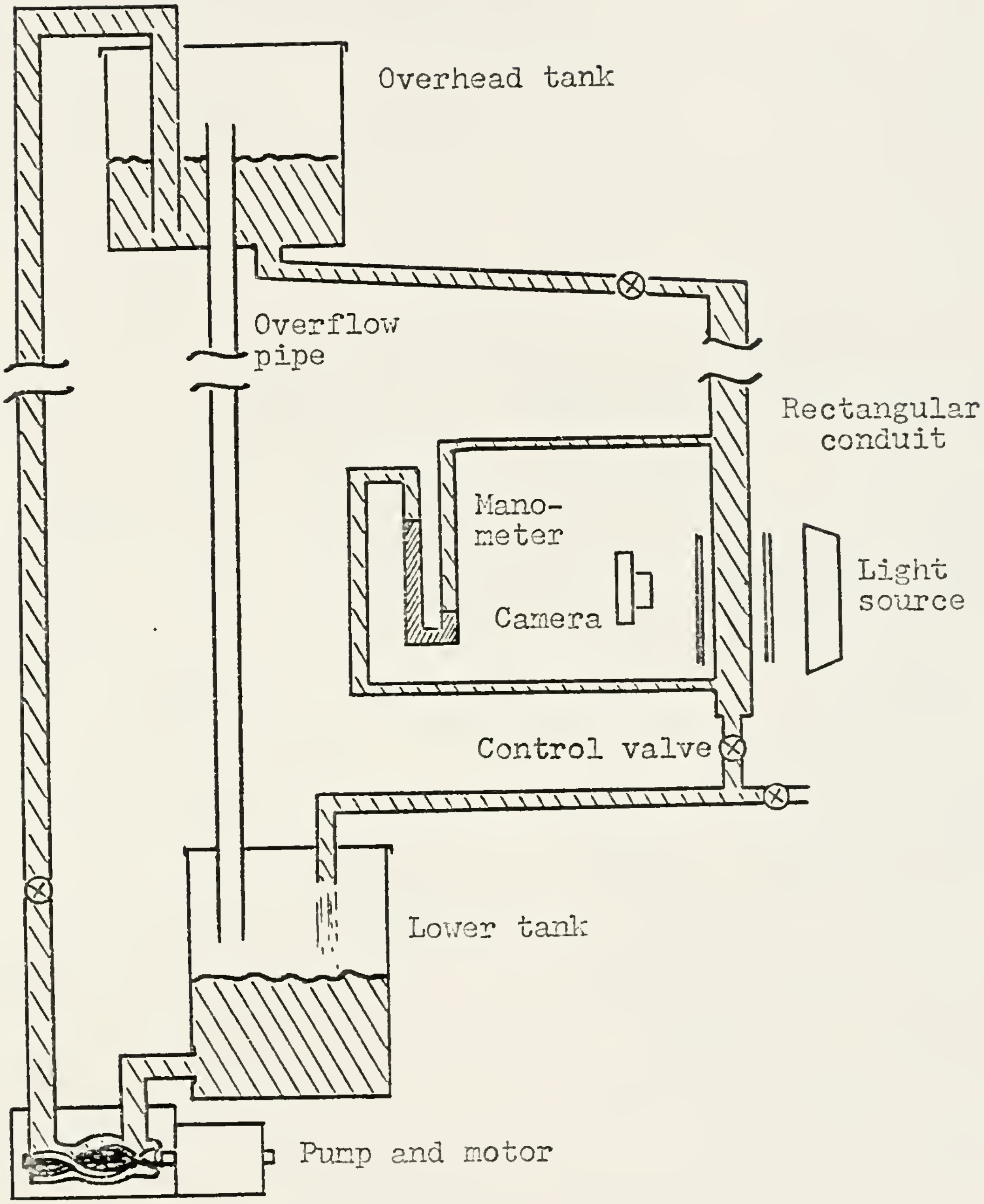

FIGURE 10. Schematic of experimental apparatus. The polarizer and analyzer are represented by vertical lines to the right and left of the rectangular conduit between the light source and the camera.

The Milling Yellow was normally stored in a lower tank which is lined with epoxy-bound fiberglass. From the tank there is a gravity feed into a Moyno EM-2304 special application pump which provides positive displacement with minimum shearing of the fluid.

At intervals, between experimental runs, the stopcock above the pump was opened and the covered, polystyrene, overhead tank was filled. When pumping was complete, normally a matter of seconds, the pump was turned off and the stopcock closed to prevent siphoning through the pump or the introduction of air into the pipe.

The fluid level in the overhead tank can be maintained at a constant head by pumping continuously and permitting the excess fluid to return to the lower tank through an overflow pipe; however, this procedure results in undesirable temperature rises and to the entrainment of air in the Milling Yellow. When it was found that the fluid level in the overhead tank had a negligible effect upon flow rate through the rectangular conduit (see Appendix C), use of the overflow pipe was restricted to providing protection against accidental overfilling of the upper tank.

A gravity feed from the overhead tank leads to a set of parallel, vertical conduits, only one of which was used at a given time. The construction of these conduits is shown in a cut-away view in Figure 11.

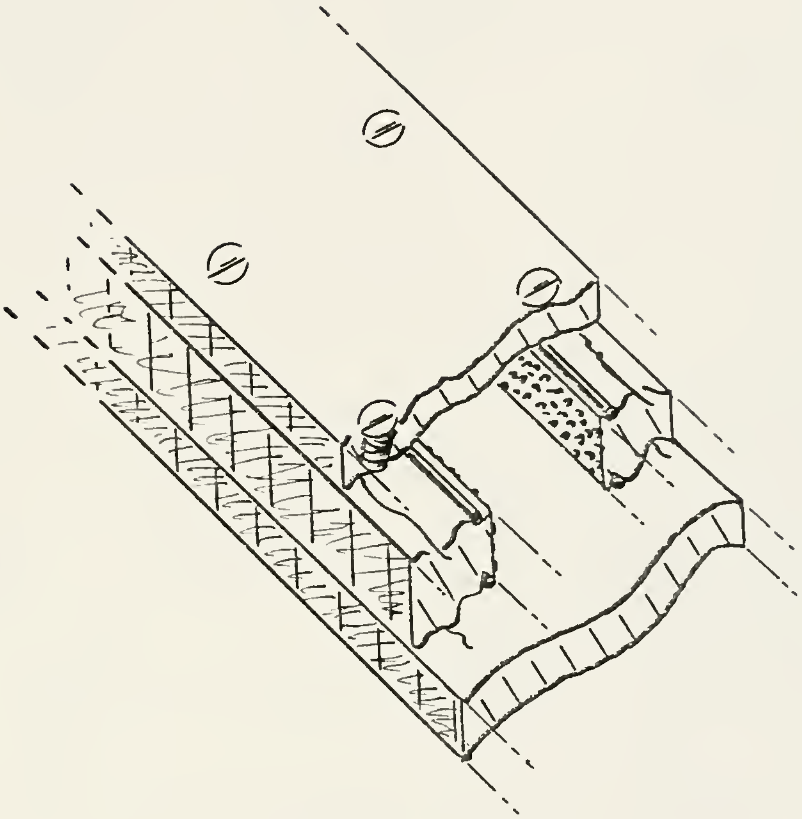

FIGURE 11. Cut-away view of rectangular conduit showing roughened walls, gaskets, and spacing wires.

The nearly square conduits are constructed by sandwiching two square, 12-mm plexiglass rods between two plexiglass strips having widths of 36 mm. Plastic gaskets in V-joints seal the flow channel, and the assembly is bolted together along the length of the conduit. Thin wires run parallel with but outside the gaskets to maintain constant internal dimensions. On certain of the channels two facing surfaces were covered with grinding cloth to provide a known roughness. The conduits are 4.87 meters in length with the internal dimensions shown in Table I.

TABLE I

INTERNAL DIMENSIONS OF CHANNELS (Lindgren, 1963)

Channel Number	Height of Roughness Elements	Distance, mm, between: Strips, $2\delta_1$	Rods, $2\delta_2$
1	Polished plexiglass	13.43	13.26
2	0.035 to 0.044 mm	13.43	12.40
6	0.59 to 0.70 mm	13.42	11.92

Because of the roughness elements, the flow can be viewed through the side walls only in the clear channel, and even in this case the view is unsatisfactory due to the gaskets which prevent a view of flow along the walls. Through the front walls there is an unimpeded view of the flow in all of the channels. Nikuradse (1933) and Moody (1944) found that surface roughness plays no significant role in the laminar flow region, and Lindgren (1963), using the present apparatus, reported no significant difference in flows through tubes with two walls roughened and flows through tubes with four walls roughened when the transition region was studied. Hence, the principal effect of the roughness elements in the present dissertation is the reduction in cross-sectional area which results.

Returning to Figure 10, note that each channel was provided with manometer taps on the smooth-faced sides of the channel. The manometer fluid was carbon tetrachloride (specific gravity: 1.584).

The flow was normally illuminated by a sodium vapor lamp from which light passed through an array of polarizers, through the transparent channel and flow field, and through an array of analyzers. The orientation of the sets of elements in the three array configurations used during the experiments is given in Figure 12 and Table II. The method of alignment is given in Appendix D. On four occasions (runs 45, 418, 419, and 424) the arrays were replaced by circular polarizers differing in phase by $\pi/2$ radians.

The fringes were photographed with an Exacta Varex IIa 35 mm camera with a Jena 58 mm lens. A bayonet extension was manufactured for the lens permitting an object 23 cm from the film plane to be focused upon and photographed. Kodak Tri-X film was used and commercially developed at an

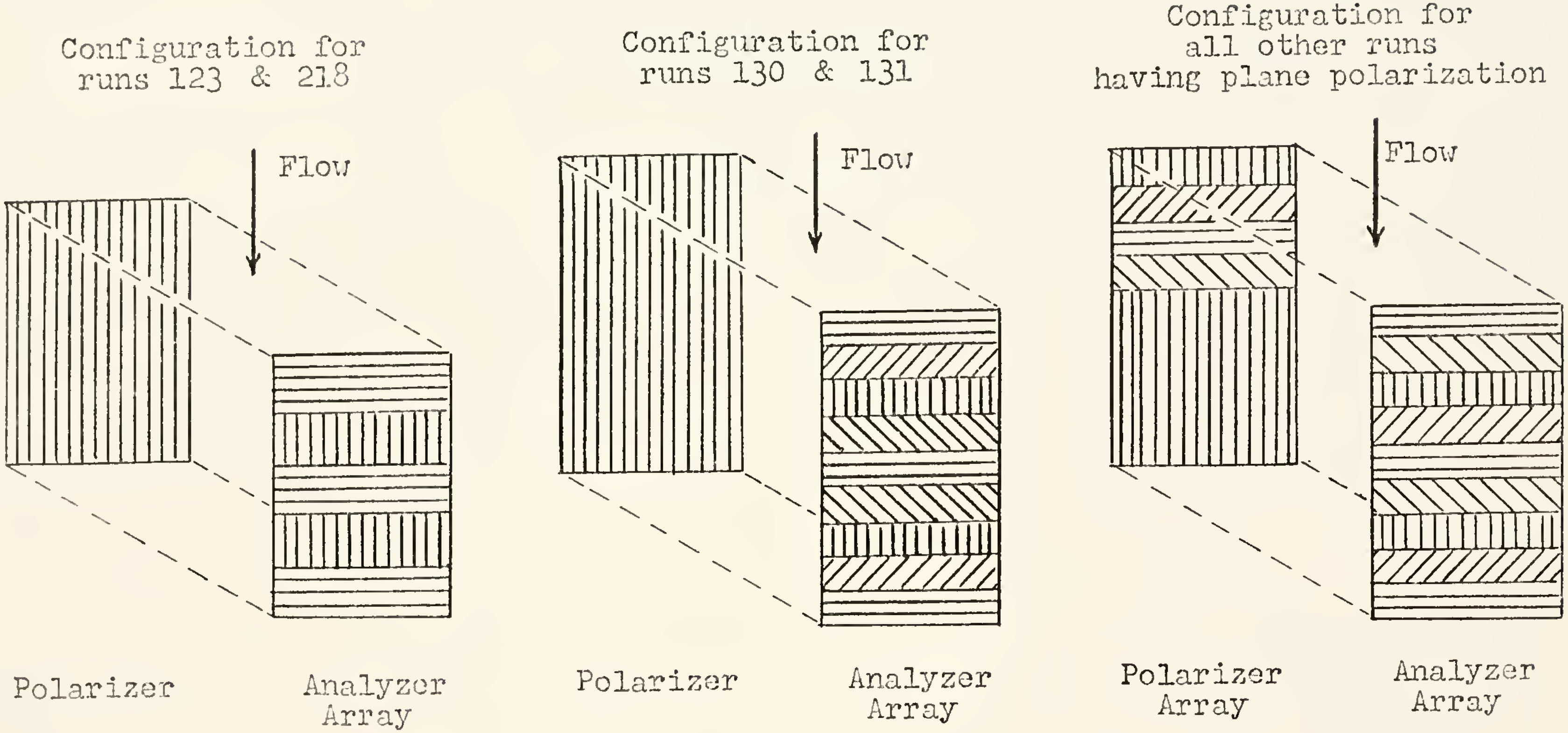

FIGURE 12. Orientation of elements in polarizer and analyzer arrays. The parallel lines indicate the direction for maximum transmission of light.

TABLE II

VALUES OF γ AND γ' FOR SUCCESSIVE ELEMENTS OF POLARIZING ARRAYS

Configuration for
runs 123 & 218

γ	γ'	γ
0	$\pi/2$	$-\pi/2$
0	0	0
0	$\pi/2$	$-\pi/2$
0	0	0
0	$\pi/2$	$-\pi/2$

Configuration for
runs 130 & 131

γ	γ'	γ
0	$\pi/2$	$-\pi/2$
0	$-\pi/4$	$\pi/4$
0	0	0
0	$\pi/4$	$-\pi/4$
0	$\pi/2$	$-\pi/2$
0	$\pi/4$	$-\pi/4$
0	0	0
0	$-\pi/4$	$\pi/4$
0	$\pi/2$	$-\pi/2$

Configuration for
all other runs with
plane-polarized
arrays

γ	γ'	γ
0	$\pi/2$	$-\pi/2$
$-\pi/4$	$\pi/4$	$\pi/2$
$\pi/2$	0	$\pi/2$
$\pi/4$	$-\pi/4$	$-\pi/2$
0	$\pi/2$	$-\pi/2$
0	$\pi/4$	$-\pi/4$
0	0	0
0	$-\pi/4$	$\pi/4$
0	$\pi/2$	$-\pi/2$

---

*Circular polarization used during runs 45, 418, 419, and 424.

equivalent exposure index of ASA 1600. A typical exposure was a lens setting of f3.5 with a shutter speed of 1/150 second.

The choice of flow channels and the rate of flow were controlled by a stopcock at the base of the flow channel. Flow rates were measured by collecting the fluid at the outlet above the lower storage tank and timing the efflux to the nearest 0.1 second with a Junghans timer. In a few instances the efflux volume was measured to the nearest milliliter with a 250-ml graduate, but in general the efflux was caught in a clean, dry vessel and its mass measured on a Harvard Trip Balance to the nearest 0.1 gm. Prior to each weighing the temperature of the efflux was measured to 0.1 C° with an ordinary laboratory thermometer.

Procedure

The fluid was circulated in the system for about twenty minutes to insure uniformity of temperature and concentration between the upper and lower tanks. When this was accomplished, as indicated by constant temperature readings in the lower container, the camera was cocked so that the shutter would release 12 seconds after the preset mechanism was actuated. The lower stopcock was adjusted until the desired flow was obtained as indicated by the birefringent fringe order at the wall of the channel. The efflux container was placed under the fluid outlet and simultaneously the timer was started. After an appropriate interval the preset mechanism on the camera was tripped so as to release the shutter at the midpoint of the efflux interval. The time at which the shutter was heard was noted, and at approximately twice this time the container was removed and the timer stopped. The temperature of the efflux was measured, and the flow rate checked by confirming that the fringe order at the wall remained unchanged. This done, the flow was stopped and the mass of the efflux measured. Finally, the fluid container was cleaned and dried, and the camera and timer readied for the next run. For the last two runs manometer readings were taken just prior to cutting off the flow. As necessary, the overhead tank was refilled.

Prediction of Results

Consider the steady flow of a fluid in a rectangular conduit having dimensions of $2\delta_1$ and $2\delta_2$. A force balance yields

$$(2\delta_1)(2\delta_2)\ dp = \overline{\tau}_W(4\delta_1 + 4\delta_2)\ dL$$

where dp/dL is the pressure gradient along the conduit and $\overline{\tau}_W$ is the average shearing stress along the perimeter. For a Newtonian fluid in a rectangular conduit, Cornish (1928) showed that

$$dp/dL = 2\delta_1\overline{u}\mu_N/\delta_2 S_0$$

where $\overline{u}$ is the mean flow velocity, μ_N is the viscosity, and S_0 is a geometric constant having the dimensions of area:

$$S_0 = \frac{2\delta_1\delta_2}{3} - \frac{128\delta_2^{\,2}}{\pi^5}\sum_{s=1,3..}^{\infty} s^{-5}\tanh(s\pi\delta_1/2\delta_2) .$$

The dimensions δ_1 and δ_2 may be interchanged in the last two equations without affecting anything but the rate of convergence of the series. Numerical values for S_0 are tabulated along with some other constants in Appendix G.

Define the apparent viscosity of a non-Newtonian fluid by

$$\mu_a = (\delta_2 S_0/2\delta_1\bar{u})\ dp/dL.$$

Substitution into the force balance yields

$$\bar{\tau}_w = 2\delta_1^{\,2}\mu_a\bar{u}/S_0(\delta_1+\delta_2).$$

Replacing the average shear stress at the wall by the product of the average shear rate and the average viscosity there,

$$\bar{g}_w = 2\delta_1^{\,2}\mu_a\bar{u}/S_0(\delta_1+\delta_2)\bar{\mu}_w.$$

The viscosity is lowest at the wall where the shear rate is highest. Replacing μ_a by $\bar{\mu}_w - \Delta\mu$, obtain

$$\bar{g}_w = \left[2\delta_1^{\,2}\bar{u}/S_0(\delta_1+\delta_2)\right](1 - \Delta\mu\bar{\mu}_w^{\,-1}).$$

By hypothesis,

$$N^2 = k_1 g + k_2,$$

so at the wall:

$$N_w^{\,2} = \left[2k_1\delta_1^{\,2}\bar{u}/S_0(\delta_1+\delta_2)\right](1-\Delta\mu\bar{\mu}_w^{\,-1}) + k_2 . \qquad (4.1)$$

If, as Peebles and Liu (1965) have shown, the viscosity is nearly constant at low flow rates, $\Delta\mu$ may be neglected and

$$N_w^{\,2} = 2k_1\delta_1^{\,2}\bar{u}/S_0(\delta_1+\delta_2) + k_2.$$

The mass flow rate is

$$G = 4\rho\delta_1\delta_2\overline{u},$$

where ρ is the density, so at low flow rates:

$$N_W^2 = k_1\delta_1 G/2S_0\delta_2\rho(\delta_1+\delta_2) + k_2. \qquad (4.2)$$

As G rises the assumption that $\Delta\mu$ is negligible becomes invalid and the slope, dN_W^2/dG, should decrease.

In the vicinity of the wall the flow approaches two-dimensionality, for which isochromatic fringes will be observed when

$$N_W = \Delta n_W\overline{\delta}/\lambda .$$

Substitution and rearrangement lead to the result

$$\Delta n^2 = \frac{\lambda^2 G k_1}{8\delta_1\delta_2 S_0\ (\delta_1+\delta_2)} + \frac{\lambda^2 k_2}{4\delta_1^{\ 2}}$$

where k_1 and k_2 are to be determined experimentally at the low flow rates for which the relationship is valid.

Experimental Data

Tests of the equation just given were conducted with the results shown in Tables III to XVI and Figures 13 to 16. It will be noted that the temperature varied during these tests.

The run numbers reflect the date in 1973 upon which the data were taken. Run 420A, for example, was the first run conducted on April 20. Run 420D was the fourth run on the same day. Although data were obtained for two other runs, 420B and 420C, these data are not presented because the flow rates were too high for the fringe order at the wall to be accurately determined.

TABLE III

FRINGE ORDER AT WALL — RUN 123

Fringe Order*	Efflux, gm	Time, sec	Flow rate, gm/sec	Temp, °C
2+	1590.8	15.6	102.0	22.0
2	1505.2	15.3	98.4	21.9
1-1/2+	1289.9	18.0	71.7	22.0
1-1/2	1453.2	20.8	69.9	22.3
2-1/2	1076.7	9.6	112.2	21.8
1+	1321.2	29.1	45.4	22.2
1/2+	1436.3	59.9	23.98	22.2
1	1391.5	46.3	30.05	22.1
1/2	1322.1	151.1	8.75	22.2

TABLE IV

FRINGE ORDER AT WALL — RUN 130

Fringe Order*	Efflux, gm	Time, sec	Flow Rate, gm/sec	Temp, °C
1	1115.7	136.2	8.19	20.0
2+	937.0	36.7	25.53	19.7
2	1251.1	45.4	27.56	20.3
3	1032.8	15.8	65.37	20.1

---

*Halved fringe orders were so identified when a fringe occurred at the wall in a light polarizing field (analyzer parallel with polarizer). A plus (+) indicates distinct separation of the fringe from the wall.

TABLE V

FRINGE ORDER AT WALL – RUN 131

Fringe Order*	Efflux, gm	Time, sec	Flow rate, gm/sec	Temp, °C
1	1029.0	39.1	26.32	22.8
2	1555.5	21.6	72.02	22.4
2	765.0	25.2	30.36	21.2
2	826.4	27.5	30.05	21.1
2	678.2	22.6	30.01	21.0
1	695.7	57.3	12.14	–
2+	718.7	18.2	39.49	21.0
3	1493.5	22.5	66.38	21.0
3-1/2	1749.2	14.2	123.18	21.0
3-1/2	1434.6	10.8	132.83	20.8
(+)	395.8	190.5	2.088	20.6
1+	885.0	69.8	12.68	20.6

TABLE VI

ORDER OF RED FRINGE AT WALL – RUN 218

Fringe Order	Efflux, gm	Time, sec	Flow rate, gm/sec	Temp °C
1	199**	35.8	5.56	23.8
2	218**	19.8	11.01	23.9
3	212**	11.7	18.12	22.8
4	1001.2	20.5	48.84	22.3
4(?)	846.2	18.3	46.24	22.2

---

*See note, Tables III-IV.

**Milliliter measurement converted to grams

TABLE VII

FRINGE ORDER AT WALL - RUN 42

Fringe Order	Efflux, gm	Time, sec	Flow rate, gm/sec	Temp, °C
1	20.7	28.1	0.736	24.3
1.5	29.8	22.3	1.337	24.6
2.3	42.1	17.4	2.416	24.7
2.45	108.8	33.7	3.23	24.8
3.5	122.6	30.5	4.02	24.8
4	131.0	25.5	5.14	25.2
5	145.1	23.8	6.10	24.7

TABLE VIII

FRINGE ORDER AT WALL - RUN 44

Fringe Order	Efflux, gm	Time, sec	Flow rate, gm/sec	Temp, °C
2.4	68.3	33.5	2.04	23.8
3	80.8	33.2	2.43	24.2
2.9	80.0	34.1	2.35	24.1
3.2	99.7	33.0	3.02	24.9
1.5	85.3	59.8	1.43	24.7
4	113.3	29.9	3.79	24.7
5	163.35	30.4	5.37	24.3
5.35	130.4	20.0	6.52	24.3
6.4	219.1*	24.0	9.13	24.2

---

*Milliliter measurement converted to grams

TABLE IX

FRINGE ORDER AT WALL – RUN 44A

Fringe Order	Efflux, gm	Time, sec	Flow rate, gm/sec	Temp, °C
1.35	41.7	34.9	1.194	24.7
1.8	57.2	34.8	1.643	24.9
2.2	68.2	29.8	2.288	25.1
2.35	105.4	36.3	2.903	25.2
3.35	66.8	14.8	4.51	25.2
5	132.2	20.4	6.48	25.1
5.5	175.4	20.7	8.47	24.8
6.5	221.1*	17.0	13.01	25.1

TABLE X

FRINGE ORDER AT WALL – RUN 45

Fringe Order**	Efflux, gm	Time, sec	Flow rate, gm/sec	Temp, °C
1	19.3	100.9	0.191	***
2	16.6	55.2	0.301	***
3	52.9	71.1	0.738	20.2
3	56.5	50.3	1.123	20.6
4	66.6	44.7	1.490	20.7
6	90.01	39.4	2.28	20.7
6	109.5	40.2	2.72	20.6
7	110.7	30.1	3.68	20.7

---

*Milliliter measurement converted to grams

**First run with circularly polarized light. Fringe orders controlled more carefully than usual.

***Efflux volume too small for temperature measurement

TABLE X (Continued)

Fringe Order	Efflux, gm	Time, sec	Flow rate, gm/sec	Temp, °C
7	153.9	29.4	5.23	20.8
10	211.1*	26.4	7.99	20.8
11	272.4*	18.2	14.96	20.4

TABLE XI

FRINGE ORDER AT WALL – RUN 418

Fringe Order	Efflux, gm	Time, sec	Flow rate, gm/sec	Temp, °C
1.27	65.7	44.0	1.49	24.7
2	92.6	36.1	3.90	24.8
2.25	110.4	25.5	4.33	24.8
3	134.5	22.8	5.90	24.9
3.32	158.0	20.2	7.82	24.8
3.46	156.0	17.4	8.97	24.7
4.3	166.1	15.2	10.93	24.6
5.0	181.0	13.7	13.21	24.7
5.6	188.7	11.3	16.70	24.8
6	222.4	10.3	21.59	24.8

---

*Milliliter measurement converted to grams

TABLE XII

FRINGE ORDER AT WALL – RUN 419

Fringe Order	Efflux, gm	Time, sec	Flow rate, gm/sec	Temp, °C
1	47.1	60.2	0.78	23.7
1.7	128.9	60.0	2.15	23.8
2.0	124.3	39.7	3.13	24.1
2.35	94.2	21.9	4.30	24.2
3.28	124.5	20.0	6.23	24.2
3.50	135.9	19.7	6.90	24.2
4.30	157.2	18.1	8.69	24.1
5.0	168.6	15.9	10.60	24.1
6.0	149.4	11.6	12.88	24.1

TABLE XIII

FRINGE ORDER AT WALL – RUN 420A

Fringe Order	Efflux, gm	Time, sec	Flow rate, gm/sec	Temp, °C
1.45	109.7	60.0	1.83	23.2
2	55.7	20.4	2.73	23.4
2.36	73.1	20.0	3.66	23.8
3.1	100.7	19.7	5.11	23.8
3.4	128.0	19.7	6.50	23.8
4.2	118.3	16.1	7.35	23.7
4.3	175.7	21.4	8.21	23.7
5.1	159.7	16.1	9.92	23.8
5.6	192.5	15.8	12.18	23.8
6.3	167.3	11.2	14.94	23.8

TABLE XIV

FRINGE ORDER AT WALL - RUN 420D

Fringe Order	Efflux, gm	Time, sec	Flow rate, gm/sec	Temp, °C
1.28	83.6	35.8	2.34	25.5
2.22	127.7	22.5	5.67	25.5
3.3	154.7	15.9	9.73	25.5
4.5	191.2	12.1	15.80	25.5
5.4	165.75	8.3	19.97	25.5
6.6	185.22	6.4	28.94	25.5
7.8	189.4	4.8	39.46	25.3

TABLE XV

FRINGE ORDER AT WALL - RUN 424

Fringe Order	Efflux, gm	Time, sec	Flow rate, gm/sec	Temp, °C
2.1	100.7	40.2	2.50	24.9
3.3	163.7	29.6	5.53	25.3
4.3	128.1	20.2	6.34	24.4
5.4	184.6	20.3	9.09	24.3
6.0	188.5	14.7	12.82	24.3
7	211.9	10.2	20.78	24.5
8	199.5	7.8	25.57	24.2

TABLE XVI

FRINGE ORDER AT WALL - RUN 425

Fringe Order	Efflux, gm	Time, sec	Flow rate, gm/sec	Temp, °C
1.58	99.8	50.1	1.99	24.2
2.26	141.0	40.3	3.50	24.2
2.43	146.0	40.5	3.60	23.8
3.6	141.6	24.8	5.71	23.8
4.4	153.3	19.7	7.78	23.8
6	175.2	14.2	12.34	23.8
7	185.6	11.4	16.00	23.8

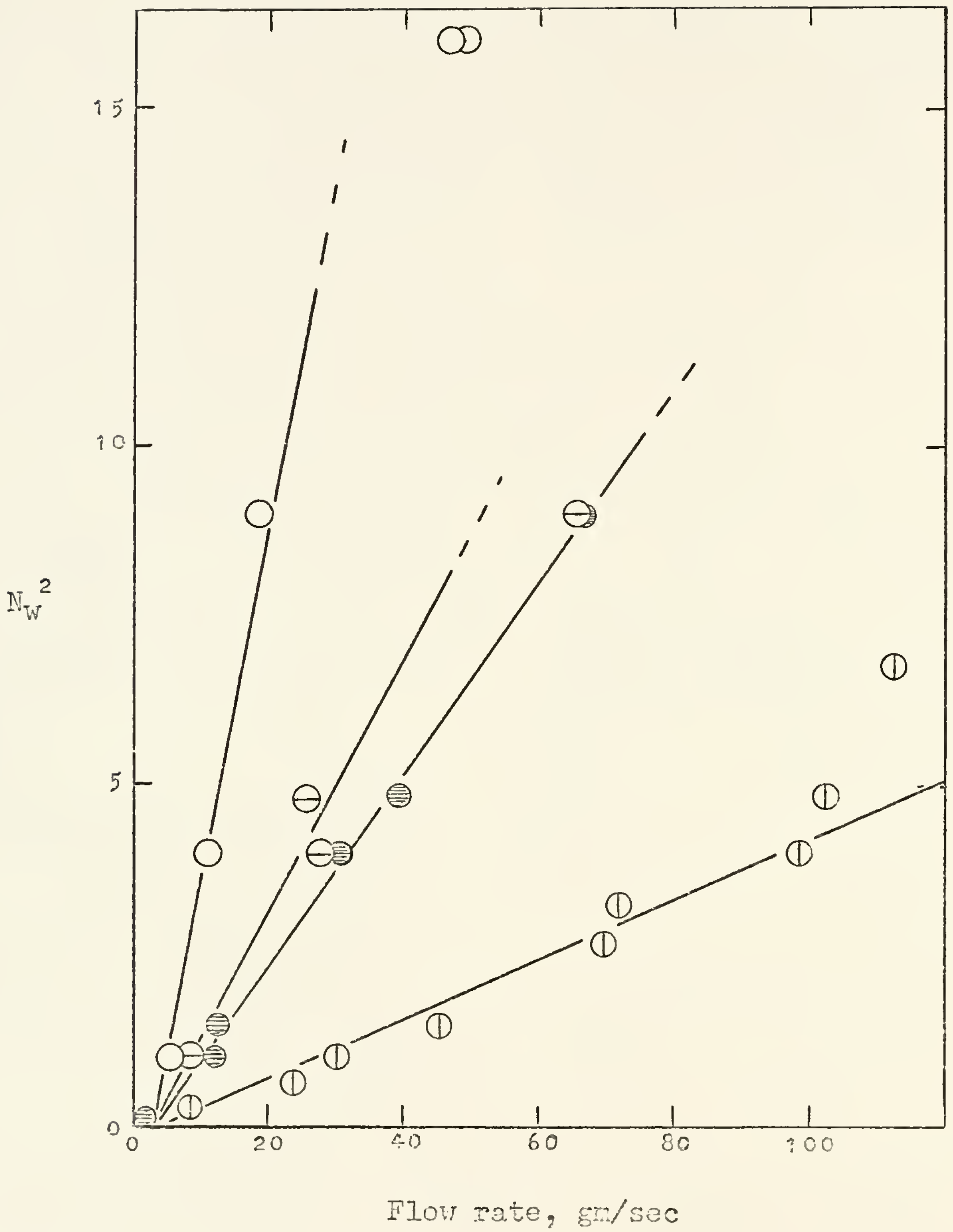

FIGURE 13. Fringe order at wall as function of mass flow rate. Runs:-⦶-123;-⊜-131;-⊖-130;-○-218.

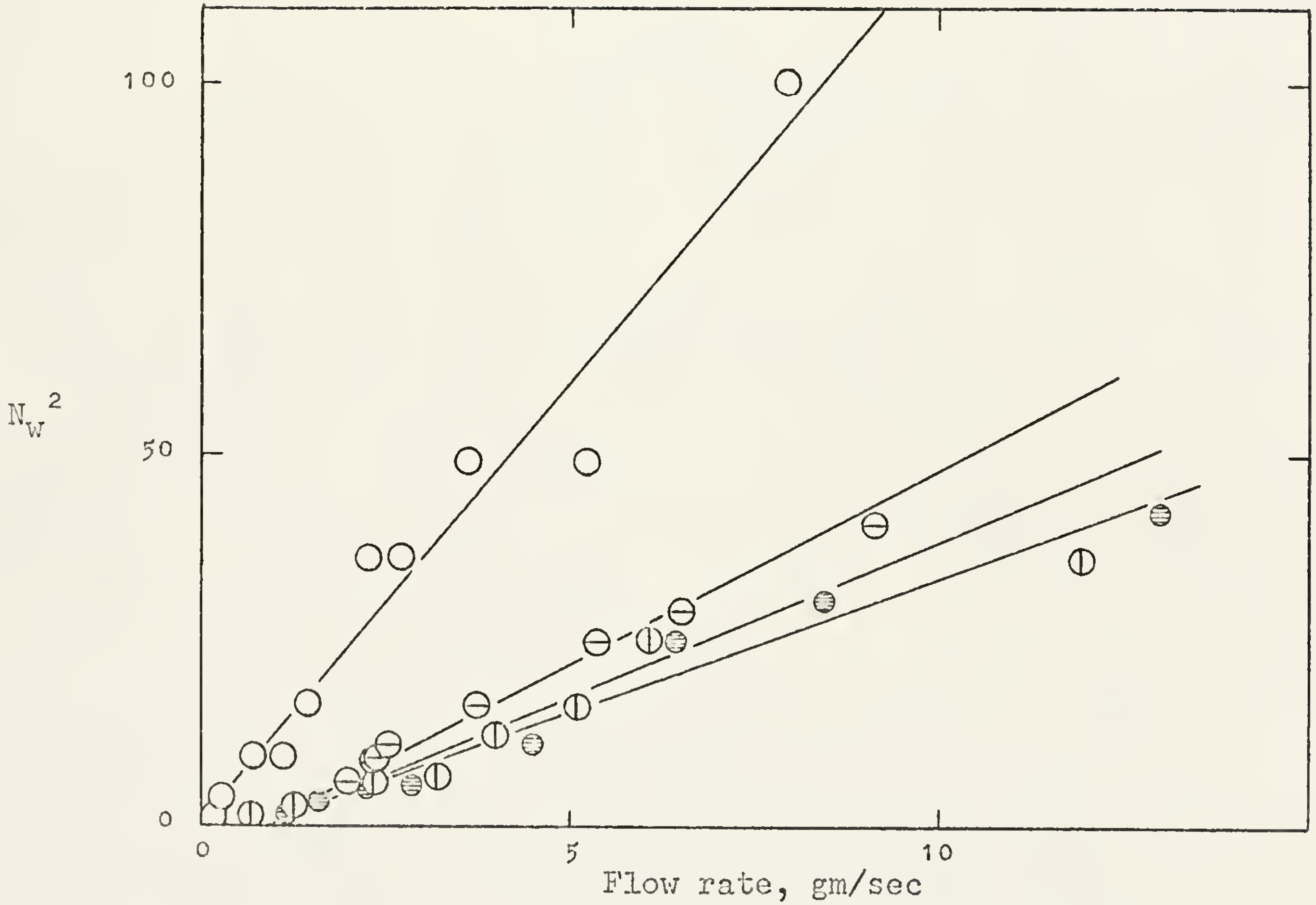

FIGURE 14. Fringe order at wall as function of mass flow rate. Runs: ⦶ 42; ⊖ 44; ⊜ 44A; ○ 45.

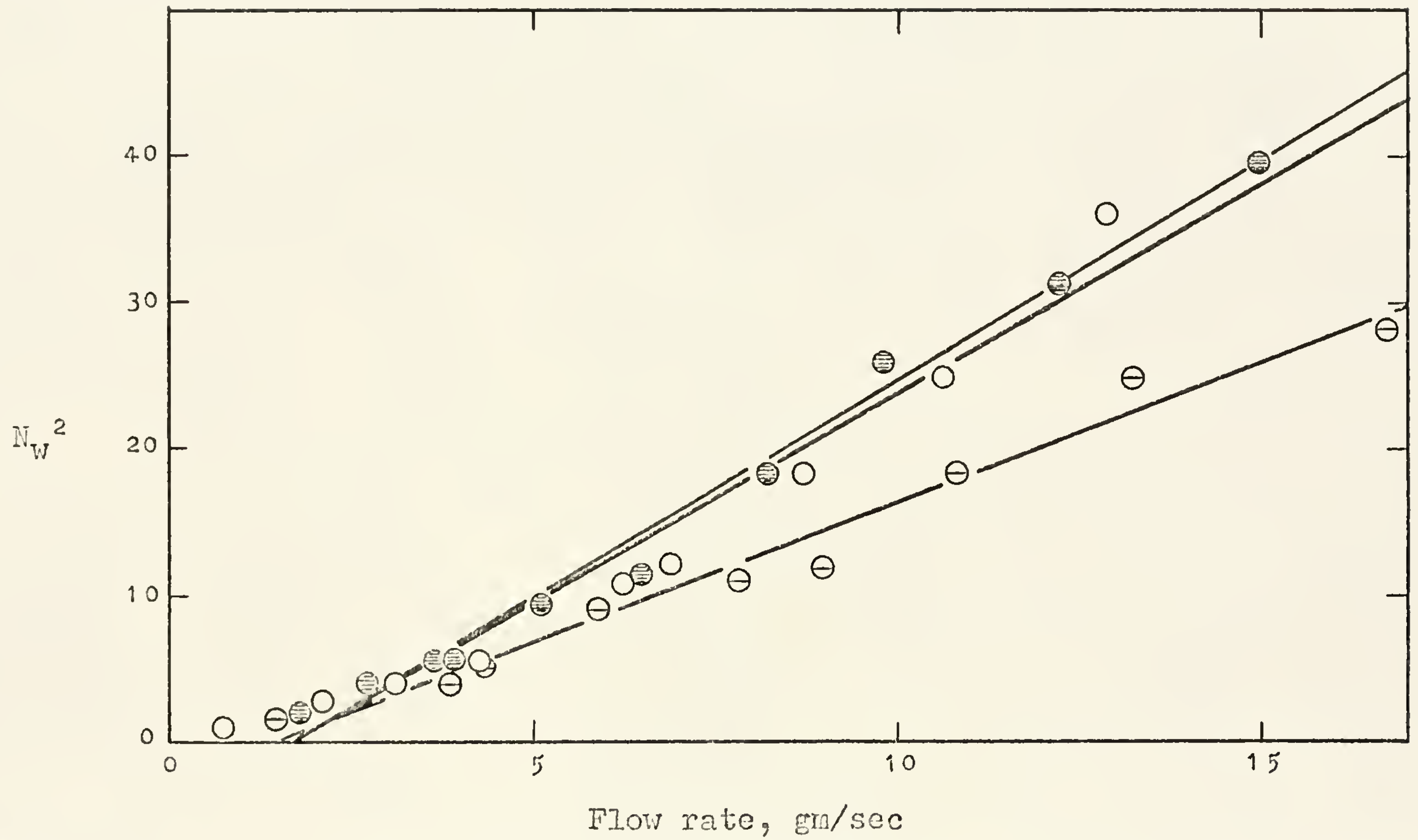

FIGURE 15. Fringe order at wall as function of mass flow rate. Runs: ⊖ 418; ○ 419; ⊜ 420A.

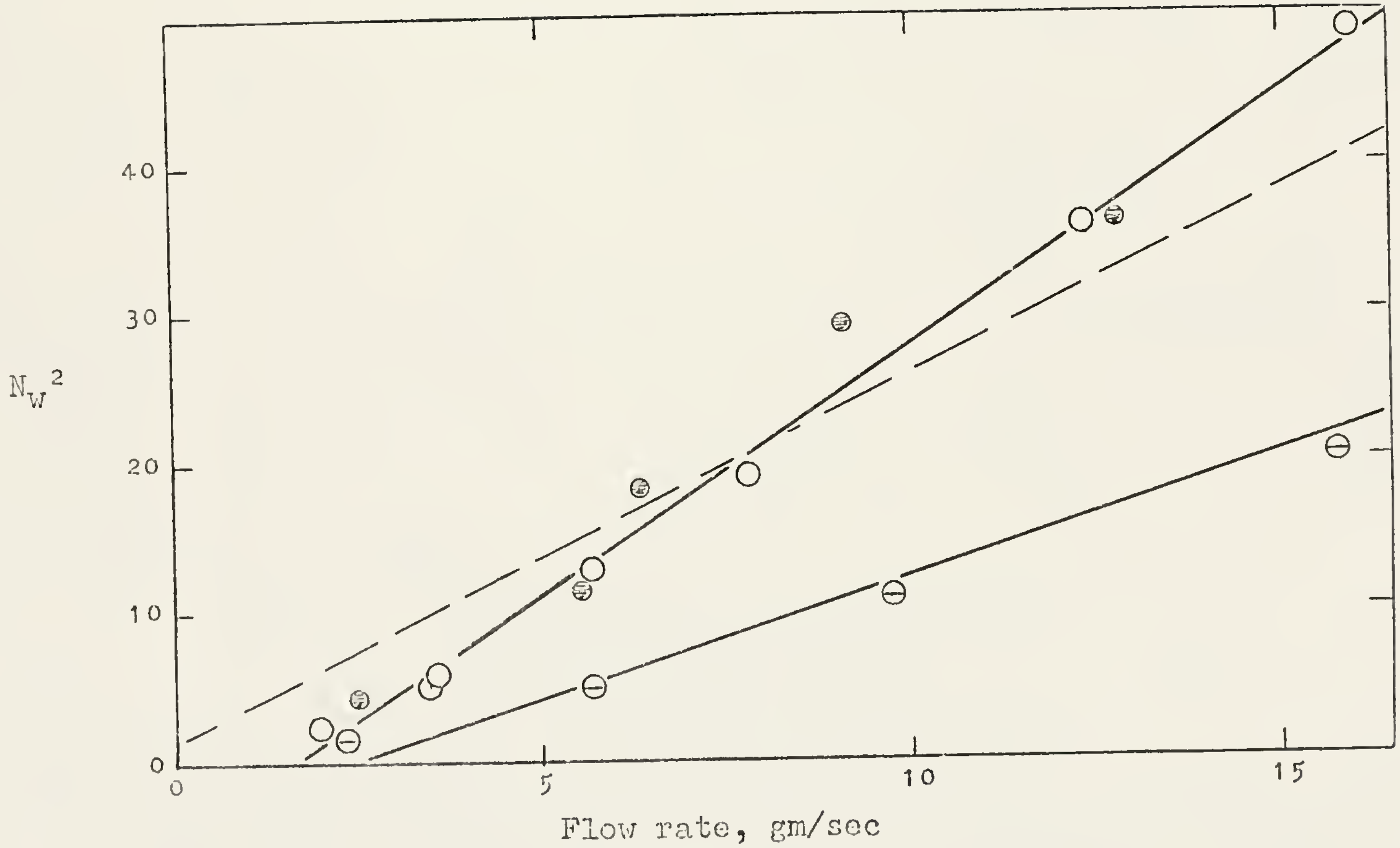

FIGURE 16. Fringe order at wall as function of mass flow rate. Runs: ⊖ 420D; ⊜ 424; ○ 425. If high flow rates are included (run 424), dashed line is result.

Discussion of Results

This discussion is in three parts. The first describes the preliminary testing used to determine the feasibility of the method. The second part describes the manner in which the data were interpreted. The last part gives the numerical values which were obtained for the optical coefficients used to calculate the birefringence.

Preliminary tests

The objective of these tests was to check the working order of the apparatus, refine the measurement technique, and confirm the validity of the form of equation (4.2). These objectives were largely fulfilled.

Run 123 was conducted in channel 6. The data for this run may be represented by a straight line when plotted as shown in Figure 13. There is an upward departure suggested by the last datum which is at odds with the falling off predicted by equation (4.1). The upward departure may be due to temperature.

Run 130 was also conducted in channel 6. No firm conclusions are possible from these few data except that the birefringence is higher than in the previous test, a result consistent with the lower mean temperature and a concentration increase due to evaporation.

Run 131 was conducted in channel 2. The data are well represented by a straight line at low flow rates and fall off, as predicted, as the flow rate increases.

Run 218 was conducted in channel 6 in white light. This was the only run in either the preliminary or the final test series in which the sodium vapor lamp was not used for illumination. Two sets of isochromatic fringes were observed, one red and the other green. Other wavelengths were hard to detect either because they were strongly absorbed by the medium or because of their similarity to the deep orange of Milling Yellow. The data plotted in Figure 13 are those from the red set of fringes. The data are too few to serve as a test of equation (4.2).

In general the preliminary tests support the analysis which predicted that the square of the fringe order would vary linearly with the mass flow rate.

Interpretation of data

If a dark polarizing field is defined as one in which polarizer and analyzer are at right angles ($\Delta\gamma = \frac{\pi}{2}$ in Table II), then it is evident that two different dark polarizing fields were used in the final testing. Associate those sets in which either the polarizer or the analyzer is parallel with the principal flow direction ($\gamma = 0$ or $\gamma' = 0$) with "parallel" fields and associate those in which both analyzer and polarizer are oriented across the flow lines ($\gamma = \pm \frac{\pi}{4}$; $\gamma' = \mp \frac{\pi}{4}$) with "crossed" fields. In the preliminary tests the dark fields were of the parallel type only.

The equation describing the emergent electric field in two-dimensional flows when $\Delta\gamma = \frac{\pi}{2}$ was given in Chapter Three as:

$$E_e = \bar{E}_0 \sin(\pi\bar{\delta}\Delta n/\lambda) \sin 2(\gamma-\psi).$$

This relationship predicts that the periodic fringe patterns will be the same for all dark polarizing fields, but that the magnitude of the emergent field will decrease progressively as the polarizer and analyzer become more and more nearly parallel with the optic axes. The latter prediction is well supported by photographs of the fringe patterns. At low flow rates, when all theories and measurements predict orientation angles near $\pi/4$ radians (see Jerrard, 1959, for examples), the crossed field is dark with diffuse fringes, while the parallel field is light with broad, lower-order fringes standing out in sharp contrast to their background. At higher rates of flow a lowered orientation angle results in a darkened parallel field, while the fringes of the crossed field are sharp and clear.

The prediction of the two-dimensional theory that the phase of the fringe pattern is independent of the orientation of the dark field is not supported by the photographic evidence. The fringe pattern in the crossed field differs by half a fringe order from its parallel counterpart. This is not surprising, since the orientation of the polarizing field cannot be neglected in the three-dimensional flow which is actually present.

This raises two questions, one theoretical and one practical. The theoretical question is: "Can equation (4.2), which postulates two-dimensionality at the wall, be used to describe a three-dimensional flow field?" To this question the answer, based upon the data, is: "Yes, provided that an error of ± 1/2 fringe is permissible, since that seems to be the maximum deviation for the two extreme orientations." The practical question is: "Given two sets of "dark field" patterns, which should be used to calculate the birefringence?" The answer is: "Whichever can be read with the greater precision."

With these considerations in mind, an error of 1/2 fringe has been accepted in the calculation of the birefringence, and the crossed field has been chosen to provide the data since the only fringes which are not clear in that field are those of the first and second order which are too broad for accurate dtermination in any field. In circularly polarized light, of course, only one set of fringes is observed and a choice of patterns is avoided.

To the 1/2-fringe bias introduced by the choice of a polarizing field must be added the experimental deviation of the measurements themselves. From equation (4.2):

$$k_1 = \left[2\delta_2(\delta_1+\delta_2)S_0\rho/\delta_1\right] d(N_W{}^2)/dG.$$

Since S_0 is an explicit function of δ_1 and δ_2, the independent variables are δ_1, δ_2, ρ, and the experimentally determined slope $d(N_W{}^2)/dG$. Since the four variables are independent, it follows that (e.g. Deming, 1964, p. 40) the variance in k_1 is

$$\sigma^2(k_1) = \sum_{S=1}^{4}\left(\frac{\partial k_1}{\partial X_S}\right)^2 \sigma^2(X_S)$$

where $\sigma^2(X_s)$ designates the variance of the s^{th} independent variable X_s. It is evident that the relative variance $\sigma^2(X_s)/X_s$ of the slope defined by

$$k_1' = d(N_w^2)/dG$$

is much larger than the relative variance of the other variables. That is,

$$\frac{\sigma^2(k_1')}{k_1'} \gg \frac{\sigma^2(X_s)}{X_s} . \qquad (k_1' \neq X_s)$$

If this assumption is valid, then

$$\sigma^2(k_1) = \left[\frac{\partial k_1}{\partial(k_1')}\right]^2 \sigma^2(k_1')$$

to a good approximation.

If k_1' is obtained from the data by the method of least squares, then according to linear regression theory (see, for example, Volk, 1969) the estimated variance of k_1' is:

$$s^2(k_1') = s^2(\overline{N}_w^2)/\Sigma' G^2 ,$$

$$= \left[\Sigma'(N_w^2) - k_1'\Sigma' GN_w^2\right]/(N_p - 2)\Sigma' G^2$$

where $s^2(\overline{N}_w^2)$ is the estimated variance of the value of N_w^2 at G predicted by the straight-line approximation and:

$$\Sigma' G^2 = \Sigma G^2 - (\Sigma G)^2/N_p ,$$

$$\Sigma' GN_w^2 = \Sigma(GN_w^2) - (\Sigma G)(\Sigma N_w^2)/N_p ,$$

$$\Sigma' N_w^2 = (\Sigma N_w^2)^2 - \left[\Sigma(N_w^2)\right]^2/N_p .$$

Summations are for the N_p pairs of data (N_w^2, G) upon which the least squares analysis was performed.

The estimated variance $s^2(k_1')$ is based upon the dispersion in the data about the straight lines in Figures 13 to 16. The half-fringe variation introduced by the arbitrary choice of a polarizing field may be presumed to have a systematic bias and must be added separately. This may be done by increasing the variance of the estimate $s^2(\overline{N}_W{}^2)$ by $(1/2)^2$. There results:

$$s^2(k_1') \quad = \quad \frac{\Sigma'(N_W{}^2) - k_1'\Sigma' GN_W{}^2 + (1/2)^2(N_p-2)}{(N_p-2)\Sigma' G^2} \;.$$

Neglecting the relative variances of the other variables,

$$s^2(k_1) \quad = \quad (k_1/k_1')\ s^2(k_1'),$$

as assumed earlier.

The estimated variance of k_2 can be obtained immediately. Since k_2 is the predicted value of $N_W{}^2$ when the flow rate is zero, the estimated variance of k_2 is the same as that of $\overline{N}_W{}^2$ increased by the systematic bias of $(1/2)^2$:

$$\begin{aligned} s^2(k_2) \quad &= \quad s^2(\overline{N}_W{}^2) + (1/2)^2 \\ &= \quad \frac{\Sigma'(N_W{}^2) - k_1'\Sigma' GN_W{}^2 + (1/2)^2(N_p-2)}{(N_p-2)} \;. \end{aligned}$$

Recalling that

$$N^2 \quad = \quad k_1 g + k_2$$

by hypothesis, and

$$N \quad = \quad \Delta n\overline{\delta}/\lambda,$$

where, in this case, $\overline{\delta} = 2\delta_1$, the variance of the birefringence will be proportional to the variances of the respective coefficients in the defining equation:

$$\Delta n^2 = (\lambda^2 k_1/4\delta_1{}^2)\ g + (\lambda^2 k_2/4\delta_1{}^2)$$

if variations in λ and δ_1 are neglected.

Computation of optical coefficients

The optical coefficients k_1, k_2, $(\lambda^2 k_1/4\delta_1{}^2)$, and $(\lambda^2 k_2/4\delta_1{}^2)$ have been defined in the preceding paragraphs. Values for these constants and their deviations are provided in Tables XVII and XVIII, and the corresponding birefringences are plotted in Figures 17 and 18. Figure 17 also includes an extrapolation of some of the data of Peebles, Prados, and Honeycutt (1965).

As indicated in Appendix B, two stock solutions of Milling Yellow were prepared. The data in Table XVII and Figure 17 are for the original stock solution which was prepared in April 1972. The concentrations cited in the plot were obtained by drying samples and weighing the residue as described in Appendix L. The effect of temperature upon the data is particularly evident in Figure 17 where testing occurred over a short enough time period so that the concentration of the solution did not change greatly. It is presumed that the higher birefringence of the less concentrated solution of Peebles, Prados, and Honeycutt is due to a different proportion of inorganic salts in the commercial dye.

The data in Table XVIII and Figure 18 are for the fresh stock solution prepared in March 1973. The tests were conducted soon after the solution was prepared, and

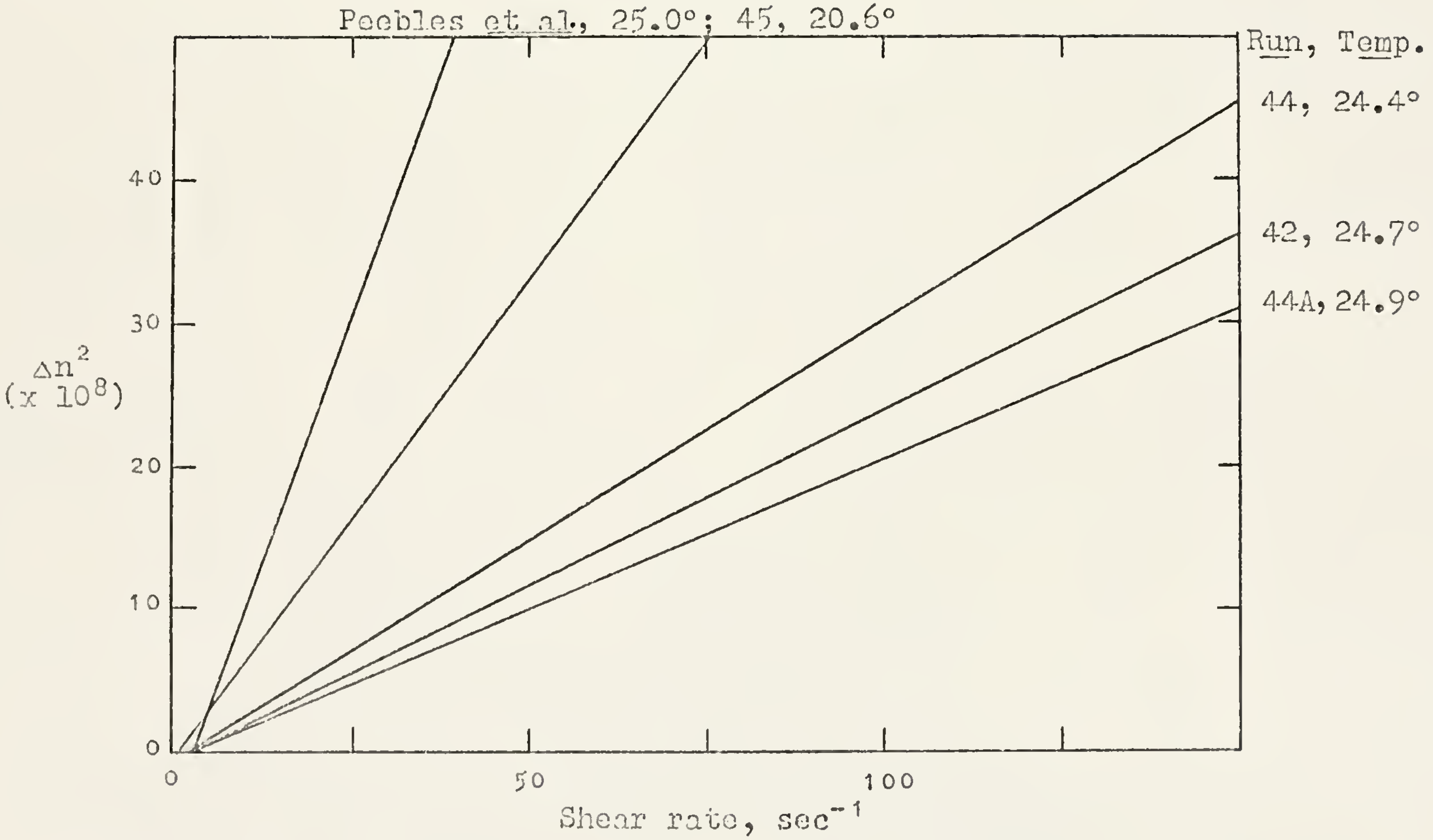

FIGURE 17. Birefringence of original stock solution compared with an extrapolation of the data of Peebles, Prados, and Honeycutt (1965). Concentrations: original stock, 1.53%; Peebles et al, 1.455 %. The mean temperature for each run has been indicated in the margin.

TABLE XVII

BIREFRINGENT CONSTANTS FOR RUNS 42, 44, 44A, AND 45 (ORIGINAL STOCK SOLUTION)

Run	Channel	Temp, °C	k_1	k_2	$\lambda^2 k_1/4\delta_1^2$ (x 10^8)*	$\lambda^2 k_2/4\delta_1^2$ (x 10^8)*
42	2	24.70 ± 0.26	1.282 ± .150	-4.22 ± 2.57	.246 ± .029	-.81 ± .49
44	2	24.31 ± 0.30	1.597 ± .075	-4.59 ± 1.15	.307 ± .014	-.88 ± .22
44A	6	24.91 ± 0.23	1.043 ± .067	-3.00 ± 2.53	.201 ± .013	-.58 ± .49
45	6	20.62 ± 0.19	3.417 ± .251	0.04 ± 6.55	.659 ± .048	.01 ± 1.26

*$\lambda = 5.892 \times 10^{-5}$ cm

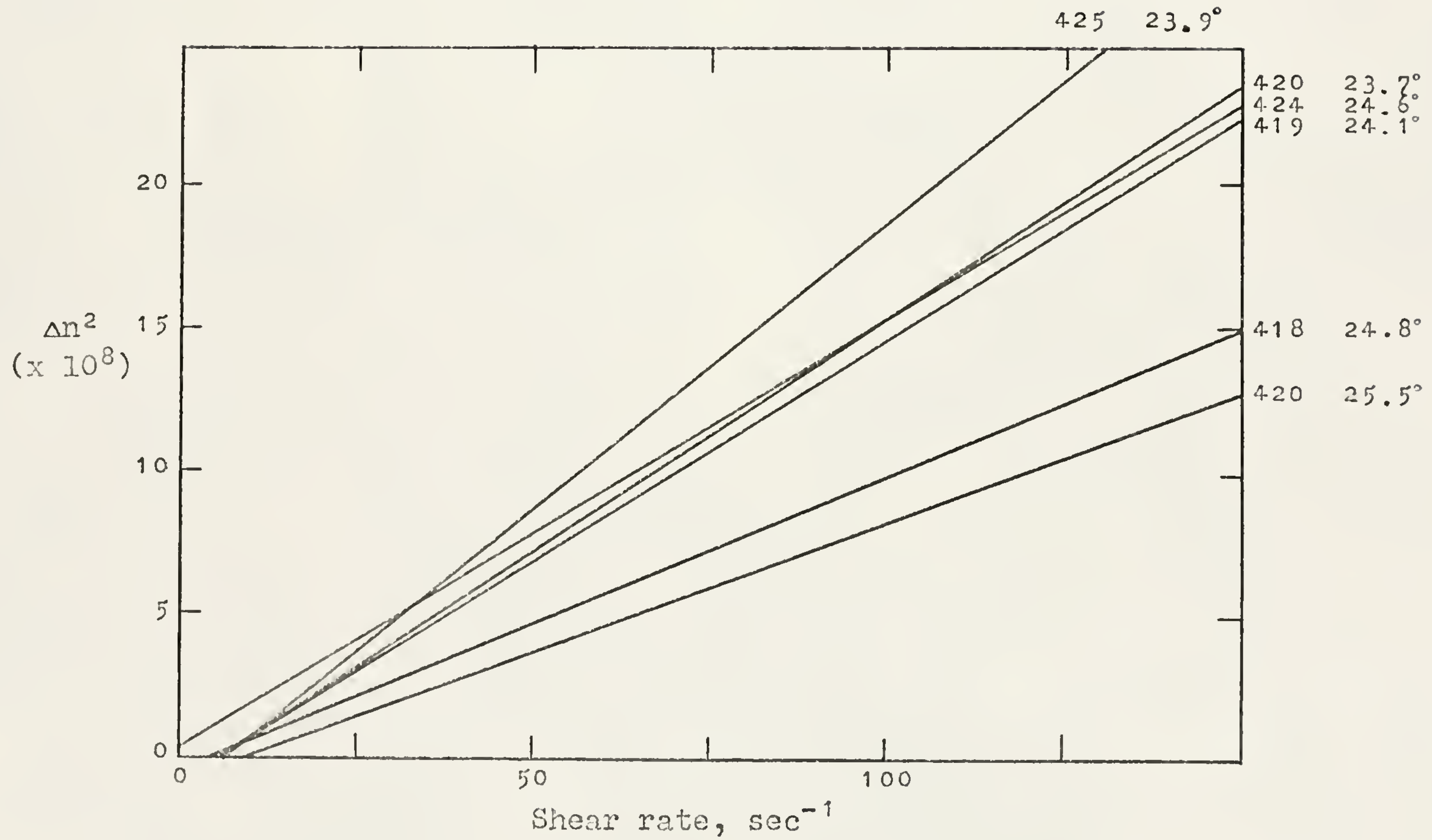

FIGURE 18. Birefringence of fresh stock solution. Concentrations: 418, 1.70 %; 419, 1.72 %; 420A and 420D, 1.75 %; 424, 1.72 %; 425, 1.70 %. The mean temperature for each run has been indicated on the margin.

TABLE XVIII

BIREFRINGENT CONSTANTS FOR RUNS 418, 419, 420A, 420D, 424, AND 425
(FRESH STOCK SOLUTION)

Run	Channel	Temp, °C	k_1	k_2	$\lambda^2 k_1/4\delta_1{}^2$ $(\times 10^8)$*	$\lambda^2 k_2/4\delta_1{}^2$ $(\times 10^8)$*
418	6	24.76 ± 0.13	0.543 ± .035	-2.77 ± 1.67	.105 ± .007	-.53 ± 0.32
419	6	24.06 ± 0.13	0.808 ± .670	-4.65 ± 2.68	.156 ± .129	-.90 ± 0.52
420A	6	23.69 ± 0.20	0.849 ± .030	-5.08 ± 1.42	.164 ± .006	-.98 ± 0.27
420D	6	25.47 ± 0.40	0.465 ± .012	-3.98 ± 1.41	.090 ± .002	-.77 ± 0.27
424	1	24.56 ± 0.40	0.825 ± .087	1.61 ± 5.43	.158 ± .017	.31 ± 1.04
425	1	23.91 ± 0.20	1.144 ± .031	-6.07 ± 1.16	.220 ± .006	-1.17 ± 0.22

---

*$\lambda = 5.892 \times 10^{-5}$ cm

day by day changes in the properties of the medium can still be observed. The birefringence plotted in Figure 18 shows simultaneous increases from run to run due to drops in temperature and to changes in the composition of the medium. For a further discussion of the stability of the solution and changes with time, see Appendix H.

Orientation Angle

In this dissertation the isoclinic fringe pattern in two-dimensional flow fields has been defined in terms of the orientation angle ψ, which is the angle between the principal flow axis and $\hat{n}_1$, the "fast" optical axis. The orientation angle, rather than the more familiar extinction angle χ, was chosen because the latter variable is defined only in two-dimensional fields when the polarizer and analyzer are at right angles. The relationship between the orientation angle and the extinction angle has been given previously at the end of the section on two-dimensional flows in Chapter Three. Recall that when χ is defined it has the value:

$$\chi = \begin{cases} |\gamma - \psi| & |\gamma - \psi| \leqslant \frac{\pi}{4} \\ \frac{\pi}{2} - |\gamma - \psi| & |\gamma - \psi| > \frac{\pi}{4} \end{cases}$$

When ψ is known, χ can be determined immediately by this relationship.

Assumption of Form

The orientation angle (extinction angle) of Milling Yellow at various shear rates was not measured in the present dissertation. Peebles, Prados, and Honeycutt (1965) found that the extinction angle decreased from 45° at zero shear rates to an asymptotic value in the vicinity of 20° at higher shear rates. Although it is probably coincidental, Taylor (1969) obtained 19.5° as the maximum inclination of a long rod falling in a viscous fluid. There may exist some model which relates these two numbers since the hydrodynamics of flows around rods and ellipsoids is a common basis for theories of birefringence, but no such claim is made here. Rather, the value of 19.5° is adopted in the absence of a better claim by some other value in the same experimental range.

Although Peebles, Prados, and Honeycutt did not choose an empirical form for their data, it appears that the equations

$$\tan 2\chi \quad = \quad \tan 2\chi_{\infty} \; + kTg^{-1}$$

or

$$\tan 2\psi \quad = \quad \tan 2\psi_{\infty} \; + k_{\psi}Tg^{-1}$$

describe them reasonably well as shown in Figure 19. This form was derived by Tsvetkov (1951) for the extinction angle of deformable, anisotropic, molecular ellipsoids which entrap their solvent. Acceptance of the Tsvetkov form is based upon its convenience and not the model; however, the Tsvetkov model is consistent with the possibility mentioned in Chapter Two that Milling Yellow has a lyotropic mesophase.

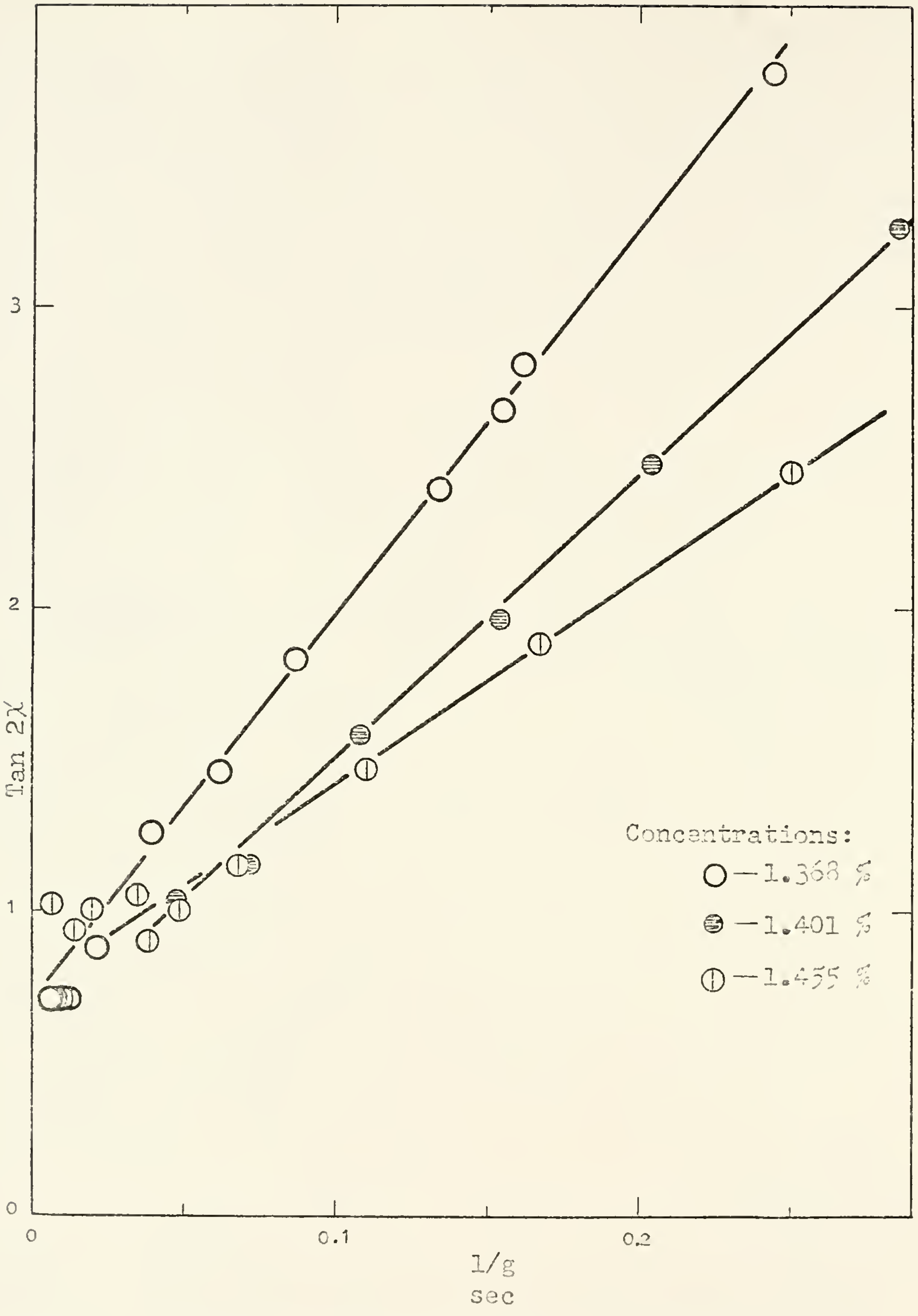

FIGURE 19. Extinction angles measured by Peebles, Prados, and Honeycutt (1965) replotted to obtain straight lines.

CHAPTER FIVE

DETERMINATION OF RHEOLOGICAL PROPERTIES

This chapter discusses the method by which the rheological properties of Milling Yellow were measured. The chapter is divided into five parts. The first discusses empiricism in rheological formulations and concludes with an equation using two constants which satisfies data reported by Pebblès, Prados, and Honeycutt (1965) in three-constant form. The second part of the chapter analyzes the Höppler Rheo-Viscometer, an instrument generally considered unsuited for the measurement of basic rheological constants. The third part tabulates the data obtained with the Rheo-Viscometer. The fourth part utilizes these data to construct a functional relationship between shear stress and shear rate in Milling Yellow. The fifth and final part considers the range of shear stresses for which the constructed relationship is valid.

Empiricism in Rheological Formulations

The late Professor Isadore Amdur once enlivened a particularly abstruse derivation of a thermodynamic relationship with the comment:*

---

*I. Amdur, Physical Chemistry Lectures, Massachusetts Institute of Technology, Cambridge, Massachusetts, Spring, 1955

> Gentlemen, you expect science to be simple. You are mistaken. It is not science, but scientists, who are simple.

The rheological behavior of Milling Yellow is not simple. As the review in Chapter Two indicates, neither continuum mechanics nor the methods of analytic model construction are able to provide useful constitutive relationships which can be applied to the solution of practical problems. In their absence an empirical approach becomes necessary, but such an approach must be provided with sufficient justification not to fly in the face of established principles. Perhaps a reasonable compromise is represented by the so-called Stokesian fluid. The discussion which follows is taken in large part from Frederickson (1964, pp. 68-89).

Consider an incompressible Stokesian fluid as defined by the constitutive relationship

$$\tau_{ij} = \tau_{ij}(g_{ij}),$$
$$\tau_{ij}(0) = 0,$$

where the stress tensor may be represented as a "polynomial" in the rate-of-deformation tensor g_{ij}. If the fluid is isotropic, the polynomial expansion reduces to

$$\tau_{ij} = -p\,\delta_{ij} + d_1\,g_{ij} + d_2\,g_{ik}g_{kj}$$

where p is the pressure, δ_{ij} is the Kronecker delta, and d_1 and d_2 are polynomials of the three principal invariants, I, II, and III, of the rate-of-deformation tensor. For flows which are steady and axial,

$$u_1 = 0, \quad u_2 = 0, \quad u_3 = u_3(x_1, x_2)$$

the tensor invariants become simply

$$I = III = 0,$$

$$II = -\left[(\partial u_3/\partial x_1)^2 + (\partial u_3/\partial x_2)^2\right]/4.$$

Thus

$$\tau_{ij} = -p\delta_{ij} + d_1(II)g_{ij} + d_2(II)g_{ik}g_{kj}$$

which is reminiscent of Ericksen's (1960a):

$$\tau_{ij} = -p\delta_{ij} - \eta g_{ij} - \tfrac{1}{2}(\theta_n + \beta)g_{ik}g_{kj} + \tfrac{1}{2}\theta_n \mathcal{D}g_{ij}/\mathcal{D}t$$

where η is the intrinsic viscosity and θ_n and β are the primary and secondary normal stress functions. The stress functions have been calculated by, among others, Giesekus (1962) and measured by Tanner (1970). The magnitude of θ_n is small in most fluids and β is smaller leading Bird* to comment humorously that integrated over the last decade of investigation, β is zero. The presence of the Jaumann derivative

$$\frac{\mathcal{D}g_{ij}}{\mathcal{D}t} = \frac{\partial g_{ij}}{\partial t} + u_k \frac{\partial g_{ij}}{\partial x_k} - w_{ik}g_{kj} - w_{ki}g_{jk}$$

reflects local anisotropy in the medium. The tensor w_{ij} is the vorticity or spin tensor.

In the present study the effect of normal stress functions upon the rheological behavior of Milling Yellow is neglected leading to the basic relationship for a "generalized Newtonian fluid" with the simple form:

---

*R. Byron Bird, Rheology Lectures, University of Florida, Gainesville, April 1973

$$\tau_{ij} = -p\delta_{ij} - \eta g_{ij}.$$

The sacrifice in dropping the terms with θ_n and β is less than it appears. Ericksen (1956) has shown that if the surfaces of constant velocity for a flow are neither planes nor circular cylinders, the only Stokesian fluid which can be described by the conditions for steady axial flow,

$$u_1 = 0, \quad u_2 = 0, \quad u_3 = u(x_1, x_2),$$

is one in which θ_n and β are either directly proportional to η or zero.

For steady axial flow, the components of τ_{ij} for a generalized Newtonian fluid are

$$\tau_{11} = \tau_{22} = \tau_{33} = -p,$$

$$\tau_{12} = \tau_{21} = 0,$$

$$\tau_{13} = \tau_{31} = -\eta(\partial u/\partial x_1)/2,$$

$$\tau_{23} = \tau_{32} = -\eta(\partial u/\partial x_2)/2.$$

Squaring the expressions for τ_{13} and τ_{23} and adding:

$$\tau_{13}^2 + \tau_{23}^2 = \eta^2\left[(\partial u/\partial x_1)^2 + (\partial u/\partial x_2)^2\right]/4.$$

The scalars τ and g are defined by comparing the terms in this expression with the corresponding terms in

$$\tau^2 = \eta^2 g^2/4.$$

Recognizing that the intrinsic viscosity was assumed to be a function of II and that $g^2/4 = -\mathrm{II}$, the final general form for the empirical relationship is just

$$\tau = \tau(g),$$

or with equal generality,

$$g = g(\tau).$$

In their analysis of viscosity measurements made in a capillary viscometer, Peebles, Prados, and Honeycutt (1965) found that Milling Yellow is well-represented, though not uniquely, by the Powell-Eyring equation:

$$\tau = \mu_{\infty} g + A_p(\mu_0 - \mu_{\infty}) \sinh^{-1}(g/A_p).$$

The flexibility of empirical representations is indicated by an alternate formulation of the same data for shear rates below 400 sec^{-1}. Peebles, Prados, and Honeycutt provide a plot of apparent viscosity versus wall shear stress. If these same data are replotted as μ_a versus $1/\tau_w{}^2$, as in Figure 20, a straight line is obtained:

$$\mu_a = \mu_{\infty} + k/\tau_w{}^2.$$

For flow in capillary tubes the classical approach of Rabinowitsch (1929) and Mooney (1931), as modified by Krieger and Maron (1952), leads to the relationship between shear rate and shear stress at the capillary wall:

$$g_w/\tau_w = (1/\mu_a) + \frac{\tau_w}{4} d(1/\mu_a)/d\tau_w$$

where

$$\tau_w = R\Delta p/2L_c$$

and

$$\mu_a = \pi\Delta pR^4/8L_cQ.$$

The variables in these expressions are R, the capillary radius, $\Delta p/L_c$, the pressure drop along capillary length L_c, and Q, the volumetric flow rate through the capillary.

When the equation for the straight line in Figure 20

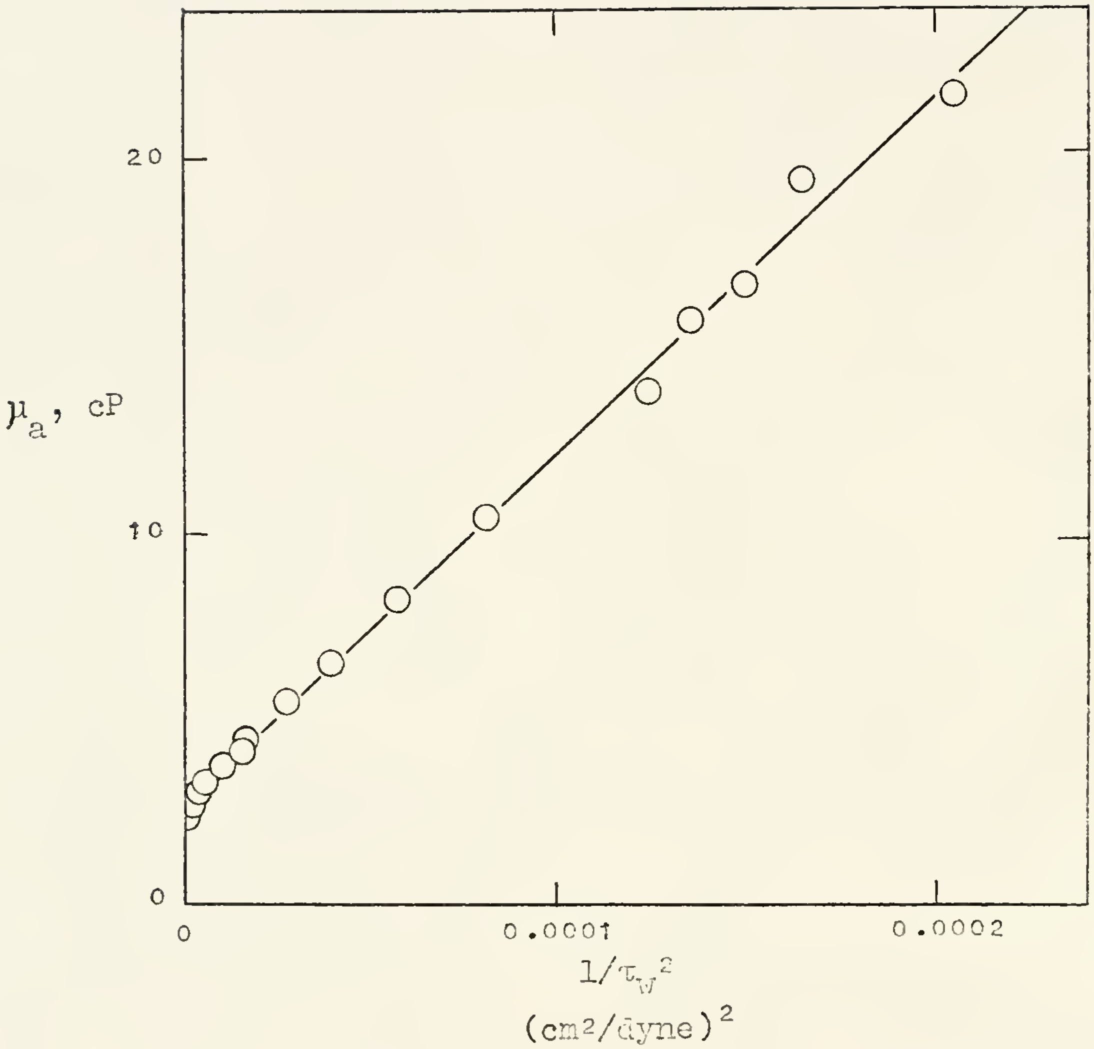

FIGURE 20. Data of Peebles, Prados, and Honeycutt (1965) replotted to obtain a linear relationship.

is substituted into Krieger and Maron's equation, the result is:

$$g_w(\tau_w) = \frac{\tau_w}{\mu_a} + \frac{k\tau_w{}^3/2}{(\mu_\infty \tau_w{}^2 + k)^2},$$

$$= \tau_w{}^3 \frac{\mu_\infty \tau_w{}^2 + (3k/2)}{(\mu_\infty \tau_w{}^2 + k)^2},$$

$$g(\tau) = \tau^3 \frac{\mu_\infty \tau^2 + (3k/2)}{(\mu_\infty \tau^2 + k)^2} .$$

This relationship differs qualitatively from the Powell-Eyring equation in being of the form $g(\tau)$ rather than $\tau(g)$. Further, it is expressed in terms of two constants, μ_∞ and k, rather than the three constants used in the Powell-Eyring equation. Inspection of the straight-line fit in Figure 20 also suggests that the expression for $g(\tau)$ given above may not be valid for values of τ above about 500 dyne/cm². Were it not for this restriction, at high values of τ the above equation would reduce to:

$$g(\tau) = \tau/\mu_\infty \qquad (\tau \text{ large}).$$

At very small values of τ it is evident that

$$g(\tau) = 3\tau^3/2k \qquad (\tau \text{ small}),$$

but this represents an extrapolation of the experimental data of Peebles, Prados, and Honeycutt much below the lowest shear stress reported.

Besides these relationships, a large number of alternate empirical forms are available for consideration. Skelland (1967, pp. 4-14) lists four equations for fluids with yield stresses,* seven for fluids without yield stresses, and four for fluids flowing in tubes where the stress at the wall is related to the volumetric flow rate. Although the form of many of these equations is influenced by molecular theory or other analysis, the spirit is empirical, and the constants are determined by experiment.

Analysis of Sliding Ball Viscometer

Since standardized samples of Milling Yellow cannot be prepared with predetermined properties, and because the properties of the solution change with time, the constants which appear in the rheological relationships describing Milling Yellow must be determined by experiment. In previous tests (e.g. Peebles, Prados, and Honeycutt, 1965) the instrument used has been a capillary viscometer. In the present instance the instrument used was the sliding ball viscometer, sometimes called a consistometer (Blair, 1949, p. 146). The sliding ball viscometer has not been considered an appropriate instrument for the determination of basic rheological properties. For this reason an analysis has been carried out by which the rheological constants may be educed from measurements made with the sliding ball viscometer. The pages which follow describe this analysis.

---

*In fluids with yield stresses, $\tau(0) \neq 0$. Although Milling Yellow has a yield stress (Thurstone and Schrag, 1962), it is negligible in most applications.

Related Investigations

The sliding ball viscometer consists of a cylindrical container inclined at a slight angle from the vertical within which a closely fitted sphere is driven downward through the liquid by a known force transmitted along a rigid shaft. The present design of the Höppler Rheo-Viscometer which is shown in Figure 21 differs little from the original (Höppler, 1941a). The variables of interest are the force applied to the ball and the time required for the ball to move downward through a set distance. Advantages of the instrument include small sample sizes (less than 20 ml), easy control of temperature and evaporation, speed and simplicity of operation, excellent reproducibility, and the traditional advantage of such instruments: the duration of shear is short. The principal disadvantage is also the traditional one: neither the shear stress nor the shear rate is constant within the instrument. Blair (1949) has discussed these advantages and disadvantages without reaching a rigid conclusion.

The sliding ball viscometer was developed in Germany at the outset of World War II. Höppler's (1941a, 1941b, 1942) descriptions were either qualitative, or the shear stress in the instrument was treated as constant and equal to the force transmitted by the shaft divided by the cross-sectional area of the ball. Following the war, analyses of the sliding ball instrument are rare (e.g. Lindgren, 1957)

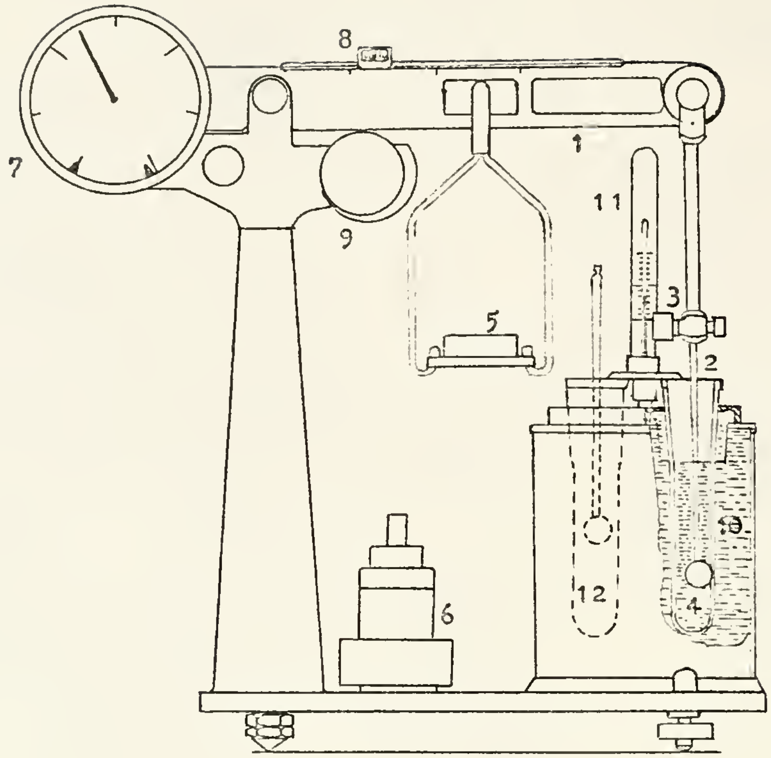

FIGURE 21. Höppler Rheo-Viscometer. Numbered items: (1) scale beam transmitting load to shaft and ball; (2) shaft and sliding ball; (3) counterweight to maintain offset position of ball; (4) fluid sample; (5) calibrated mass determining load on ball; (6) unused masses; (7) dial indicating position of ball in cylinder to nearest 0.1 mm; (8) slider to compensate for buoyancy effects arising from samples of varying density; (9) eccentric knob which is used to raise and release beam; (10) water from constant temperature circulator; (11) precision thermometer; (12) receptacle for next sample.

and to the present day the instrument manual furnished by the manufacturer speaks only of the "shear stress" defined by Höppler's original papers.

If the sliding ball viscometer is absent from the literature, the same cannot be said for its cousins: the rolling ball viscometer, the ball and tube flowmeter, and the falling cylinder viscometer. Ewing (1925) set some sort of record for *ex post facto* reminiscences by describing his experiments with the ball and tube flow meter in 1876. He points out that the ball's position in the tube is not stable when the tube is vertical and provides photographs of colored dye flowing up the center of the tube, around the ball, and up the wall while the inclination of the tube maintains the ball off-center in an eccentric position. Höppler's (1933) measurements with a rolling ball viscometer demonstrated the dependence of fall times upon the ratio of ball radius to cylinder radius and showed that accurate viscosity measurements could be made with a variety of materials following calibration with water. Höppler's photograph of dye flowing around the ball is, unlike Ewing's, symmetric above and below the ball.

Hubbard and Brown (1943a) derived a general equation for the rolling ball viscometer. A calibration constant was necessary for this equation and was found to vary by about 10 percent when used with fluids ranging from air to benzene (1943b). An analytic form for this constant was provided by Lewis (1953). The corresponding analyses of the falling cylinder viscometer are those of Lawaczeck (1919) and Lohrenz, Smith, and Kurata (1960). Christopherson and Dowson (1959) have considered the falling, rotating ball. Bauer and DuPuis (1967) discuss drag on a sphere rolling in a closed tube. Floberg (1968) is the author of a treatise on the ball and tube flowmeter and the rolling ball viscometer. All of these studies have been concerned with Newtonian fluids.

The extension of this work to non-Newtonian fluids requires an accurate description of the flow in the viscometer annulus. For a close fitting sphere or cylinder the usual first assumption has been to assume that the flow pattern is essentially that of two-dimensional flow along a channel having as its boundaries two circular surfaces.

Except for the elementary case of Newtonian flow in a concentric annulus (e.g. Lea and Tadros, 1931), the first solution of this problem appears to be that of Stevenson (1948), who solved the analogous problem of torsion in hollow tubes. The analogy between steady axial flows and torsion in cylindrical bars has been discussed in Chapter Two. For unit eccentricity, when the ball or cylinder slides along the cylindrical wall, the bounding surface is simply connected satisfying the necessary condition for the mathematical solutions of the two problems to be the same.

Ashare, Bird, and Lescarboura (1965) considered the flow of non-Newtonian fluids in a concentric annulus and found that non-Newtonian flow could be approximated by slit flow if one is interested only in the average fluid velocity in the channel. Chen, Lescarboura, and Swift (1968) studied the effect of eccentricity upon the flow, obtaining an exact expression for the velocity of a Newtonian fluid in an eccentric annulus. An extension of their method to non-Newtonian fluids was also indicated. Both Ashare's group and Chen's applied their results to the falling cylinder viscometer. They assumed that the cylinder was long enough so that entrance and exit effects could be neglected.

The sliding ball viscometer, despite a superficial resemblance to the rolling ball instrument, resembles the falling cylinder device when the flow is analyzed. The similarity lies in the fact that neither the sliding ball nor the cylinder rotate as they move downward. The difference in the two falling bodies is more apparent than real. At the close tolerances for which the sliding ball viscometer is used in the present dissertation, it may be shown that the resistance of the ball occurs over an "effective length" which is less than 10 percent of the ball's diameter. Over this effective length, the radius of the "cylinder" which the ball approximates changes by less than 1 percent.

Analysis

Paralleling the derivation for constitutive relationships in a capillary as carried out by Rabinowitsch (1929), Mooney (1931), and Krieger and Maron (1952), it is first necessary to define the volumetric flow of the liquid upward in the cylinder as the ball descends. The ball moves so slowly compared with the mean speed of the liquid (less than 1 percent) that the speed of the ball can be neglected and the flow becomes that of a non-Newtonian liquid in an eccentric annulus. Using the parameters shown in Figure 22, one obtains:

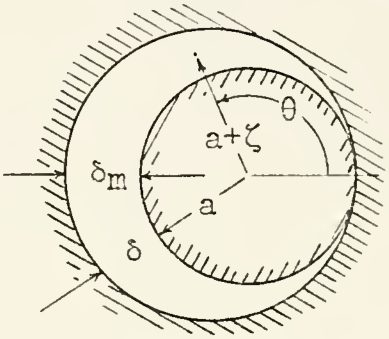

FIGURE 22.
Geometry in annulus.

$$Q = \int^{A} u \, dA = 2 \int_{0}^{\pi} \left[\int_{0}^{\delta} u(a+\zeta) d\zeta \right] d\theta$$

where Q is the volumetric flow rate, u is the axial speed at coordinates (ζ,θ), and δ is the width of the annulus. The magnitude of δ is

$$\delta = \delta_m(1-\cos\theta)/2 \pm \delta_m^2(1-\cos 2\theta)/16a \mp O(\delta_m^3/a^2)$$

where the sign of the second and higher order terms depends upon whether δ is measured along an outward normal from the ball or an inward normal from the cylinder. Since $\delta_m/a = 0.0088$ for the Höppler Rheo-Viscometer used in the present study, no serious error is introduced if one neglects the terms in δ_m^2 and higher to obtain

$$\delta = \delta_m(1-\cos\theta)/2.$$

Consider the term

$$I = \int_0^\delta u(a+\zeta)d\zeta$$

in the expression for Q just given. Set $\zeta = \eta_0 + \frac{\delta}{2}$ and obtain

$$I = \int_{-\delta/2}^{0} u(a + \frac{\delta}{2} + \eta_0)\, d\eta_0 + \int_0^{\delta/2} u(a + \frac{\delta}{2} + \eta_0)\, d\eta_0.$$

In a narrow annulus $u(-\eta_0) = u(\eta_0)$, so

$$I = 2\int_0^{\delta/2} u(a + \frac{\delta}{2} + \eta_0)\, d\eta_0.$$

Integrating by parts,

$$I = 2u\left[(a + \frac{\delta}{2})\eta_0 + \frac{1}{2}\eta_0^2\right]\Bigg|_{u = 0,\ \eta_0 = \delta/2}^{u = u_{max};\ \eta_0 = 0}$$

$$- 2\int_{u_{max}}^{0}\left[(a + \frac{\delta}{2})\eta_0 + \frac{1}{2}\eta_0^2\right] du.$$

Recognizing that the first term is zero at both limits, and replacing η_0 by $\zeta - \frac{\delta}{2}$, obtain

$$I = 2\int_0^{u_{max}} (a + \frac{\delta}{2})(\frac{\delta}{2} - \zeta)\, du. \qquad \zeta \leqslant \frac{\delta}{2}$$

Substituting into the original integral for Q yields

$$Q = 4\int_0^{\pi}\int_0^{u_{max}} (a + \frac{\delta}{2})(\frac{\delta}{2} - \zeta)\, du\, d\theta.$$

The unknown constitutive relationship which is sought for in the viscometric measurements is

$$du/d\zeta = g(\tau).$$

Substituting,

$$Q = 4\int_0^{\pi}\int_0^{\delta/2} (a + \frac{\delta}{2})(\frac{\delta}{2} - \zeta)\, g(\tau)\, d\zeta\, d\theta.$$

At this point it is necessary to draw a force balance on an annular element of the fluid subtending an arc $d\theta$, having a thickness $d\zeta$ and a length z. It is assumed that the change in the shearing stress in the angular direction $d\theta$ is negligible compared with the change in the direction $d\zeta$, and that the flow is steady and axial so that the shearing stress is unchanged throughout the length z. Under these assumptions the force balance can be written as

$$p(a + \zeta)\, d\theta\, d\zeta = - d\tau\, (a + \zeta)\, d\theta\, z$$

which reduces to

$$-d\tau/d\zeta = \Delta p/z.$$

The change in pressure from one side of the ball to the other is due, in the Höppler Rheo-Viscometer, to the force applied to the ball. Hence, identify the pressure drop Δp along the annular element with the force applied to the shaft divided by the cross-sectional area of the ball. This is the quantity which the instrument manual designates as P, the "average shear stress" in the fluid.* There is no analytical expression for the "effective length" L which replaces z:

$$\Delta p/z = P/L.$$

The effective length will be obtained experimentally.

Since P and L are constants, the force balance can be integrated from $\zeta = 0$ to $\zeta = \delta/2$ to obtain

---

*The units of P, according to the manufacturer, are gm/cm.^{2} A conversion to dyne/cm^2 is required before the numerical values given for P can be used consistently.

$$\tau = P(\tfrac{\delta}{2} - \zeta)/L.$$

At the wall,

$$\tau_W = P\delta/2L = P\delta_m(1-\cos\theta)/4L.$$

Substituting the value for the shear stress into the integral for Q yields

$$Q = \frac{4L^2}{P^2}\int_0^{\pi}(a + \tfrac{\delta}{2})\int_0^{\tau_w}\tau\, g(\tau)\, d\tau\, d\theta\ .$$

It is a simple matter to rewrite Q in terms of the "fall time" t for the ball. Applying the continuity requirement,

$$Q = (\bar{U}A)_{\text{annulus}} = (UA)_{\text{ball}} = \frac{\ell}{t}\pi a^2,$$

where ℓ is the distance (normally 3 cm) through which the ball is driven in time t. Substitution and rearrangement leads to:

$$1/t = \frac{4L^2}{\pi a^2 \ell P^2}\int_0^{\pi}(a + \tfrac{\delta}{2})\int_0^{\tau_w}\tau\, g(\tau)\, d\tau\, d\theta\ . \qquad (5.1)$$

In the analyses which follow it will be noted that $\frac{\delta}{2}$ has usually been neglected compared with a in order to reduce the complexity of the integration procedures. Although justified by the relative magnitudes of the quantities ($\frac{\delta}{2} = 0.0044a$), this assumption has been made for convenience rather than necessity. Typically a rigorous integration has been possible even when it was not performed.

For a Newtonian fluid the response of the viscometer can be obtained directly. Substituting $g(\tau) = \tau/\mu_N$ into equation (5.1) yields (when the $\delta/2$ term is neglected):

$$1/t = \frac{4L^2}{\pi a \ell P^2 \mu_N} \int_0^{\pi} \int_0^{\tau_w} \tau^2 \, d\tau \, d\theta,$$

$$= \frac{4L^2}{\pi a \ell P^2 \mu_N} \int_0^{\pi} \frac{1}{3} \tau_W{}^3 \, d\theta.$$

Substituting the value for the stress at the wall given on the previous page,

$$1/t = \frac{4L^2}{3\ a \ell P^2 \mu_N} \int_0^{\pi} \frac{\delta_m{}^3 P^3}{8L^3} (1-\cos\theta)^3 \, d\theta,$$

$$= 5P\delta_m{}^3/96\mu_N a \ell L.$$

Hence, for a Newtonian fluid,

$$\mu_N = 5\delta_m{}^3 Pt/96a\ell L.$$

Calibration of the viscometer yields a numerical value for the ratio $5\delta_m{}^3/96a\ell L$ from which the effective length may be calculated. When this is done for the Höppler instrument the effective length is found to be 0.1365 cm, compared with a ball diameter of 1.596 cm. Details of this calibration may be found in Appendix E. Since the credibility of the present analysis depends upon the concept of a fixed effective length, it appears desirable to give some attention to the experimental value for L and the inferences to be drawn from its magnitude.

In assuming that the flow past a sliding ball can be modeled on the flow in an eccentric annulus of the same cross-section it is implicit that the ball be replaced by a cylinder of length L.* Three questions naturally arise:

---

*When this analysis is applied to a falling cylinder viscometer the length of the actual cylinder should approximate L.

1. – Why use a ball instead of a cylinder?

2. – How valid is the assumption that the ball can be modeled by a cylinder?

3. – How constant is the effective length from fluid to fluid and from one force on the ball to another?

These questions will be answered individually.

1. Why use a ball? – All of the analysis which is provided in this chapter models flow past a ball at the point of minimum clearance on flow past a cylinder of the same dimensions; hence, the analysis should be valid without significant change for a sliding cylinder viscometer. Naturally the primary impetus for the analysis was the need to analyze the instrument which was actually used. It is valid to inquire, nevertheless, whether an instrument with a fitted cylinder would have been preferable to the present instrument. It appears likely that the sliding ball possesses the advantage that a smaller force is required to overcome the shearing stresses in the eccentric annulus than would be the case with a cylinder of sufficient length that entrance and exit effects could be neglected. On the other hand, the effective length of the sliding cylinder, even if a correction for end effects is necessary, corresponds more closely to an actual physical dimension than the effective length of the sliding ball. Which instrument would be preferable in a general case would depend upon the relative importance of these considerations.

2. How well does the ball model a cylinder? — In terms of changes in the radius of the cylinder which the ball models, the assumption that the ball is a cylinder over the effective length L = 0.1365 cm is a good one. If it is assumed that the position of the effective length is such that it extends equally above and below the point of minimum clearance, then the change in the radius of the ball is about 0.72 percent. Despite the instability of flow in divergent channels, as calculated by Millsaps and Pohlhausen (1953) extending the work of Jeffery (1915), Hamel (1916) and others, it appears that at the Reynolds numbers which are present in the channel (see Appendix J) a back flow does not occur within the computed effective length. The width of the eccentric annulus does change significantly over the effective length. Above and below the ball, at points corresponding to the limits of the effective length, the channel has a width twice that at the point of minimum clearance. The angle which the tangent to the ball makes with the cylinder wall at these points is about 5 degrees.

An alternate model has been considered by Šesták and Ambros (1973) who assumed that the flow remains parallel with the cylinder walls, but that the flow rate decreases in proportion to the increase in cross-sectional area. Integrating along the boundary of the sphere in the direction of flow, they obtained viscometer responses for

Newtonian and power-law substances. Their results for the latter extended a similar analysis by Bird and Turian (1964). While the model of Šesták and Ambros overcomes one assumption of the present model — that the flow rate is unchanged along the effective length of the annulus — it retains another: that the radial components of the velocity are negligible. While this assumption appears reasonable for integrations orthogonal to the flow path at the point of minimum clearance, as in the present dissertation, it appears less reasonable when the integration occurs, as it does in the Šesták and Ambros analysis, in the direction of flow. Since the assumption made in the present dissertation permits the determination of the rheological properties when the form of the constitutive relationship is not known, a determination which is not possible when the model of Šesták and Ambros is employed, it would appear that the advantages of modeling a cylinder by means of a ball overweigh the corresponding objections.

3. How constant is the effective length? — The constancy of the effective length as various fluids are placed in the viscometer is a matter of conjecture. It is clear from the calibration in Appendix E that the change is negligible for Newtonian fluids through a wide range of shear rates and between Newtonian fluids when the viscosity varies by more than a factor of ten. The

assumption made in this dissertation is that the change in the effective length is also negligible for non-Newtonian substances.

Integration of the viscometer equation

The viscometer equation, equation (5.1), has already been integrated for a Newtonian fluid. Another important class of fluids for which the equation may be integrated directly are the power-law fluids which may be represented in the one-dimensional form

$$\tau = K g^{m}$$

where K and m are constants. Substitution into the viscometer equation yields

$$1/t = (4L^2/\pi a^2 \ell P^2 K^{1/m}) \int_0^{\pi} (a + \frac{\delta}{2}) \int_0^{\tau_w} \tau^{\frac{m+1}{m}} \, d\tau \, d\theta .$$

Neglecting $\delta/2$ compared with a,

$$1/t = (4L^2/\pi a \ell P^2 K^{1/m}) \int_0^{\pi} \int_0^{\tau_w} \tau^{\frac{m+1}{m}} \, d\tau \, d\theta .$$

Integrating once and setting $(1+2m)/m = M$,

$$1/t = (4L^2/\pi a \ell P^2 M K^{1/m}) \int_0^{\pi} (P\delta_m/4L)^M (1-\cos\theta)^M \, d\theta ,$$

$$= \frac{\delta_m{}^M P^{M-2}}{4^{M-1} \pi a \ell L^{M-2} M K^{1/m}} \int_0^{\pi/2} 2^M \sin^{2M}\varphi' \, (2\, d\varphi')$$

where $2\varphi' = \theta$. Integration yields

$$1/t = \frac{\delta_m{}^M \Gamma(M+1/2)}{2^{M-2}\sqrt{\pi}\, a \ell L^{M-2} M K^{1/m} \Gamma(M+1)} P^{1/m}$$

where $\Gamma(M+1/2)$ and $\Gamma(M+1)$ are gamma functions. Thus the response of the viscometer to a power-law substance shows the same exponential characteristics as in one-dimensional shear flow. The model of Šesták and Ambros (1973) yields a similar result.

The treatment of materials with yield stresses (such as a Bingham plastic) or bilinear responses is similar, but a separate consideration of the limits of integration is required. An example of a bilinear material having the response

$$g = \begin{cases} \tau/\mu_0 & \tau < \tau_c \\ \dfrac{\tau}{\mu_\infty} - k & \tau \geqslant \tau_c \end{cases}$$

is treated in Appendix F.

If the form of the constitutive equation is unknown or resists integration in explicit form it is possible to obtain a plot of $g(\tau)$ versus τ from experimental values of P and t.

Replace τ_w in equation (5.1) by $P\delta/2L$ to obtain ($a \gg \delta_m$)

$$P^2/t = (4L^2/\pi a\ell)\int_0^\pi\int_0^{P\delta/2L} \tau\, g(\tau)\, d\tau\, d\theta. \tag{5.2}$$

Differentiating with respect to P yields

$$d(P^2/t)/dP = (P/\pi a\ell)\int_0^\pi \delta^2\, g(\delta P/2L)\, d\theta.$$

Expand $g(\tau)$ as a power series in τ:

$$g(\tau) = \alpha_0 + \alpha_1\tau + \alpha_2\tau^2/2! + ..$$

At the wall, where $\tau_w = \delta P/2L = P\delta_m(1-\cos\theta)/4L$,

$$g(\tau_w) = g(\delta P/2L) = \sum_{n=0}^{\infty}\alpha_n\delta_m{}^n P^n(1-\cos\theta)^n/4^n L^n n!$$

Substituted into the expression for $d(P^2/t)/dP$ with $\delta_m/4L$ set equal to β_0, there results:

$$\frac{1}{P}\,\frac{d(P^2/t)}{dP} = \frac{\delta_m{}^2}{4\pi a\ell}\int_0^{\pi}\sum_{n=0}^{\infty}\alpha_n\beta_o{}^nP^n(1-\cos\,\theta)^{n+2}\;d\theta/n!\ ,$$

which is integrated to yield:

$$\frac{1}{P}\,\frac{d(P^2/t)}{dP} = \frac{\delta_m}{4\pi a\ell}\sum_{n=0}^{\infty}\frac{\alpha_n\beta_o{}^nP^n2^{n+3}}{n!}\,\frac{\pi}{2}\,\frac{1\cdot3\cdot5\cdot\cdot(2n+3)}{2\cdot4\cdot6\cdot\cdot(2n+4)}\ .$$

The quantity on the left hand side of this equation is obtained experimentally. By least squares analysis or other suitable technique, fit a polynomial of the form

$$\frac{1}{P}\,\frac{d(P^2/t)}{dP} = a_o + a_1P + a_2P^2 + \,..\; a_nP^n$$

to the experimental data. Alternately one may find an empirical fit in the form

$$1/t = b_o + b_1P + b_2P^2 + \,..\; b_nP^n,$$

in which case

$$a_n = (n+2)b_n.$$

Once the coefficients have been obtained for the experimental data, a term by term comparison yields:

$$\alpha_n = \frac{an!\ell a_n}{\delta_m{}^n\beta_o{}^n2^n}\,\frac{2\cdot4\cdot6\cdot\cdot(2n+3)}{1\cdot3\cdot5\cdot\cdot(2n+4)}\ .$$

Substituted into the series expansion for $g(\tau)$:

$$g(\tau) = \frac{a\ell}{\delta_m{}^2}\sum_{n=0}^{\infty}\frac{a_n}{2^n\beta_o{}^n}\,\frac{1\cdot3\cdot5\cdot\cdot(2n+3)}{2\cdot4\cdot6\cdot\cdot(2n+4)}\,\tau^n\ . \qquad (5.3)$$

This is the desired constitutive relationship.

As a simple example of this technique, consider again the Newtonian fluid. Previously it was found that

$$1/t = 5P\delta_m{}^3/96\mu_N a\ell L,$$

so that

$$b_1 = 5\delta_m{}^3/96\mu_N a\ell L,$$

and

$$b_0 = b_2 = b_3 = b_4 = .. = 0.$$

Hence,

$$a_1 = 3b_1 = 5\delta_m{}^3/32\mu_N a\ell L.$$

Recalling that $\beta_0 = \delta_m/4L$ and substituting into equation (5.3),

$$g(\tau) = \tau/\mu_N,$$

as, of course, it should.

If the analytical form of the experimental data can be induced, then equation (5.2) may be solved by quadrature without the necessity for a power law expansion. Recall that differentiation of the viscometer equation, equation (5.1), yielded

$$d(P^2/t)/dt = (P/\pi a\ell)\int_0^\pi \delta^2\ g(\delta P/2L)\ d\theta.$$

Setting

$$\tau_m = P\delta_m/2L,$$

and recalling that

$$\tau_w = P\delta_m(1-\cos\ \theta)/4L,$$

substitute

$$2\tau_w/\tau_m = (1-\cos\ \theta)$$

and

$$\frac{d\tau_w}{\sqrt{\tau_w(\tau_m - \tau_w)}} = d\theta$$

to obtain:

$$\frac{1}{P}\,\frac{d(P^2/t)}{dP} = \frac{\delta_m{}^2}{\pi a \ell \tau_m{}^2}\int_0^{\tau_m} \tau_w{}^{3/2}\, g(\tau_w)\,\frac{d\tau_w}{\sqrt{\tau_m-\tau_w}}\,.$$

The left side of this equation may also be expressed in terms of τ_m:

$$\frac{1}{P}\,\frac{d(P^2/t)}{dP} = \frac{1}{\tau_m}\,\frac{d(\tau_m{}^2/t_m)}{d\tau_m}\,,$$

where the subscript on the symbol t_m is a reminder that in place of $t(P)$ one must write $t(2L\tau_m/\delta_m)$.

The result of this manipulation is an equation of the form

$$\tau_m\,\frac{d(\tau_m{}^2/t_m)}{d\tau_m} = \frac{\delta_m{}^2}{\pi a \ell}\int_0^{\tau_m} \tau_w{}^{3/2}\, g(\tau_w)\,\frac{d\tau_w}{\sqrt{\tau_m-\tau_w}}$$

which is recognizable as Abel's equation for which the solution, as given by Tricomi (1957, pp. 39-40) among others, is:

$$\tau_m{}^{3/2}\, g(\tau_m) = \Upsilon(0)\,\frac{1}{\sqrt{\tau_m}} + \int_0^{\tau_m} \Upsilon'(\tau_w)\,\frac{d\tau_w}{\sqrt{\tau_m-\tau_w}}\,,$$

where

$$\Upsilon(\tau_m) = \frac{a\ell\tau_m}{\delta_m{}^2}\,\frac{d(\tau_m{}^2/t_m)}{d\tau_m} \tag{5.4}$$

and

$$\Upsilon'(\tau_w) = \left.\frac{d\Upsilon(\tau_m)}{d\tau_m}\right|_{\tau_m=\tau_w}\,.$$

The corresponding constitutive equation is simply

$$g(\tau) = \frac{\Upsilon(0)}{\tau^2} + \frac{1}{\tau^{3/2}}\int_0^{\tau} \Upsilon'(\tau_w)\,\frac{d\tau_w}{\sqrt{\tau-\tau_w}}\,. \tag{5.5}$$

To illustrate the use of this equation, consider for the third time a Newtonian fluid. Again,

$$1/t = 5P\delta_m{}^3/96\mu_N a\ell L,$$

so

$$1/t_m = 5\tau_m\delta_m{}^2/48\mu_N a\ell,$$

in which case,

$$\Upsilon(\tau_m) = 5\tau_m{}^3/16\mu_N$$

$$\Upsilon(0)/\tau^2 = \lim\ (\tau_m \rightarrow 0)\quad 5\tau_m{}^3/16\mu_N\tau^2 \qquad (\tau < \tau_m)^*$$

$$= 0$$

$$\Upsilon'(\tau_w) = 15\tau_w{}^2/16\mu_N,$$

and

$$g(\tau) = \frac{1}{\tau^{3/2}}\,\frac{15}{16\mu_N}\int_0^{\tau} \tau_w{}^2\,\frac{d\tau_w}{\sqrt{\tau-\tau_w}},$$

$$= \tau/\mu_N,$$

as, again, it must.

---

*Recall that $\tau_m = P\delta_m/2L$ is the maximum value of the shear stress anywhere in the annulus.

Experimental Results

Besides the measurements made to determine the rheological constants, several other investigations were carried out. These included the change in apparent viscosity of Milling Yellow with time (Appendix H) and with concentration and temperature (Appendix I). It was found that the range of the Höppler Rheo-Viscometer could be extended to viscosities less than the minimum of 4 centipoise recommended by the manufacturer by observing the restriction (Appendix J):

$$P/\mu_a^2 < 15.5 \text{ gm/(cm-cP)}^2.$$

Confirmation of the calibration of the instrument using distilled water (Appendix E) is an example of this usage.

During the time that the medium was being used to measure the birefringence, as described in Chapter Four, nine samples were taken. Each of these was tested in the Höppler Rheo-Viscometer at 20° and 25° C. These data are tabulated in Tables XIX to XXVII. The fall times listed are for a displacement of 3.00 cm. The temperatures are those of the precision thermometer located adjacent to the viscometer cylinder in the water bath of the instrument.

TABLE XIX

VISCOMETER MEASUREMENTS - RUN 42*

P, gm/cm²	t, sec	T, °C	P, gm/cm²	t, sec	T, °C
160	3.2	20.00	80	4.7	25.00
	3.4	20.02		4.6	25.00
	3.4	20.02		4.7	25.00
	3.4	20.02			
	3.8	20.02			
80	6.3	20.02	60	6.7	25.00
	6.0	20.02		6.8	25.00
	6.1	20.00		6.8	25.00
	6.0	20.02			
	6.5	20.02			
40	16.8	20.02	40	12.1	25.00
	16.4	20.02		12.1	25.00
	16.6	20.00		12.1	24.98
	16.8	20.02			
	16.5	20.02			
30	26.9	20.00	30	18.6	25.00
	26.5	20.00		18.6	25.00
	26.3	20.00		18.6	25.00
	26.6	20.00			
	27.0	20.00			
20	54.8	20.00	20	35.5	25.00
	54.9	20.00		35.6	25.00
	55.6	20.00		35.7	25.00
	54.5	20.00			
	54.4	20.00	15	58.6	25.00
				58.5	25.00
15	99.4	20.00		58.5	25.00
	96.8	20.00			
	99.3	20.00	10	128.3	25.00
	95.1	20.00		128.1	25.00
	95.6	20.00		128.3	25.00
10	264.7	20.00	7.5	237.2	25.00
	249.1	20.02			
	240.5	20.00	5	603.1	25.00
	241.2	20.00		604.4	25.00

---

*Sample 42 contained sedimentation. This caused variability in the run at 20° C. The run at 25° C was conducted with fluid decanted from the top of the sample bottle.

TABLE XX

VISCOMETER MEASUREMENTS - RUN 44

P, gm/cm^2	t, sec	T, °C	P, gm/cm^2	t, sec	T, °C
160	3.4	20.00	80	5.1	25.00
	3.5	20.00		5.1	25.02
	3.4	20.00		5.0	25.00
80	6.1	20.00	60	6.9	25.00
	6.1	20.00		7.1	25.00
	6.2	20.00		7.0	25.02
40	17.2	20.00	40	12.3	25.00
	17.2	20.00		12.4	25.00
	17.2	20.00		12.4	25.02
				12.3	25.02
30	27.4	20.00	30	19.1	25.00
	27.4	20.00		19.1	25.00
	27.3	20.00		19.3	25.00
20	57.0	20.00	20	36.8	25.00
	57.7	20.02		36.9	25.00
	58.6	20.00		36.9	25.00
	58.0	20.00			
	57.1	20.00			
15	103.3*	20.00	15	60.5**	25.00
	108.4*	20.00		60.8**	25.00
	100.6	20.00		61.2**	25.00
	100.2	20.00		61.5**	25.00
	100.2	20.00		62.9**	25.00
				60.5	25.00
				60.7	25.00
				60.5	25.00
10	254.6	20.04	10	136.6	25.00
	254.1	20.04		136.0	25.00
	254.3	20.00		136.8	25.00
			7.5	255.7	25.00
5	1853.9	20.00	5	672.4	25.00
				666.6	25.00

---

*Rejected as spurious

**Rejected as spurious after a pause to clean viscometer ball produced a reproducible result.

TABLE XXI

VISCOMETER MEASUREMENTS — RUN 418

P, gm/cm²	t, sec	T, °C	P, gm/cm²	t, sec	T, °C
160	3.6	20.00	80	4.9	25.00
	3.6	20.00		4.9	25.00
	3.5	20.00		4.9	25.00
80	5.9	20.00	60	6.7	25.00
	5.9	20.00		6.8	25.00
	6.0	20.00		6.7	25.00
	6.0	20.00			
40	16.6	20.00	40	11.9	25.00
	16.6	20.00		11.9	25.00
	16.6	20.00		11.9	25.00
30	26.4	20.00	30	18.3	25.00
	26.5	20.00		18.2	25.00
	26.5	20.00		18.3	25.00
20	56.3	20.00	20	34.6	25.00
	54.0	20.00		34.8	25.00
	53.8	20.00		34.9	25.00
	54.0	20.00			
	53.8	20.00			
15	92.8	19.96	15	56.3	25.00
	92.7	20.00		56.3	25.00
	93.4*	20.00		56.3	25.00
	92.8	20.00			
	92.9	20.00			
10	220.8	20.00	10	118.3	25.00
	221.0	20.00		119.0	25.00
	220.7	20.00		119.1	25.00
7.5	445.0	20.02	7.5	210.0	25.00
5	1253.1	20.00	5	485.8	25.00
	1240.7	20.00		482.1	25.00

---

*Rejected as spurious

TABLE XXII

VISCOMETER MEASUREMENTS – RUN 419

P, gm/cm²	t, sec	T, °C	P, gm/cm²	t, sec	T, °C
160	3.5	20.00	80	4.9	25.00
	3.4	20.00		4.7	25.00
	3.5	20.00		4.7	25.00
80	5.9	20.00	60	6.7	25.00
	6.0	20.02		6.9	25.00
	6.0	20.02		6.8	25.00
40	16.4	20.00	40	12.0	25.00
	16.3	20.00		12.0	25.00
	16.3	20.00		12.0	25.00
30	25.9	20.00	30	18.4	25.00
	25.8	20.00		18.3	25.02
	26.0	20.00		18.2	25.00
20	52.0	20.00	20	34.6	25.00
	52.1	20.00		34.6	25.00
	52.1	20.00		34.7	25.00
15	90.3	20.00	15	55.7	25.00
	89.6	20.00		55.7	25.00
	89.7	19.98		55.7	25.00
	89.8	20.00			
	89.8	19.98			
	89.8	20.00			
10	211.4*	20.04	10	116.4	25.00
	213.3	20.00		116.9	25.02
	214.3	20.00		117.1	25.00
	214.5	20.00			
7.5	419.6	20.04	7.5	205.6	25.02
5	1150.9	20.00	5	474.9	25.00**
	1157.1	20.00		477.2	25.00

---

*Rejected as spurious

**Difficulty with circulator. Temperature varied during run from 24.94° to 25.04° C.

TABLE XXIII

VISCOMETER MEASUREMENTS - RUN 420

P, gm/cm²	t, sec	T, °C	P, gm/cm²	t, sec	T, °C
160	3.7	20.00	80	5.1	25.02
	3.6	20.00		5.1	25.02
	3.5	20.00		5.1	25.02
80	6.0	20.00	60	6.8	25.00
	6.1	20.00		6.8	25.00
	6.1	20.00		6.9	25.00
40	17.0	20.00	40	12.1	25.00
	16.9	20.00		12.1	25.00
	16.9	20.00		12.2	25.00
30	26.9	20.00	30	18.6	25.00
	27.0	20.00		18.6	25.00
	27.1	20.00		18.8	25.00
20	54.8	20.00	20	35.4	25.00
	55.1	20.00		35.4	*
	55.1	20.00		35.4	25.00
	55.0	20.00			
	55.2	20.00			
10	227.1	20.00	10	122.8	25.00
	227.1	20.00		123.3	25.00
	227.4	20.02		122.9	25.00
7.5	440.3	20.00	7.5	214.0	25.00
5	1220.3	20.00	5	497.6	25.00
	1218.2	20.00		497.4	25.00

---

*Measurement omitted

TABLE XXIV

VISCOMETER MEASUREMENTS – RUN 420B

P, gm/cm^2	t, sec	T, °C	P, gm/cm^2	t, sec	T, °C
160	3.7	20.00	80	5.0	25.00
	3.6	20.00		5.0	25.00
	3.7	20.00		5.0	25.00
80	6.0	20.00	60	6.8	25.00
	6.1	20.00		6.8	25.00
	6.0	20.00		6.8	25.00
	6.0	20.00			
40	16.9	20.00	40	12.0	25.00
	17.0	20.00		12.0	25.00
	16.9	20.00		12.0	25.02
30	27.1	20.00	30	18.4	25.00
	27.1	20.00		18.4	25.00
	26.9	20.00		18.4	25.00
20	55.3	20.00	20	34.9	25.00
	55.3	20.00		34.8	25.00
	55.2	20.00		34.9	25.00
15	96.0	19.98	15	56.4	25.00
	96.4	20.00		56.3	25.00
	96.2	20.00		56.5	25.00
	96.3	20.00			
	96.3	20.00			
10	230.0	20.00	10	119.6	25.02
	230.7	20.00		120.2	25.00
	231.5	20.00		120.2	25.02
	230.3	20.00			
	230.7	20.00			
7.5	448.7	20.00	7.5	214.1	25.00
5	1237.5	20.00	5	508.3	25.00
	1236.4	20.00		500.0	25.00*

---

*Difficulty with circulator. Temperature varied during run from 24.98° to 25.02° C.

TABLE XXV

VISCOMETER MEASUREMENTS - RUN 424

P, gm/cm^2	t, sec	T, °C	P, gm/cm^2	t, sec	T, °C
160	3.6	20.00	80	4.9	25.00
	3.5	20.00		4.8	25.00
	3.4	20.00		4.9	25.00
80	6.3	20.00	60	7.1	25.00
	6.3	20.00		7.1	25.00
	6.4	20.00		7.1	25.00
40	17.8	20.00	40	12.6	25.00
	17.8	20.00		12.7	25.02
	17.8	20.00		12.6	25.00
30	28.5	20.00	30	19.6	25.00
	28.6	20.00		19.6	25.00
	28.4	20.00		19.5	25.00
20	58.7	20.00	20	37.5	25.00
	58.8	20.00		37.7	25.00
	58.8	20.00		37.6	25.00
15	102.0*	20.00	15	61.8	25.00
	102.3*	20.02		61.7	25.00
	102.5*	20.00		61.6	25.00
	102.8*	20.00			
	103.1*	20.00			
10	254.2	19.98	10	134.6	25.00
	253.9	19.98		134.8	25.00
	253.4	20.00		134.9	25.00
7.5	510.8	20.00	7.5	243.1	25.00
5	1480.8	20.00	5	591.3	25.00
				591.4	25.01**

---

*The systematic increase in these values is unexplained.

**Difficulty with circulator. Temperatures varied during run from 24.98° to 25.04° C.

TABLE XXVI

VISCOMETER MEASUREMENTS – RUN 424B

P, gm/cm²	t, sec	T, °C	P, gm/cm²	t, sec	T, °C
160	3.3	20.00	80	5.0	25.00
	3.4	19.98		4.9	25.00
	3.4	19.98		5.0	25.00
80	6.4	20.00	60	7.3	25.00
	6.4	20.00		7.3	25.00
	6.4	20.00		7.3	25.00
40	18.2	20.00	40	12.9	25.00
	18.2	20.00		13.0	25.00
	18.2	20.00		13.0	25.00
30	29.3	20.00	30	20.1	25.00
	29.3	20.00		20.1	25.02
	29.3	20.00		20.1	25.00
20	60.9	20.00	20	38.9	24.94
	60.9	20.00		39.0	25.00
	61.1	20.00		39.0	25.00
15	107.3	20.00	15	64.3	25.00
	107.1	20.00		64.4	25.00
	106.9	20.00		64.3	25.00
10	267.4	20.00	10	141.1	25.02
	271.3	20.00		139.6	25.02
	268.0	20.00		140.7	25.00
7.5	549.4	20.00	7.5	257.6	25.00
5	1632.6	20.00	5	634.8	25.02
				640.6	25.00

TABLE XXVII

VISCOMETER MEASUREMENTS - RUN 425

P, gm/cm²	t, sec	T, °C	P, gm/cm²	t, sec	T, °C
160	3.5	20.00	80	5.1	25.00
	3.5	20.00		4.9	24.98
	3.5	20.00		5.0	24.96
80	6.4	20.00	60	7.3	25.00
	6.4	20.00		7.4	25.00
	6.4	20.00		7.3	24.98
40	18.3	20.00	40	13.1	25.00
	18.2	20.00		13.2	25.00
	18.3	20.00		13.2	25.00
				13.1	25.00
30	29.5	20.00	30	20.3	25.00
	29.6	20.02		20.3	25.00
	29.6	20.00		20.4	25.00
20	61.5	20.00	20	39.5	25.00
	61.6	20.02		39.5	25.00
	61.8	20.00		39.6	25.00
15	109.7	20.00	15	65.4	25.00
	109.6	20.00		65.3	25.00
	109.6	20.00		65.4	25.00
10	273.8	20.00	10	144.2	25.00
	274.6	20.00		144.7	25.00
	274.6	20.00		145.0	25.00
7.5	562.2	20.01*	7.5	264.9	25.00
5	1661.7	20.00	5	656.2	25.00
				660.8	25.00

---

*Difficulty with circulator. Temperature varied during run from 20.00° to 20.02° C.

Discussion of Results

This discussion is in two sections. The first describes the reduction of the data to an analytic form by the method of least squares. The second section is concerned with the calculation of the rheological constants for Milling Yellow from this analytic form.

Curve Fitting

Three of the experimental runs are plotted in Figure 23. Inspection of the preceding tables indicates that the plotted data are typical.

In all of what follows the values of P which appear in Tables XIX to XXVII have been reduced by 0.28 gm/cm^2 to correct for instrumental friction. The need for this correction is provided in Appendix E.

The data in Figure 23 appear to have a slope d(ln P)/d(ln t) which has a value of -2 at low values of P and which approaches -1 as P becomes large. A straight line of slope -2 has been passed through the data for the lower values of P (run 425). The logarithm of the difference between the experimental value of t and the value obtained from this straight line was plotted versus ln P and a nearly straight line was obtained. This suggested a test of the functional form

$$1/t \quad = \quad P^2/(k_1+k_2P)$$

or

$$Pt \quad = \quad \frac{k_1}{P} + k_2 \; .$$

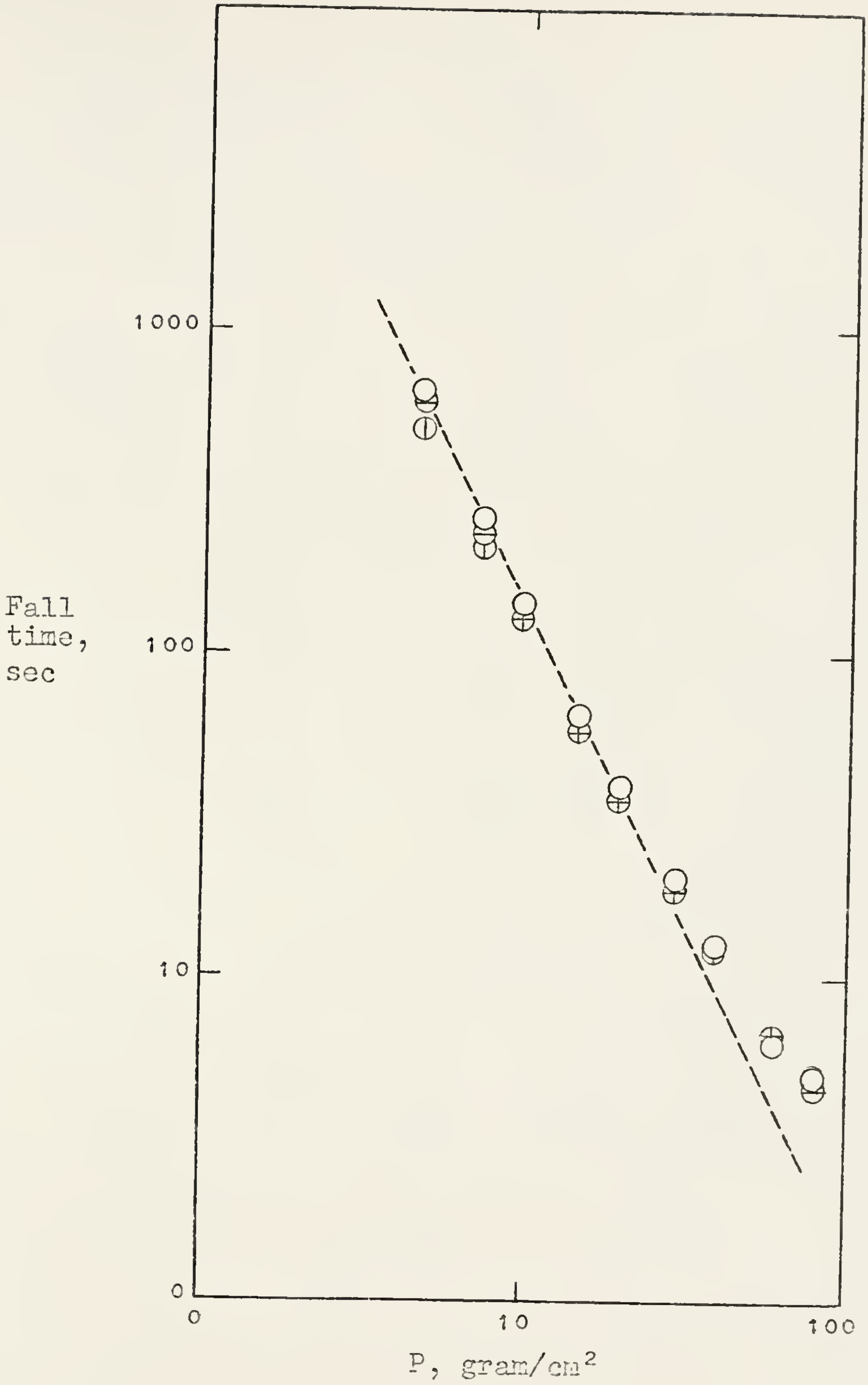

FIGURE 23. Response of viscometer, runs: ⊖ 42; ⦶ 420; ○ 425.

The scale of the log-log plot (Figure 23) is too small to provide a serious test of the hypothetical functional form just given, so the data were replotted on a cartesian scale as Pt versus 1/P. The result shown in Figure 24 is for the same experimental runs plotted previously. The predicted linearity is reasonable only at higher values of P.

Again the departure from the predicted functional form served as the new variable for improved curve-fitting. Following the example of Lindgren (1957), who was interested in the viscosity at infinite shear rates, the value of the product Pt as 1/P approaches zero was taken from Figure 24, and a new correlation was attempted between $[Pt - (Pt)_\infty]$ and P, where $(Pt)_\infty$ is the value for Pt as P increases without limit. As shown in Figure 25, a linear result is obtained when $P[Pt - (Pt)_\infty]$ is plotted versus 1/P. The corresponding functional form is

$$Pt = (Pt)_\infty + k_1/P + k_2/P^2$$

or

$$1/t = P^3 \left[(P+C_1)^{-1} - (P+C_2)^{-1}\right]/C_0.$$

Values of the constants C_0, C_1, and C_2 are given in Table XXVIII for each of the experimental runs. Also tabulated are the viscosity values corresponding to $(Pt)_\infty$,

$$\mu_\infty = 0.00534(Pt)_\infty = 0.00534\ (C_2-C_1)/C_0;$$

and an estimate of the goodness of fit of the functional form.

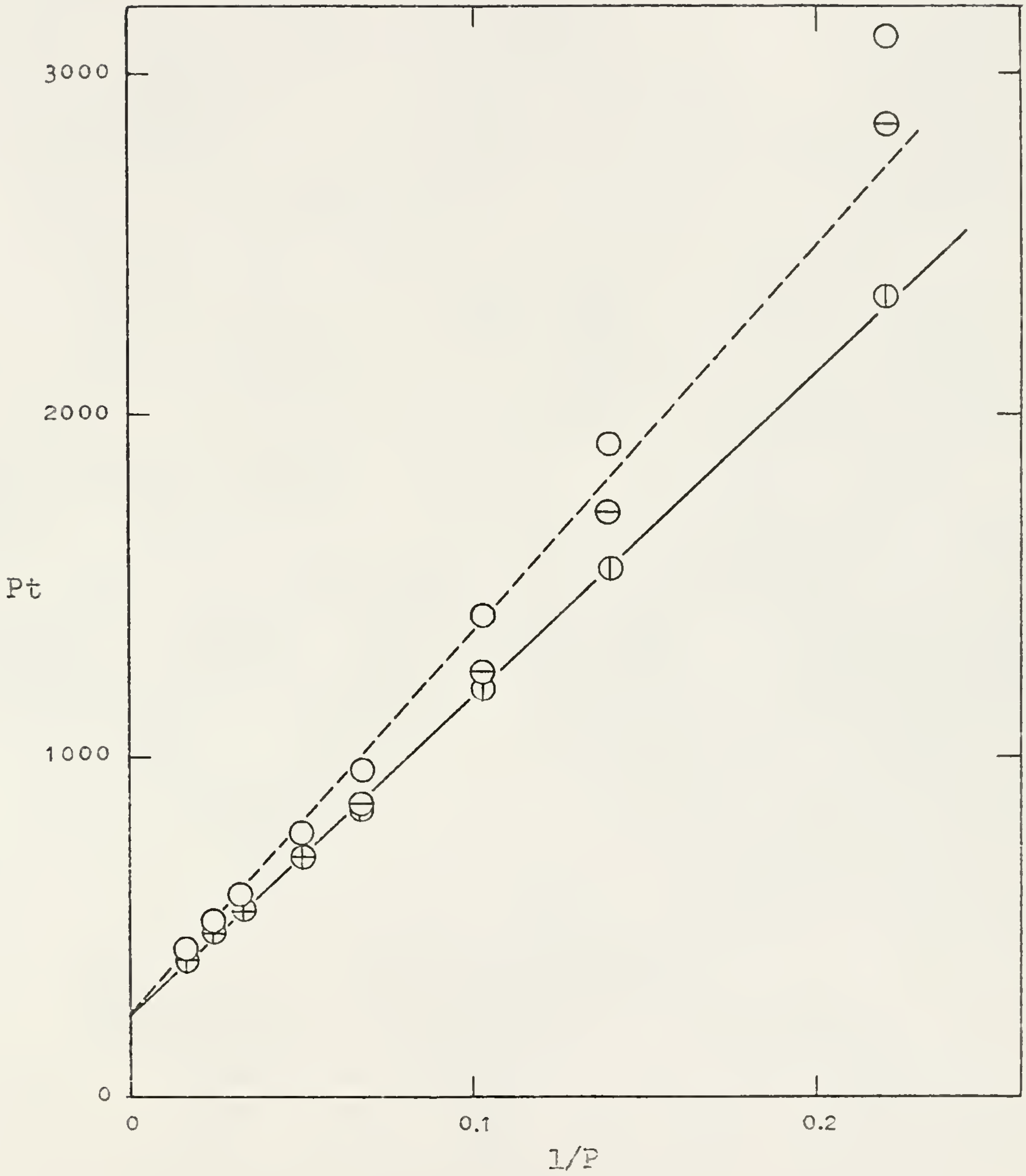

FIGURE 24. Test of functional form: $Pt = \frac{k_1}{P} + k_2$. Runs: ⊖ 42; ⦶ 420; ○ 425.

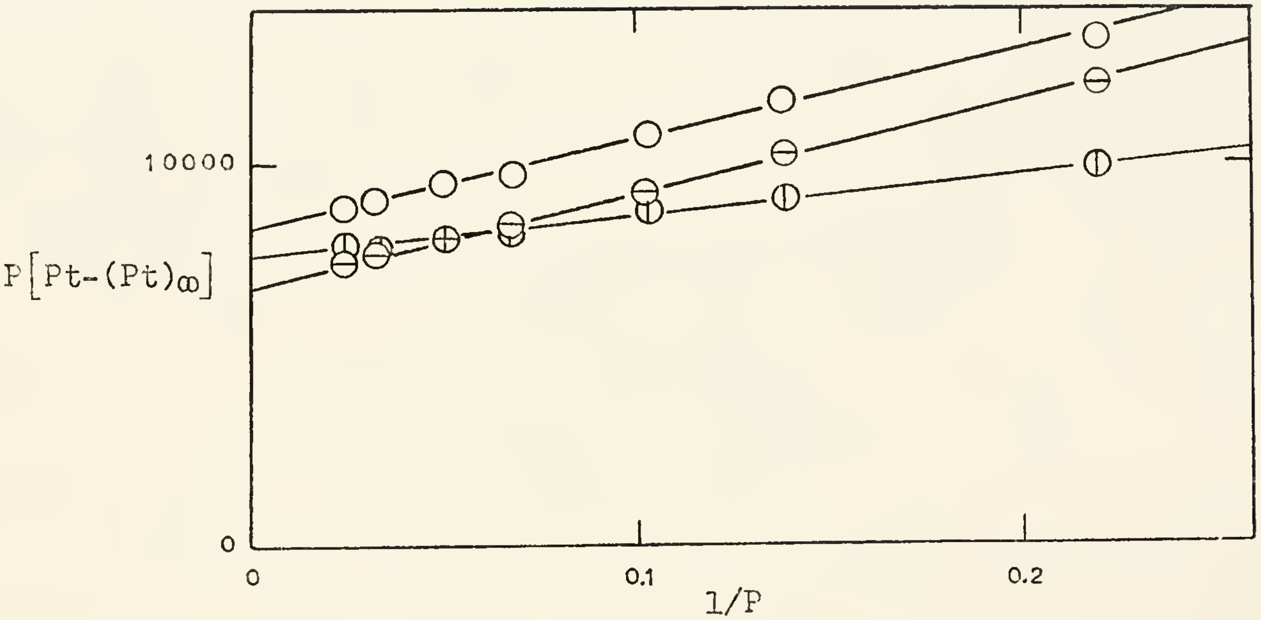

FIGURE 25. Test of functional form: $P[P_t-(P_t)_\infty] = k_1 + \frac{k_2}{P}$. Runs: ⊖ 42; ⦶ 420; ○ 425.

TABLE XXVIII

RHEOLOGICAL CONSTANTS

Run	Temp, °C	C_0	C_1	C_2	μ_∞, cP	Percent error in 1/t*
42	20	7733	1.91	22.96	1.96	0.95
	25	4013	4.68	18.45	1.56	1.75
44	20	18892	-16.52	20.16	2.75	13.7
	25	2173	7.36	14.54	1.62	1.19
418	20	3801	8.38	19.06	1.90	3.31
	25	7262	1.06	28.14	1.43	1.00
419	20	3669	9.49	20.18	1.83	1.27
	25	6660	1.29	24.86	1.51	0.75
420	20	5072	8.54	23.18	1.85	2.27
	25	7479	1.06	28.65	1.45	1.13
420B	20	6401	7.66	26.95	1.77	1.39
	25	6555	1.65	25.19	1.49	1.13
424	20	7845	2.51	22.77	2.07	4.04
	25	6931	2.27	26.86	1.51	1.17
424B	20	10052	-0.79	24.26	4.28	5.17
	25	6567	2.91	25.39	1.56	0.66
425	20	9042	1.35	24.68	2.07	4.25
	25	6846	2.93	26.63	1.54	1.12

---

*Maximum percentage deviation when measured values of 1/t are compared with values calculated using the estimate $1/t = P^3\left[(P+C_1)^{-1}-(P+C_2)^{-1}\right]/C_0$.

Determination of $g(\tau)$ from Experimental Measurements

Previous analysis yielded equation (5.5)

$$g(\tau) = \frac{\Upsilon(0)}{\tau^2} + \frac{1}{\tau^{3/2}} \int_0^\tau \Upsilon'(\tau_w) \frac{d\tau_w}{\sqrt{\tau-\tau_w}}$$

where

$$\Upsilon(\tau_m) = \frac{a\ell\tau_m}{\delta_m{}^2} \frac{d(\tau_m{}^2/t_m)}{d\tau_m} .$$

Using the functional form for $1/t$ obtained in the previous section and recalling that

$$t(P) = t_m(2L\tau_m/\delta_m),$$

it follows that

$$1/t = \frac{2L\tau_m{}^3}{d_0\delta_m}\left[\frac{1}{\tau_m+d_1} - \frac{1}{\tau_m+d_2}\right]$$

where

$$d_0 = C_0\delta_m/2L,$$

$$d_1 = C_1\delta_m/2L,$$

$$d_2 = C_2\delta_m/2L.$$

Hence,

$$\Upsilon(\tau_m) = \frac{2a\ell L}{\delta_m{}^3}\left\{\frac{5\tau_m{}^5}{d_0}\left[\frac{1}{\tau_m+d_1} - \frac{1}{\tau_m+d_2}\right] - \frac{\tau_m{}^6}{d_0}\left[\frac{1}{(\tau_m+d_1)^2} - \frac{1}{(\tau_m+d_2)^2}\right]\right\} ;$$

$$\Upsilon(0) = 0,$$

and $g(\tau)$ is given in integral form by:

$$g(\tau) = \frac{2a\ell L}{d_0\delta_m{}^3\tau^{3/2}}\int_0^\tau\left\{25\tau_W{}^4\left[\frac{1}{\tau_W+d_1} - \frac{1}{\tau_W+d_2}\right] - 11\tau_W{}^5\left[\frac{1}{(\tau_W+d_1)^2} - \frac{1}{(\tau_W+d_2)^2}\right] - 2\tau_W{}^6\left[\frac{1}{(\tau_W+d_1)^3} - \frac{1}{(\tau_W+d_2)^3}\right]\right\}\frac{d\tau_W}{\sqrt{\tau-\tau_W}}\,.$$

The integration, though tedious, is not difficult and yields the desired relationship between shear stress and shear rate for Milling Yellow:

$$\begin{aligned}g(\tau) = \frac{a\ell L}{d_0\delta_m{}^3}\Bigg\{&\frac{3d_1{}^5}{\tau(\tau+d_1)^2} - \frac{3d_2{}^5}{\tau(\tau+d_2)^2} - \\ &\frac{6628d_1{}^3}{105\ \tau} + \frac{6628d_2{}^3}{105\ \tau} + \\ &\frac{14368d_1{}^2(\tau+d_1)}{105\tau} - \frac{14368d_2{}^2(\tau+d_2)}{105\tau} - \\ &\frac{3744d_1(\tau+d_1)^2}{35\tau} + \frac{3744d_2(\tau+d_2)^2}{35\tau} + \\ &\frac{1024(\tau+d_1)^3}{35\tau} - \frac{1024(\tau+d_2)^3}{35\tau} + \\ &\left[\frac{3d_1{}^6}{\sqrt{\tau^3(\tau+d_1)^5}} - \frac{2d_1{}^5}{\sqrt{\tau^3(\tau+d_1)^3}}\right]\tanh^{-1}\sqrt{\tau/(\tau+d_1)} - \\ &\left[\frac{3d_2}{\sqrt{\tau3(\tau+d_2)^5}} - \frac{2d_2}{\sqrt{\tau^3(\tau+d_2)^3}}\right]\tanh^{-1}\sqrt{\tau/(\tau+d_2)}\Bigg\}\,.\end{aligned} \qquad (5.6)$$

At very high values of τ, this becomes simply

$$g(\tau_\infty) = \frac{96a\ell L(d_2-d_1)\tau}{5d_0\delta_m{}^3} = \frac{\tau}{\mu_\infty}\,.$$

At very low values of τ,

$$g(\tau) = \frac{a\ell L}{d_o\delta_m{}^3}\,\frac{2560}{63}\,\frac{(d_2-d_1)}{d_1d_2}\,\tau^3 \qquad (\tau\rightarrow 0),$$

or in terms of the constants tabulated in Table XXVIII,

$$g(\tau) = \frac{a\ell L^3}{C_o\delta_m{}^5}\,\frac{10240}{63}\,\frac{(C_2-C_1)}{C_1C_2}\,\tau^3 \qquad (\tau\rightarrow 0).$$

In the first part of this chapter it was found that the data of Peebles, Prados, and Honeycutts (1965) could be represented by the two-constant empirical relationship

$$g(\tau) = \frac{\mu_\infty\tau^2 + (3k/2)}{(\mu_\infty\tau^2 + k)^2}\,\tau^3 \qquad (5.7)$$

which had the limiting value as τ becomes small:

$$g(\tau) = 3\tau^3/2k. \qquad (\tau\rightarrow 0)$$

Comparison of this equation with the one just above provides the constant k to be used in the two-constant relationship based upon the present data:

$$k = \frac{21}{5120}\,\frac{C_o\delta_m{}^5}{a\ell L^3}\,\frac{C_1C_2}{(C_2-C_1)} \qquad (5.8)$$

A similar comparison for very high rates of shear yields the value of μ_∞ previously cited and tabulated:

$$\mu_\infty = \frac{5}{96}\,\frac{\delta_m{}^3}{a\ell L}\,(Pt)_\infty = 0.00534\,\frac{(C_2-C_1)}{C_2C_1}\,. \qquad (5.9)$$

Several typical plots of the rheological response of Milling Yellow are provided in Figure 26, based upon equation (5.6). Figure 27 provides a comparison between equations (5.6) and (5.7). Clearly k and μ_∞ are poorly predicted by equations (5.8) and (5.9).

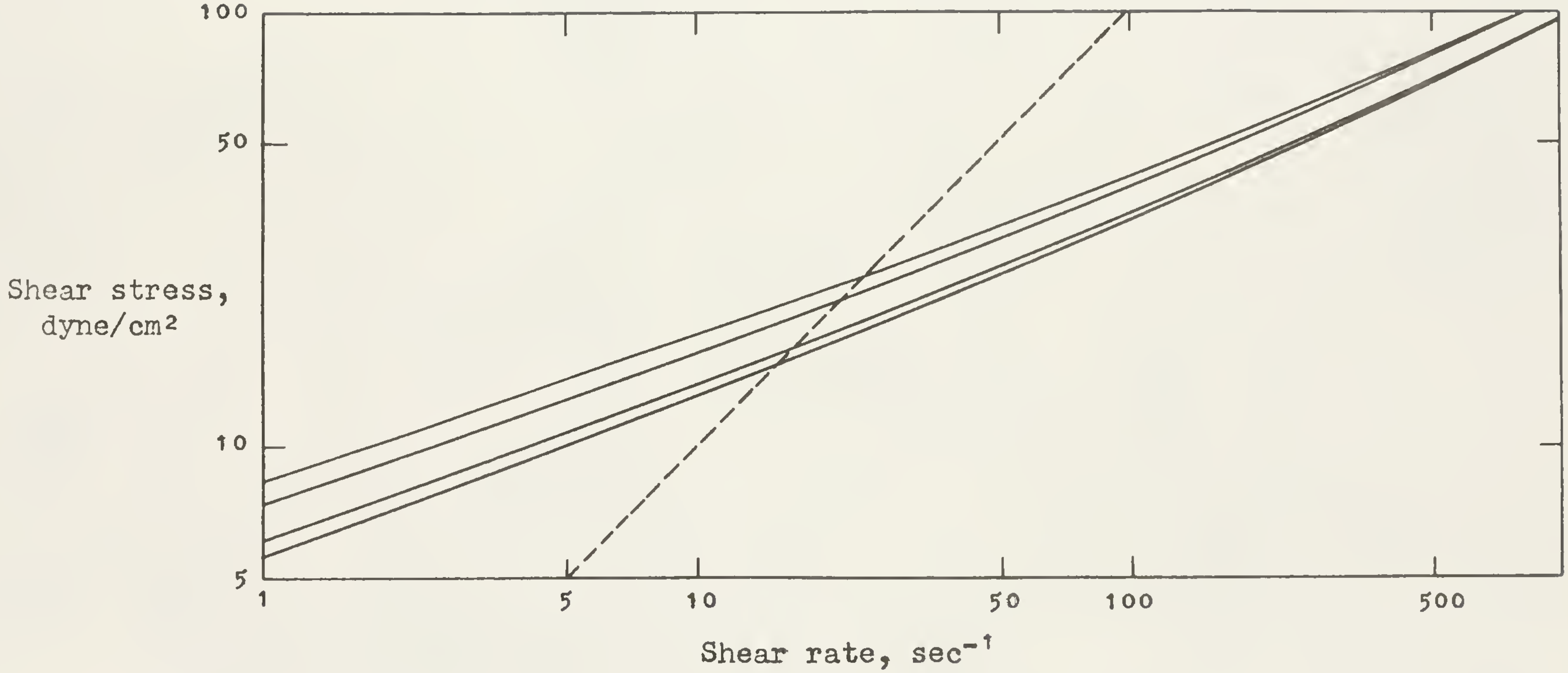

FIGURE 26. Constructed relationship between shear stress and shear rate for Milling Yellow at 25° C. From top to bottom, solid lines are runs 44, 424B, 420B, and 419. The dashed line represents a Newtonian fluid with a viscosity of 100 cP.

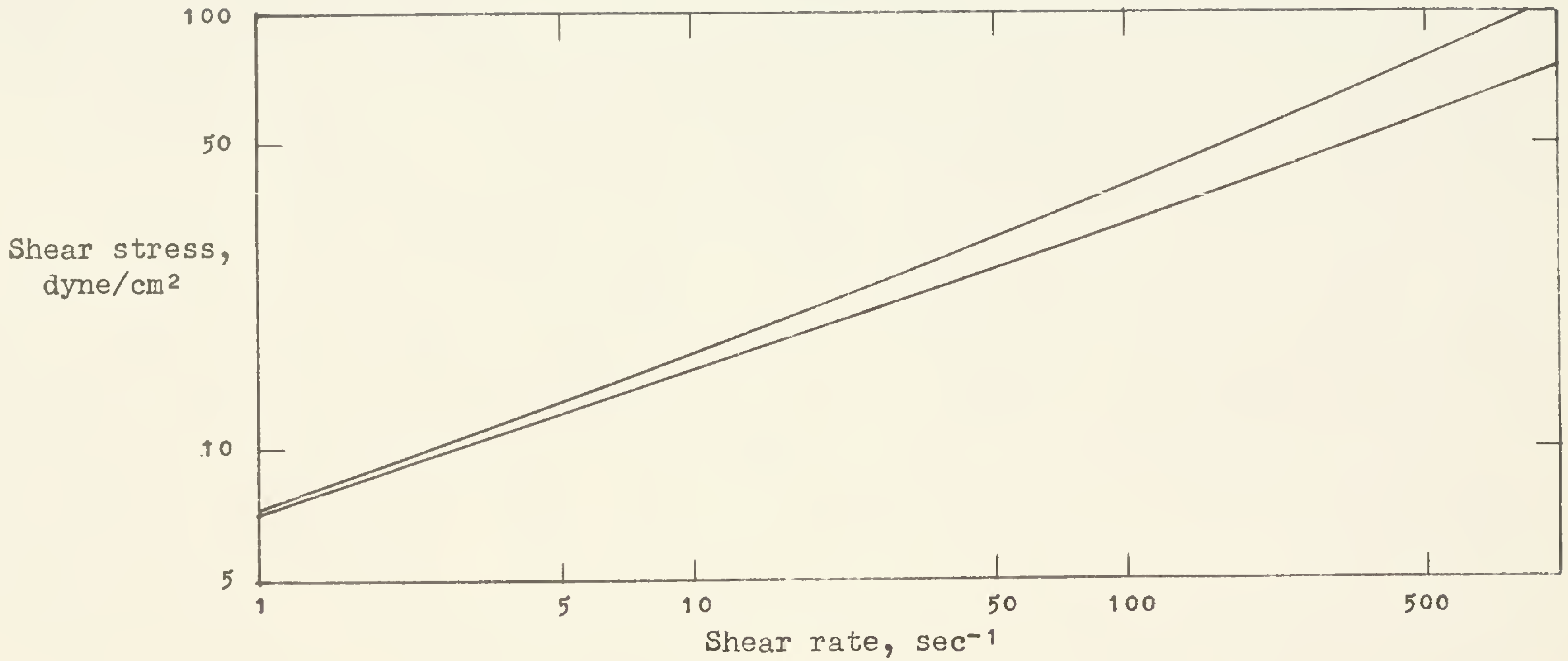

FIGURE 27. Comparison of equations (5.6) and (5.7), run 424B, at 25° C. Top line is calculated using equation (5.6); bottom line represents equation (5.7). At very high shear rates the lines will be parallel and have a slope of unity.

It should be noted that whatever form for $g(\tau)$ is chosen for a given application, there is a requirement that d_0, d_1, and d_2 (C_0, C_1, and C_2) be positive. This requirement fails in runs 44 and 424B at 20° C. There is no explanation for the anomalous measurements of run 44 which, due to the poor fit indicated by the last column of Table XXVIII, was not analyzed further. In run 424B the fit of the data is only slightly poorer than that for runs 424 and 425 suggesting that these data are valid. Since C_1 in this case is small, it seems appropriate to replace C_1 by zero in the fit of the data to obtain:

$$1/t = P^2\left(\frac{1}{P+C_2}\right)C_2/C_0.$$

This relationship may now be used in equation (5.5) to obtain the corresponding relationship between shear stress and shear rate. This has not been done in the present case.

Range of Application

The data of previous investigators, beginning with Prados (1957), have indicated that the viscosity remains constant when the shearing stress is less than about 5 to 10 dyne/cm^2 for 1.3 to 1.7 percent solutions at temperatures around 20° to 25° C. This point was discussed at some length in Chapter Two. It would be helpful if the experimental measurements reported in this chapter were able to cast some light into this area of concern. Unfortunately, the Höppler Rheo-Viscometer is an inappropriate instrument for the measurement of viscosities at lower shear stresses. Even when the force applied to the ball is reduced to its minimum value, so that the ball falls as slowly as 0.025 mm/sec, the shearing stress at the wall of the annulus will reach

$$\tau_w = \frac{P\delta}{2L} = \frac{(5\text{x}981 \text{ dyne/cm}^2)(0.007 \text{ cm})}{(2)(0.1365 \text{ cm})}$$

$$= 125 \text{ dyne/cm}^2$$

according to the previously derived relationship. Although the stress will become smaller at other points on the wall and drops linearly to zero as one passes from the wall to the center of the annulus, the shearing stress is much higher than the 5 to 10 dyne/cm² value at which a constant viscosity might be observed.

Evidence for a constant viscosity at low shear stress can be inferred from the success of the technique in Chapter Four which was used to calculate the birefringence based upon the assumption that at low flow rates the viscosity would remain constant. More direct data are available in the form of manometer readings made during the last two of the birefringence measurements.

According to Cornish (1928) the pressure gradient in a rectangular conduit flowing a Newtonian fluid will be

$$dp/dz = -2\delta_1\bar{u}\mu_N/\delta_2 S_0$$

where δ_1, δ_2, and S_0 are channel parameters defined in Chapter Two with numerical values tabulated in Appendix G, $\bar{u}$ is the average flow rate, and μ_N is the viscosity. The manometer estimate of the pressure gradient is well known:

$$dP/dz \;=\; (\rho_f - \rho)g_c h/\Delta z$$

where ρ_f is the density of the manometer fluid, ρ is the density of the medium, g_c is the gravitational constant, h is the difference in fluid levels in the manometer, and Δz is the distance between the manometer taps.

Values for the manometer readings, flow rates, and corresponding viscosities are tabulated in Table XXIX. If the first two readings of run 424 are discarded due to their anomalous temperatures, the remaining data for both trials indicate a reasonable likelihood that constant viscosities in the neighborhood of 100 and 125 cP were observed at the beginning of the two runs. It must be noted that this conclusion could be invalidated if a previous assumption — that normal stress functions are negligible for Milling Yellow solutions — fails.

When the response of a Newtonian fluid having a viscosity of 100 cP is superposed on the previous plot of Milling Yellow's rheological response given in Figure 27, it will be noted that the intersection occurs at τ = 20 dyne/cm^2, about twice the upper end of the linear range observed by Prados (1957) and others. In the absence of more convincing evidence, it will be assumed that this intersection is valid, and the following relationship for $g(\tau)$ is recommended for Milling Yellow over the full range of shear stresses:

TABLE XXIX

ESTIMATION OF APPARENT VISCOSITY

Run 424:

Flow rate, gm/sec	Temp, °C	Manometer head, cm*	Apparent viscosity, cP
2.50	24.9	8.13	157.5
5.53	25.3	8.26	72.0
6.34	24.4	13.21	100.5
9.09	24.3	18.80	99.8
12.82	24.3	23.62	88.8
20.78	24.5	28.96	69.8
25.57	24.2	32.77	60.8

Run 425:

Flow rate, gm/sec	Temp, °C	Manometer head, cm*	Apparent viscosity, cP
1.99	24.2	5.33	129.0
3.50	24.2	9.14	125.8
3.60	23.8	9.91	132.5
5.71	23.8	13.72	115.8
7.78	23.8	17.53	109.5
12.64	23.8	21.59	82.2
16.00	23.8	29.46	88.8

---

*Manometer fluid was reagent grade CCl_4, S.G. = 1.584; manometer taps were separated by 200.0 cm.

$$g(\tau) = \begin{cases} \tau/\mu_o & \tau \leqslant \tau_c \\ g(\tau) \text{ from equation (5.6)} & \tau > \tau_c \end{cases}$$

where

$$\mu_o = \tau_c/g(\tau_c)$$

and

$$\tau_c = 20 \text{ dyne/cm}^2.$$

When convenience of form is an important consideration, $g(\tau)$ may be obtained from equation (5.7) over the upper range of shear stresses; however, the constants in the equation must be obtained by experiment since comparisons of equations (5.6) and (5.7) at very low and very high shear rates do not provide adequate estimates for the interrelationship between the constants in the two expressions.

CHAPTER SIX

DISTRIBUTION OF SHEAR RATES IN RECTANGULAR CONDUITS

Even if the functional dependence of the rheological and optical properties upon shear rates is well defined for a birefringent medium, the prediction of fringe patterns for steady axial flow through a given cross-section requires a hypothetical velocity distribution within the channel. Once this is obtained, the distribution of shear rates follows by differentiation.

The velocity distribution for Milling Yellow flowing in rectangular conduits has not been calculated and is not determined in this dissertation. The distribution of other fluids in rectangular sections has been discussed at length in Chapter Two. The present chapter evaluates these distributions in terms of their applicability to Milling Yellow.

Power-Law Fluids

Of the non-Newtonian materials for which flows in rectangular pipes have been studied, only power-law fluids have received significant attention. Since there is some evidence that Milling Yellow has a behavior similar to a power-law fluid over a certain range of lower shear rates, it appears appropriate to compare predicted pressure drops for power-law substances with the pressure drop measured in the rectangular conduit with Milling Yellow.

The relationship $g = g(\tau)$ has been plotted in Figures 26 and 27 for run 424B. At shear rates less than 10 sec^{-1} these data are well represented by the power-law expression:

$$\tau = 7.35\ g^{1/3}.$$

Substituting $K = 7.35$ and $m = 1/3$ into equation (2.5), obtained by Wheeler and Wissler (1965) for square pipes, there results, for mass flow rate G,

$$-dp/dz = 38.1\ G^{1/3}$$

where the sides of the square in equation (2.5) have been replaced by the geometric mean of the average length of the walls in the nearly square conduit. For the manometer described in the previous chapter,

$$-dp/dz = 2.83\ h.$$

Hence, if Milling Yellow behaves as a power-law fluid, the manometer readings should vary with the flow rate according to the simple relationship:

$$h = 13.5\ G^{1/3}.$$

The manometer readings predicted by this equation are plotted in Figure 28 together with the manometer readings given in Table XXIX for runs 424 and 425. Manometer values predicted for Newtonian fluids having viscosities of 100 and 125 cP are represented by dashed lines in the same figure. The $g(\tau)$ relationship for run

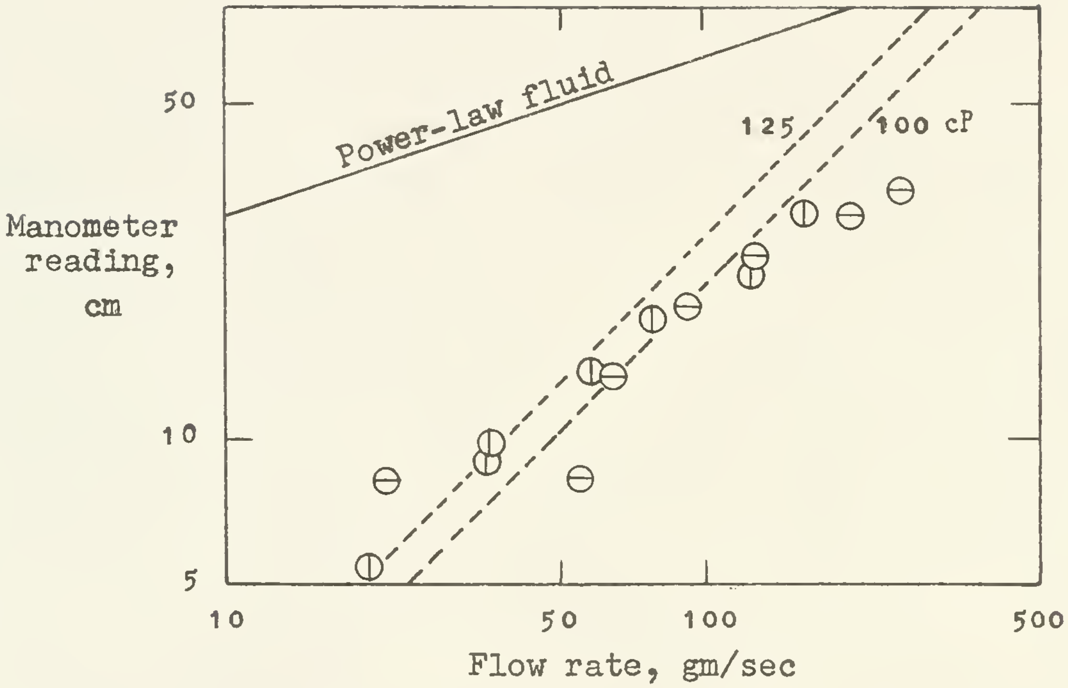

FIGURE 28. Manometer readings compared with those expected for Newtonian fluid (dashed lines having the indicated viscosities) or a power-law fluid. Runs: ⊖ 424; ⦶ 425.

425 ($\tau = 7.46\ g^{1/3}$) differs so little from that for run 424 that the separate manometer prediction for run 425 ($h = 13.7\ G^{1/3}$) is not plotted.

It will be noted that the $g(\tau)$ relationships are based upon viscometric measurements made at 25° C, while the average temperature for runs 424B and 425 in the conduit were 24.6° and 23.9° C respectively. Variations in the apparent viscosity of Milling Yellow with temperature (Appendix I) average 10 to 15 percent per degree Celsius. A correction of this order would yield a good correlation between runs 424B and 425, but the disparity between the data and the power-law model would persist.

Since the power-law model predicts pressure gradients inaccurately, it is unlikely that an accurate velocity distribution can be derived from the model. Yet even an insufficient solution for the distribution may represent an improvement over the Newtonian assumption that the viscosity is constant.

Although Wheeler and Wissler (1965) have criticized Schechter's (1961) variational coefficients as imprecise, Schechter's solution for power-law flow in square pipes has two advantages: the coefficients are tabulated and the velocity distribution is scaled to the measured flow rate in the channel. In a square pipe symmetry reduces the number of coefficients in Schechter's solution (equation 2.4) from six to four. Three of these are plotted as a function of the power-law exponent in Figure 29. The

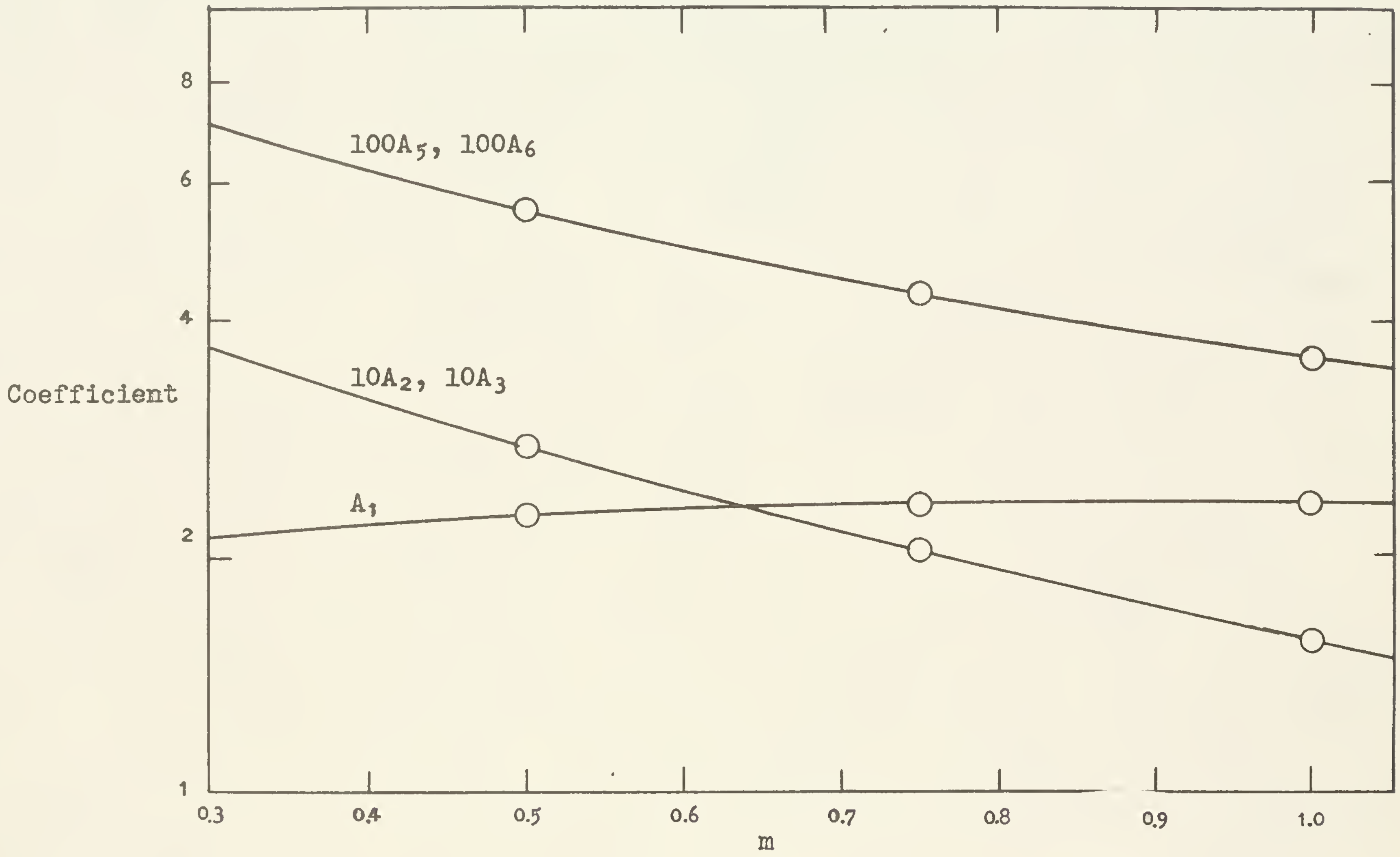

FIGURE 29. Schechter's (1961) coefficients plotted as function of power-law exponent.

fourth, which cannot be plotted on a logarithmic scale, has values of 0.0289 at $m = 1$, 0.0007 at $m = 0.75$, and -0.0285 at $m = 0.5$. Extrapolation gives $A_4 = -0.0472$ at $m = 1/3$. Using this estimate and obtaining the remaining coefficients by extrapolating in Figure 29 as shown, equation (2.4) becomes:

$$\begin{aligned} u = (4G/\delta_1\delta_2) \Big\{ & 2.16 \sin(\pi x/2\delta_1) \sin(\pi y/2\delta_2) + \\ & 0.349 \big[\sin(3\pi x/2\delta_1) \sin(\pi y/2\delta_2) + \\ & \quad \sin(\pi x/2\delta_1) \sin(3\pi y/2\delta_2) \big] - \\ & 0.0472 \sin(3\pi x/2\delta_1) \sin(3\pi y/2\delta_2) + \\ & 0.0683 \big[\sin(5\pi x/2\delta_1) \sin(\pi y/2\delta_2) + \\ & \quad \sin(\pi x/2\delta_1) \sin(5\pi y/2\delta_2)\big]\Big\}. \end{aligned}$$

The shear rate is obtained directly by differentiation.

Some Alternatives

Neither Cornish's (1928) relationship for a Newtonian fluid, equation (2.3), nor the power-law approximation just cited may be used with confidence to predict the velocity distribution for Milling Yellow in a rectangular pipe. Alternatives require the adoption of more realistic rheological relationships such as those derived in Chapter Five and the choice of a suitable analytical technique for its utilization. These choices are not independent since the analytical technique will be influenced by the complexity of the differential equation which results from substitution of the rheological relationship into the equilibrium equation. Of the analytical methods surveyed in Chapter Two, those of Litvinov (1968) and Röthemeyer (1970) seem to possess the necessary generality. It also seems necessary to resolve the possibility raised by Wheeler and Wissler (1966) that significant secondary flows are present in the channel.

CHAPTER SEVEN

SUMMARY AND CONCLUSIONS

This dissertation has consisted of three nearly separate studies which have been discussed individually in Chapters Three, Four, and Five. The major findings of these chapters may be summarized as follows.

Optical Analysis of Birefringent Flow Fields

An aqueous solution of Milling Yellow provides an excellent medium for the visualization of flows in a variety of processes. At very low flow rates the fringe patterns which result from its birefringence may be used to calculate directly the velocity and pressure distributions of two-dimensional flows.

A like determination of three-dimensional flow fields directly from birefringent patterns is not practical, but the inverse process — hypothesizing a flow field and checking it from the fringe pattern — is indeed practical, even at flow rates for which the optical and rheological properties of the medium do not vary linearly with the shear rate. In such cases it is shown that the fringe pattern will depend upon the effective optical parameters Ψ and ΔN which are in turn related explicitly to the optical properties of the medium: Δn, ψ, and Θ.

It is assumed that Δn and ψ are uniquely determined by the magnitude of the shear rate:

$$\Delta n = \Delta n(g),$$

$$\psi = \psi(g),$$

and that

$$\Theta = \tan^{-1}\left[\frac{\partial g/\partial y}{\partial g/\partial x}\right].$$

Any hypothetical velocity which can be differentiated will yield a distribution of shear rates from which the optical coefficients may be calculated point by point. The fringe pattern may then be computed by an iterative process which, in effect, replaces the medium by a succession of linear wave plates.

Optical Properties of the Medium

Standard solutions of Milling Yellow cannot be prepared with reproducible properties from the commercial dyestuff. For this reason the birefringence Δn has been measured in the past either just prior to a given test or just after, using a two-dimensional flow regime. The present study shows that at low flow rates, in the vicinity of the wall, the square of the birefringence varies linearly with the mass flow rate, providing a simple means of determining either once the other is known. Plots of the fringe order at the wall, squared, versus the flow rate confirm this finding, and birefringences for the various test samples are calculated from the data.

The orientation angle ψ is not measured in the present study, but an empirical form is provided for previously published data.

Rheological Properties of the Medium

Previous authors have demonstrated that Milling Yellow is well represented, though not uniquely, by a three-constant empirical relationship, the Powell-Eyring equation. The same data are shown in the present study to be satisfied by a two-constant relationship in which the general form $g = g(\tau)$ is used rather than the previous form $\tau = \tau(g)$. There is evidence that the two-constant form is invalid at shear stresses above about 500 dyne/cm^2.

Data are presented, both in the text and in the appendices, which show the variation of Milling Yellow's rheological properties with time, with temperature, and with concentration. Based on measurements made with the Höppler Rheo-Viscometer, a sliding ball viscometer, rheological constants are provided from which the relationship between shear stress and shear rate for Milling Yellow may be obtained. The resultant expression, though complicated, requires only three coefficients which are tabulated for the samples in the present investigation.

The use of the Höppler Rheo-Viscometer to obtain basic rheological information is supported by an analysis of the flow in the instrument and a full discussion of the assumptions upon which the analysis is based. A principal advantage of the method given is that the constitutive form for the material's rheological response to stresses need not be known to employ the instrument, and indeed, this form may be constructed by quadrature from the mathematical form of the experimental results. For the Höppler Rheo-Viscometer it is necessary to assume that flow past the sliding ball may be modeled on flow through an eccentric annulus having a fixed "effective length" which is obtained by calibration. In a falling cylinder viscometer it is hypothesized that the effective length will be approximated by the actual length of the cylinder. The effective length of the Höppler instrument is shown to vary less than 1 percent for a wide range of shear stresses in the annulus and for a change in the viscosity of the Newtonian calibration fluid of more than an order of magnitude. Solutions are provided to the viscometer equation for Newtonian fluids, power-law substances, bilinear materials, and, as stated earlier, Milling Yellow.

Other Findings

The prediction of fringe patterns requires a knowledge of the distribution of shear rates in the conduit through which the fluid flows. For the special case of a rectangular conduit (in which the birefringence was measured) methods for obtaining such relationships were reviewed, but a solution of the problem was not attempted.

APPENDIX A

THE EFFECTIVE BIREFRINGENCE AND ORIENTATION ANGLE OF THE OPTICAL ELLIPSE FORMED BY THE INTERSECTION OF THE OPTICAL ELLIPSOID WITH THE PLANE ORTHOGONAL TO THE PATH OF LIGHT

Consider an ellipsoid of circular cross-section (prolate spheroid) with the surface

$$(x'/n_2)^2 + (y'/n_2)^2 + (z'/n_1)^2 = 1,$$

where n_1 and n_2 are the major and minor axes respectively. In the initial position the x'y'z'-coordinate system is coincident with the xyz-coordinate system. If the x'y'z' system is rotated first through an angle Θ about the z'-axis and then through an angle ψ about the y'-axis, then the relation between the coordinate systems will be:

$$\begin{bmatrix} x' \\ y' \\ z' \end{bmatrix} = \begin{bmatrix} \cos\psi & 0 & \sin\psi \\ 0 & 1 & 0 \\ -\sin\psi & 0 & \cos\psi \end{bmatrix} \begin{bmatrix} \cos\Theta & \sin\Theta & 0 \\ -\sin\Theta & \cos\Theta & 0 \\ 0 & 0 & 1 \end{bmatrix} \begin{bmatrix} x \\ y \\ z \end{bmatrix}.$$

If the center of the coordinate system (x',y',z') is translated to the point (x_0,y_0,z_0), then the new relation can be obtained by substituting $(x-x_0)$ for x and $(y-y_0)$ for y in the column matrix to the right. Expanding the matrices and substituting into the equation for the surface of the ellipsoid yields:

$$1 = \frac{[(x-x_0)\cos\psi\cos\Theta + (y-y_0)\cos\psi\sin\Theta + z\sin\psi]^2}{(\bar{n} - \frac{\Delta n}{2})^2}$$

$$+ \frac{[(x-x_0)\sin\Theta + (y-y_0)\cos\Theta]^2}{(\bar{n} - \frac{\Delta n}{2})^2}$$

$$+ \frac{[-(x-x_0)\sin\psi\cos\Theta - (y-y_0)\sin\psi\sin\Theta + z\cos\psi]^2}{(\bar{n} + \frac{\Delta n}{2})^2}$$

where the major and minor axes have the dimensions $\bar{n} \pm \frac{\Delta n}{2}$.

The ellipsoid so defined conforms to the description of the optical ellipsoid shown in Figure 3. The corresponding optical ellipse is formed by the intersection of this surface, $F(x,y,z) = 0$, with the plane $x = x_0$:

$$\frac{[(y-y_0)\cos\psi\sin\Theta + z\sin\psi]^2}{(\bar{n} - \frac{\Delta n}{2})^2} + \frac{[(y-y_0)\cos\Theta]^2}{(\bar{n} - \frac{\Delta n}{2})^2}$$

$$+ \frac{[-(y-y_0)\sin\psi\sin\Theta + z\cos\psi]^2}{(\bar{n} + \frac{\Delta n}{2})^2} = 1 .$$

Designating

$$A_1 = \cos\psi\sin\Theta / (\bar{n} - \tfrac{\Delta n}{2}),$$
$$A_2 = \cos\Theta / (\bar{n} - \tfrac{\Delta n}{2}),$$
$$A_3 = -\sin\psi\sin\Theta / (\bar{n} + \tfrac{\Delta n}{2}),$$
$$A_4 = \sin\psi / (\bar{n} - \tfrac{\Delta n}{2}),$$
$$A_5 = \cos\psi / (\bar{n} + \tfrac{\Delta n}{2}),$$

and substituting yields upon rearrangement:

$$(A_1{}^2+A_2{}^2+A_3{}^2)(y-y_0)^2 + 2(A_1A_4+A_3A_5)(y-y_0)z$$
$$+ (A_4{}^2+A_5{}^2)z^2 = 1.$$

To remove the cross-product term, set

$$(y-y_0) = -N_1 \sin\Psi + N_2 \cos\Psi,$$

$$z = N_1 \cos\Psi + N_2 \sin\Psi,$$

and substitute into the equation just given to obtain

$$B_1N_1{}^2 + B_2N_1N_2 + B_3N_2{}^2 = 1$$

where

$$\begin{aligned} B_1 &= (A_1{}^2+A_2{}^2+A_3{}^2) \sin^2\Psi - 2(A_1A_4+A_3A_5) \sin\Psi \cos\Psi \\ &\quad + (A_4{}^2+A_5{}^2) \cos^2\Psi, \\ B_2 &= 2(A_1A_4+A_3A_5) \cos 2\Psi - \\ &\quad (A_1{}^2+A_2{}^2+A_3{}^2-A_4{}^2-A_5{}^2) \sin 2\Psi, \\ B_3 &= (A_1{}^2+A_2{}^2+A_3{}^2) \cos^2\Psi + 2(A_1A_4+A_3A_5) \sin\Psi \cos\Psi \\ &\quad + (A_4{}^2+A_5{}^2) \sin^2\Psi. \end{aligned}$$

If N_1 and N_2 are to be identified as the principal axes of the ellipse, then it is necessary that

$$B_2 = 0$$

which is satisfied if

$$\Psi = \tfrac{1}{2} \tan^{-1}\left[\frac{2\,(A_1A_4+A_3A_5)}{A_1{}^2+A_2{}^2+A_3{}^2-A_4{}^2-A_5{}^2}\right].$$

The birefringence and the orientation angle have been defined respectively as the difference between the lengths of the major and minor axes of the optical ellipse and the angle between the principal flow direction ($\hat{k}$) and the major optic axis. From these definitions it is clear that the effective orientation angle is identically Ψ as just derived. The effective birefringence is simply

$$\Delta N = \frac{1}{\sqrt{B_1}} - \frac{1}{\sqrt{B_2}}$$

or

$$\begin{aligned}\Delta N = {} & \left[(A_1{}^2+A_2{}^2+A_3{}^2)\sin^2\Psi - 2(A_1A_4+A_3A_5)\sin\Psi\cos\Psi \right.\\ & \left. + (A_4{}^2+A_5{}^2)\cos^2\Psi\right]^{-1/2} \\ - {} & \left[(A_1{}^2+A_2{}^2+A_3{}^2)\cos^2\Psi + 2(A_1A_4+A_3A_5)\sin\Psi\cos\Psi \right.\\ & \left. + (A_4{}^2+A_5{}^2)\sin^2\Psi\right]^{-1/2} .\end{aligned}$$

APPENDIX B

PREPARATION OF MILLING YELLOW SOLUTIONS

Two stock solutions of Milling Yellow were prepared, the first in April, 1972, and the second in March, 1973. The procedures were the same in principle as those followed by previous investigators such as Peebles, Garber, and Jury (1953). Changes in the properties of these solutions with time are discussed in Appendix H. The manner in which the concentration was measured is discussed in Appendix L.

Original Stock Solution

Seven and one-half liters of tap water were heated to about 60° C in a galvanized iron pail using an immersion heating element. To the warm water was added 113 grams of commercial dye, Milling Yellow NGS, supplied by Keystone Aniline and Chemical Company, Chicago, Illinois. The mixture was stirred until all of the dye particles had sunk beneath the surface, after which an agitator of the egg-beater type was introduced and heating continued. The temperature was raised to and maintained at a temperature just below the boiling point, typically 93° C. No attempt was made to control the nominal 1.5 percent concentration for evaporation losses.

Periodically the mixture was inspected. The preparation was considered complete when three criteria were met:

Clarity. — Though deeply colored, the solution was clear. Specifically, the end of a stirring rod could be seen 5 cm beneath the surface within the opaque container.

Absence of residue. — A sample of the hot solution, taken from the bottom of the pail with a hollow tube, could be released at the surface of the fluid without observing any undissolved dye.

Birefringence. — A small sample, rapidly cooled, remained clear and exhibited birefringence when stirred or swirled between crossed polarizers.

Having met these criteria, the solution was added to the polystyrene container in which the bulk stock was stored. The earlier preparations were allowed to stand and cool for a sufficient time that the temperature of the bulk stock would never rise above 45° C in the polystyrene container.

It was noticed that any preparation which was allowed to stand contained a small amount of sedimentation despite the test for residue. The warm solution has a viscosity not appreciably different from water, and it was easy to decant the clear solution and include the residue in the bottom of the pail at the beginning of the next preparation. The sediment which remained at the bottom of the pail at the end of the preparation sequence was discarded.

Fresh Stock Solution

Preparation of the fresh stock solution followed the procedure used for the original stock solution with the following changes:

The fresh dye, though provided by the same supplier, was from a different lot.

The galvanized pail was replaced by two 3-gallon, heavy-weight aluminum containers. Both were heated on hot plates. One was agitated with a magnetic stirrer. The other was not. No difference between stirred and unstirred samples was evident.

Distilled water was used in place of tap water.

The amount of Milling Yellow used in the preparation of the separate batches was not controlled, two "heaping cupfuls" being used each time for each container; however, the total amount of Milling Yellow was weighed as a single quantity before preparation of the fresh stock solution began, and the total mass of the bulk stock was determined when preparation was complete. On this basis the nominal dye concentration was:

$$q = \frac{1351.8 \text{ gm of dye}}{83500 \text{ gm of solution}}(100) = 1.62 \text{ percent.}$$

Criteria for lack of residue and for clarity were retained. The criterion for birefringence was eliminated as unnecessary.

Following the separate preparation of the individual batches, the entire bulk stock was heated to 50° C and then cooled slowly while the stock was circulated between two containers. The temperature difference between the containers was never greater than 0.1 C°, so that a corresponding uniformity of concentration was inferred. The 50° C temperature was determined by the heating capacity of the immersion heating elements which were used; however, this temperature exceeds by a comfortable margin the transition temperature of about 30° C below which Milling Yellow becomes birefringent.

APPENDIX C

VARIATION IN FLOW RATE AS AMOUNT OF LIQUID IN OVERHEAD TANK DECREASES

Referring to Figure 10, and recalling that the pump is not operated continuously, it will be evident that the amount of fluid in the overhead tank decreases during each run with a corresponding reduction in the pressure head. A test was conducted to determine if this reduction had a significant effect upon the flow rate in the channel.

The flow rate used during the test was about six times higher than any used during later testing so that the magnitude of the effect was increased proportionately. The procedure was as follows.

The test was conducted in Channel 6. Thirty seconds after the control valve at the bottom of the conduit was opened, four consecutive samples of the efflux were taken for timed intervals of roughly ten seconds each. A photograph of the birefringent pattern was taken before each of these samplings. At the end of this sequence, about two minutes in all after the valve was opened, the flow was halted and the efflux for each of the timed intervals was weighed and its temperature recorded. These data are given in Table C-I.

TABLE C-I

CHANGE IN FLOW RATE AS OVERHEAD TANK EMPTIES

Order sampled	Efflux, gm	Time, sec	Flow Rate, gm/sec	Temp, °C	Order, temp measurement
1	1831.9	10.1	181.4	21.2	2
2	1699.8	9.5	178.9	21.4	1
3	2010.9	11.1	181.2	21.2	3
4	1110.1	6.3	176.2	20.8	4

From these data the flow rate during the test was $G = 179.4 \pm 2.4$ gm/sec. The standard deviation in the flow rate is only slightly higher than the 1 percent variation to be expected from the ±0.1-sec precision of the timer. The photographs taken during the run are indistinguishable. The temperature variation appears to have resulted from cooling of the samples which remained on the floor between weighings. The floor temperature is noticeably cooler than the ambient temperature in the vicinity of the overhead tank.

On the basis of this test it was concluded that variations in the fluid level of the overhead tank have a negligible effect upon the flow rate in the channels.

APPENDIX D

ALIGNMENT OF POLARIZING ARRAYS

The polarizing material used in this dissertation was commercial Polaroid sheeting secured to the inside surfaces of two parallel plates of transparent plexiglass. One of the two longer edges of each plate was milled to provide a reference surface, after which the two plates were clamped together and drilled. When the clamp was removed threaded rods were passed through the holes and provided with nuts which could be tightened to secure the plates at any desired location on the rectangular conduit through which the Milling Yellow was observed in flow. The individual elements of the polarizing arrays shown in Figure 12 were aligned with the milled edge of the plastic plates in the following manner.

On a piece of graph paper were drawn a series of 30 mm by 5 mm rectangles. These rectangles were oriented so that some were horizontal, some vertical, some were sloped at 45° angles to the right, and some at 45° to the left. The Polaroid sheeting was laid on top of the graph paper and secured to it by a thin coating of rubber cement, the optical axis of the sheeting lying parallel with one axis of the graph paper. Rectangular strips were then cut from the Polaroid sheet along the lines already drawn.

One of the plastic plates was laid on a second sheet of graph paper having the same scale, the milled edge of the plate coinciding with one axis of the paper. One of the rectangular bits of sheeting was selected by observing the orientation of its optic axis by means of the graph paper still cemented to its under side. This rectangle was slid carefully beneath the plate and maneuvered until, looking through both the transparent plastic and the polarizing material, it could be seen that the grid on the rectangle was aligned with the grid on the underlying sheet. When this was accomplished the small strip was taped in place and its alignment reconfirmed, after which the graph-paper backing was carefully peeled away. The process was repeated until all of the elements shown in Figure 12 had been secured in place. For strips having 45° orientations it was necessary to align the milled edge with a line drawn at 45° on the underlying graph paper, but this posed no difficulties.

After the plexiglass plates were secured to the conduit, the alignment was completed by aligning the milled edges with each other outside the wall of the conduit and parallel with that wall, or, alternately, by aligning each milled edge in turn to a common vertical reference, usually the centerline of the bolts which hold the conduit together.

APPENDIX E

CALIBRATION OF THE HÖPPLER RHEO-VISCOMETER

The instrument used in this investigation was the "Rheo-Viscometer nach Höppler," serial number 002770, manufacturer: VEB Prüfgeräte-Werk Medingen, Sitz Freital, D. D. R. The serial number of the cylinder was 31871.

According to the instruction booklet provided by the manufacturer, the viscosity of a Newtonian fluid is obtained by use of the simple expression

$$\mu_N = KPt$$

where K is a calibration constant, P is the force applied to the ball divided by the cross-sectional area of the ball, and t is the time of fall for a displacement of 3.00 cm. Although both cylinder and ball have dimensions which are specified to a few thousandths of a centimeter, the closeness of fit requires calibration for each combination of cylinder and ball. Further, it is necessary that the orientation of both ball and cylinder be noted so that there is no rotation of the one relative to the other each time the cylinder is removed and replaced.

The ball and cylinder used in this dissertation were calibrated on May 3, 1973, using a "normal fluid" supplied by the manufacturer. The viscosity of the normal fluid was certified as 11.06 cP at 20° C if used within three months of April 2, 1973, the date at which it was standardized. Temperature control at 20° C was provided by a Haake Constant Temperature Circulator, Model F423, serial 71011. A partially insulated container of ice water was immersed in the bath of the Haake circulator during the calibration to provide ambient cooling. The ice water was replaced at about ten-minute intervals.

The calibration data are provided in Table E-I. The temperature recorded here are from the gas-jacketed, precision thermometer located adjacent to the cylinder in the constant temperature bath of the viscometer (see Figure 21). From these calibration data a separate calibration constant K was calculated for each value of P, the so-called "average stress" on the sliding ball. These data are plotted in Figure E-1. It will be noted that K varies very little along the ordinate of the graph.

The form of this curve suggests the presence of a frictional resistance in the viscometer bearings. This supposition led to a corrected viscometer equation of the form

$$\mu_N = K(P-P_f)t$$

where P_f is the frictional resistance. Rearrangement of this equation into the form

$$Pt = P_f t + \mu_N/K$$

shows that the slope d(Pt)/dt would have a value P_f when

TABLE E-I

CALIBRATION DATA

P, gm/cm^2	t, sec	T, °C
250	8.4	20.00
	8.4	20.00
	8.4	20.00
	8.4	20.00
	8.4	20.00
K_{250} = 0.00527		
200	10.5	20.00
	10.5	20.00
	10.4	20.00
	10.4	20.00
	10.5	20.00
K_{200} = 0.00529		
160	13.0	20.00
	13.1	20.00
	13.0	20.00
	13.0	20.00
	13.0	20.00
K_{160} = 0.00531		
100	20.9	20.00
	20.8	20.00
	20.8	20.00
	20.7	20.00
	20.7	20.00
K_{100} = 0.00532		
80	25.9	20.00
	26.0	20.00
	26.0	20.00
	26.0	20.00
	25.8	20.00
K_{80} = 0.00533		
50	41.5	20.00
	41.6	20.00
	41.5	20.00
	41.6	20.00
	41.6	19.98
K_{50} = 0.00532		

P, gm/cm^2	t, sec	T, °C
40	51.9	20.00
	51.9	20.00
	51.9	20.00
	51.9	20.00
	51.8	20.02
K_{40} = 0.00533		
25	83.3	20.02
	83.3	20.00
	83.4	19.96
	83.4	19.94
	83.5	20.02
	83.3	20.02
	83.3	20.00
K_{25} = 0.00531		
20	104.5	20.00
	104.8	20.00
	104.8	20.02
	104.5	20.04
	104.9	20.00
K_{20} = 0.00528		
15	139.5	20.00
	139.9	20.00
	139.7	20.04
	139.7	20.02
	140.4	19.98
K_{15} = 0.00527		
10	211.6	19.96
	212.2	20.00
	212.8	20.00
	212.0	20.00
	212.2	20.00
K_{10} = 0.00521		
5	434.9	20.04
	435.8	20.02
	435.9	20.00
K_{5} = 0.00508		

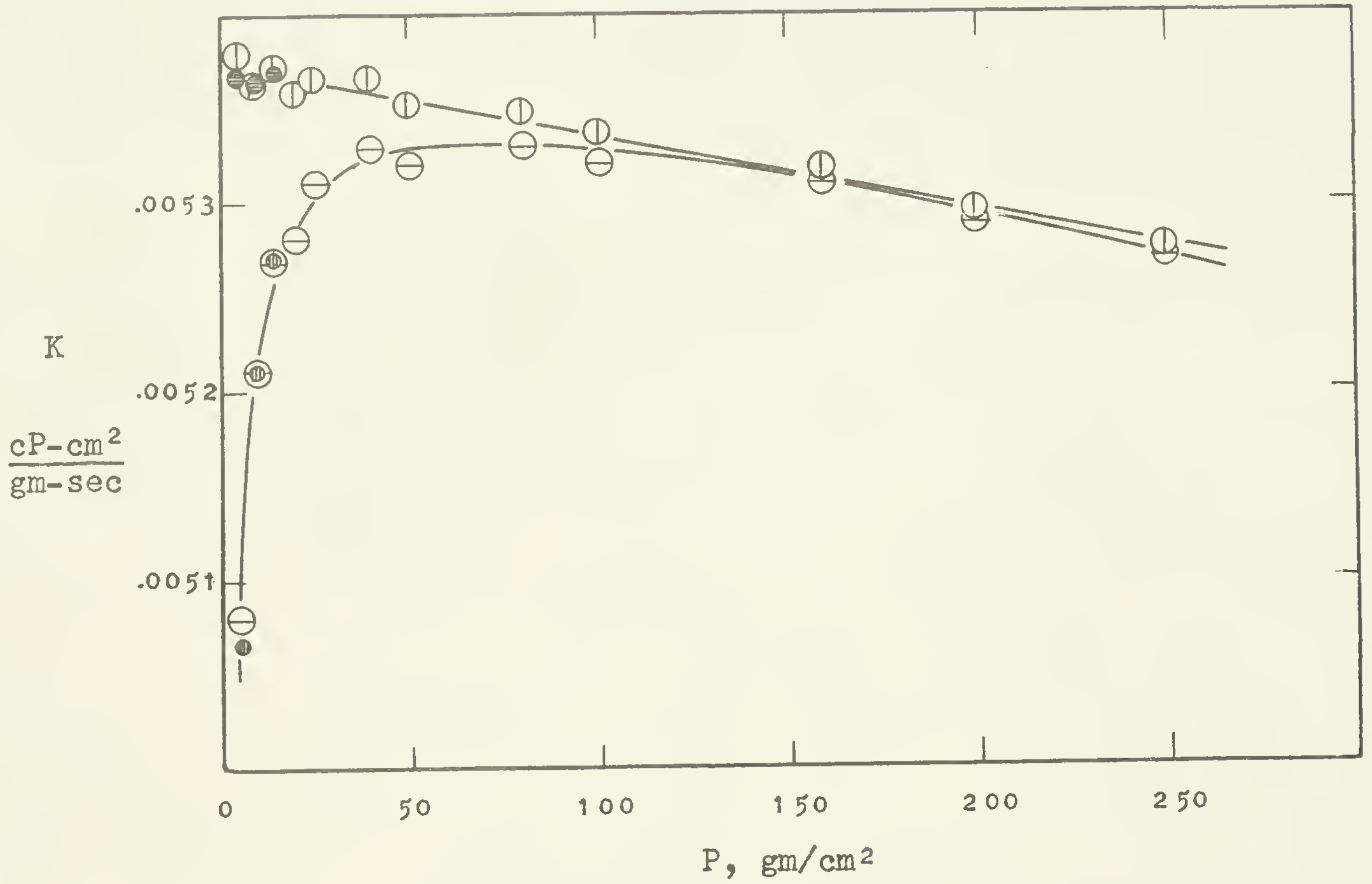

FIGURE E-1. Variation in calibration constant with load on ball. The larger circles are for the standardized calibration fluid, viscosity: 11.06 cP at 20° C. The smaller, shaded circles are for water, viscosity: 1.002 cP at 20°. The lower curve represents raw data. The straight line at the top represents the same data corrected for friction.

the product Pt was plotted versus t. When this was done (not shown) the result was $P_f = 0.28$ gm/cm^2. With this correction the calibration constant could be expressed as

$$K = \mu_N/(P-0.28)t.$$

Values of K calculated in this manner are plotted at the top of Figure E-1 and show a nearly linear variation in K with P. For the line drawn in Figure E-1,

$$K = \mu_N/(P-0.28)t = 0.00538 - 0.000000388P.$$

For most applications it may be stated with sufficient accuracy that

$$K = 0.00534 \text{ cP-cm}^2/\text{gm-sec},$$

the units to be used for μ_N in cP, P in gm/cm^2, and t in seconds. In consistent units (μ_N in poise, P in dyne/cm^2, t in seconds) $K = 5.44 \times 10^{-8}$.

As a check of the calibration, a distilled water sample ($\mu_N = 1.002$ cP at 20° C, according to Swindells, Coe, and Godfrey, 1966) was tested in the instrument. Because of a restriction on the use of the viscometer at lower viscosities (see Appendix J), only three points could be obtained, but these lay in the range ($P \leq 15$ gm/cm^2) where the frictional correction is most significant. As Table E-II and Figure E-1 confirm, the calibration previously performed is also valid for distilled water.

TABLE E-II

CALIBRATION CHECK (WATER)

P, gm/cm²	t, sec	T, °C
15	12.6	20.02
	12.7	20.02
	12.7	20.00
	12.7	20.00
	12.7	20.02
$K_{15} = 0.00527$		
10	19.3	20.02
	19.2	20.02
	19.3	20.04
	19.2	20.04
	19.2	20.04
	19.2	20.02
	19.3	20.02
	19.2	20.00
	19.2	20.00
	19.2	20.00
$K_{10} = 0.00521$		
5	39.7	20.00
	39.5	20.00
	39.6	20.00
	39.5	20.00
	39.5	20.00
$K_5 = 0.005065$		

Analysis of the viscometer in Chapter Five resulted in the following equation for the viscosity of a Newtonian fluid:

$$\mu_N = \frac{5\delta_m{}^3}{96a\ell L} Pt^3$$

where δ_m is the maximum width of the eccentric annulus, a is the radius of the ball, ℓ is the distance moved by the ball in time t, and L is the effective length to be obtained by calibration. Comparison of this result with the calibration equation yields

$$L = 5\delta_m{}^3/96a\ell K$$

and on substitution,

$$\begin{aligned} L &= (5)(.007)^3/(96)(.798)(3.00)(5.44 \times 10^{-8}) \\ &= 0.1365 \text{ cm.} \end{aligned}$$

Following the correction for friction, the variation in the calibration constant with P is less than 1 percent. A much more serious uncertainty is that due to δ_m for which the value given above was based upon the subtraction of a micrometer-read diameter for the ball from manufacturer's specification for the inside diameter of the cylinder:

$$\delta_m = 1.603 - 1.596 = 0.007 \text{ cm.}$$

This value is accurate to only one significant figure. To illustrate the effect of this uncertainty, consider the expression for the calibration constant proposed by Hubbard and Brown (1943a) for the rolling ball viscometer:

$$K = \frac{\delta_m^{5/2}}{6\pi \ell J_L (2a+\delta_m)^{3/2}}$$

where J_L was calculated by Hubbard and Brown to be 0.398 and K has been corrected to compensate for the fact that the force in the Hubbard-Brown analysis was due to the weight of the ball, while in the present case a force was applied along a rigid shaft. This equation may be rearranged to solve for δ_m when, as in the present case, the value of K is known from calibration. When this is done it is found that

$$\delta_m \doteq 0.00552 \text{ cm},$$

in which case the corresponding effective length becomes

$$L \doteq 0.0670 \text{ cm}.$$

Since the Hubbard-Brown analysis was for the rolling ball instrument a difference in δ_m is not surprising, but the variation in L with δ_m is dramatized by the comparison.

In the present study the values $\delta_m = 0.007$ and $L = 0.1365$ were accepted as the most likely ones.

APPENDIX F

BILINEAR MATERIALS

An important class of empirical constitutive equations are those which postulate two separate relationships, often linear, with a critical value of the shear stress at which the transition occurs. Figure F-1 is an example.

The integration of the viscometer equation in this case requires the separate treatment of two regions of flow, one in which all the stresses are below the critical value, τ_c, and the other in which the transition occurs within the annulus. As shown in Figure F-2, corresponding to each value of τ_c there will exist an angle θ_c representing the maximum value of θ for which a single region of flow may be assumed.

In this case the equation for the viscometer is no longer equation (5.1), but its analogue:

$$1/t = \frac{4L^2}{\pi a \ell P^2} \left[\int_0^{\theta_c} \int_0^{\tau_w} \tau \, g_1(\tau) \, d\tau \, d\theta + \int_{\theta_c}^{\pi} \int_0^{\tau_c} \tau \, g_1(\tau) \, d\tau \, d\theta + \int_{\theta_c}^{\pi} \int_{\tau_c}^{\tau_w} \tau \, g_2(\tau) \, d\tau \, d\theta \right],$$

where

$$g(\tau) = \begin{cases} g_1(\tau) & \tau < \tau_c \\ g_2(\tau) & \tau \geq \tau_c \end{cases},$$

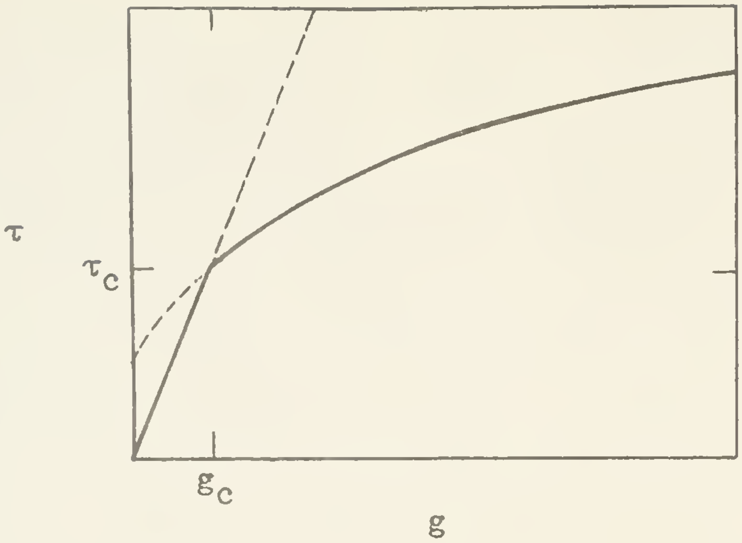

FIGURE F-1. Bi-functional material.

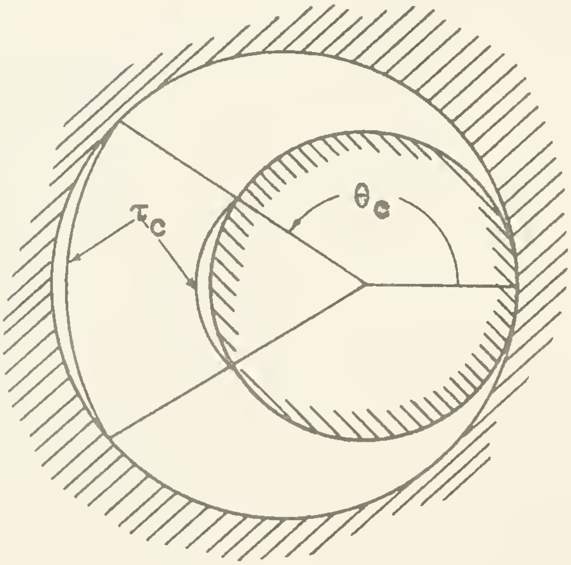

FIGURE F-2. Flow field within viscometer showing boundary between regions obeying separate constitutive equations. Along the boundary, $\tau = \tau_c$.

and θ_c is related to τ_c by

$$\tau_c = \frac{P\delta m}{2L}(1-\cos\theta_c).$$

Of special importance is the bilinear case:

$$g = \begin{cases} \tau/\mu_0 & \tau < \tau_c \\ (\tau/\mu_\infty) - k & \tau \leqslant \tau_c \end{cases}$$

In this instance,

$$1/t = \frac{4L^2}{\pi a\ell P^2}\left[\int_0^{\theta_c}\int_0^{\tau_w}\frac{\tau^2}{\mu_0}\,d\tau\,d\theta + \int_{\theta_c}^{\pi}\int_0^{\tau_c}\frac{\tau^2}{\mu_0}\,d\tau\,d\theta + \int_{\theta_c}^{\pi}\int_{\tau_c}^{\tau_w}\left(\frac{\tau^2}{\mu_\infty} - k\tau\right)d\tau\,d\theta\right].$$

Integrating once and substituting

$$\tau_w = P\delta_m(1-\cos\theta)/4L$$

yields

$$1/t = \frac{4L^2}{\pi a\ell P^2}\left[\frac{P^3\delta m^3}{192\mu_0 L^3}\int_0^{\theta_c}(1-\cos\theta)^3\,d\theta + \int_{\theta_c}^{\pi}\frac{\tau_c}{3u_0}\,d\theta + \frac{P^3\delta m^3}{192\mu_\infty L^3}\int_{\theta_c}^{\pi}(1-\cos\theta)^3\,d\theta - \int_{\theta_c}^{\pi}\frac{\tau_c}{3u_\infty}\,d\theta + \frac{kP^2\delta m^2}{32\ L^2}\int_{\theta_c}^{\pi}(1-\cos\theta)^2\,d\theta + \int_{\theta_c}^{\pi}\frac{k\tau_c^2}{2}\,d\theta\right].$$

Integrating again and collecting terms, a final expression for 1/t is obtained. The result is given on the next page.

$$
\begin{aligned}
1/t \quad = \quad & \frac{P\delta_m{}^3\sigma_0}{48\pi a\ell L}\left[5\theta_c \; - \; 8\sin\theta_c \; + \; \frac{3\sin 2\theta_c}{2}\right. \\
& + \; \frac{2\sin^3\theta_c}{3} \; + \; \frac{5\pi}{\sigma_0\mu_\infty} \; + \; \left.(1-\cos\theta_c)^2(\pi-\theta_c)\right] \\
& - \; \frac{\delta_m{}^2}{16\pi a\ell}\left[3(\pi-\theta_c) \; + \; 4\sin\theta_c \; - \; \frac{\sin 2\theta_c}{2}\right. \\
& - \; \left.k(1-\cos\theta_c)^2(\pi-\theta_c)\right].
\end{aligned}
$$

The substitution

$$\sigma_0 \quad = \quad (1/\mu_0) - (1/\mu_\infty)$$

has been made to reduce slightly the number of terms, and where τ_c appeared it was replaced by $\delta_m P(1-\cos\theta_c)/4L$.

APPENDIX G

SOME CHANNEL CONSTANTS

Channel	δ_1, cm	δ_2, cm	S_0, cm^2	$2\delta_2(\delta_1+\delta_2)S_0\rho/\delta_1$ gm	$\lambda^2/4\delta_1{}^2$ ($\times 10^8$)
1	.672	.663	.127	.336	.192*
2	.672	.620	.126	.303	.192*
6	.671	.596	.126	.285	.193*

---

*λ = 5892 Angstrom

APPENDIX H

VARIATION IN MILLING YELLOW SOLUTIONS WITH TIME

As alluded to in Chapter Two, other investigators, beginning with Prados (1957), have reported difficulty with the stability of Milling Yellow in solution. The experience of the present study confirms these earlier findings.

Two factors contribute especially to the variability of Milling Yellow solutions: evaporation and sedimentation.

If evaporation is not rigidly controlled, the concentration of the dye increases with a disproportionate rise in both birefringence and intrinsic viscosity. This was evident in the current work as shown in Figure 18, where the birefringence rises markedly between runs 418 and 419 due to the accidental displacement for about ten hours of the lid on the lower storage tank. Evaporation also occurred during the testing when the lid was set aside to permit the efflux from the conduits to be caught and measured. A deliberate concentration by evaporation was carried out on the original stock solution in January 1973 just prior to initial testing.

A more insidious change in Milling Yellow properties occurs as the result of slow but continuous sedimentation to which the organic dye, with its limited solubility, contributes the chief constituent. This is particularly true when the solution is diluted to concentrations near the limit of birefringence. The original stock solution set in a tightly sealed container from May to December, 1972. During this time, as mentioned in Chapter Two, a continuous process of evaporation and recondensation occurred beneath the lid. The result is shown in Figure H-1. The apparent viscosity as measured with the Höppler Rheo-Viscometer according to the manufacturer's instructions (*i.e.*, as opposed to the method of analysis in Chapter Five) is plotted as a function of the reciprocal of the average shear stress at four different times during 1972. The reduction in viscosity with time, particularly at lower shear rates, is very evident.

During the testing of both the original and the freshly made stock solutions described in Appendix B there was evaporation and sedimentation occurring, the former having the dominant role. The results in Chapters Four and Five confirm that the optical and rheological properties of Milling Yellow vary significantly with time and must be measured at the time of use if quantitative results are to be obtained.

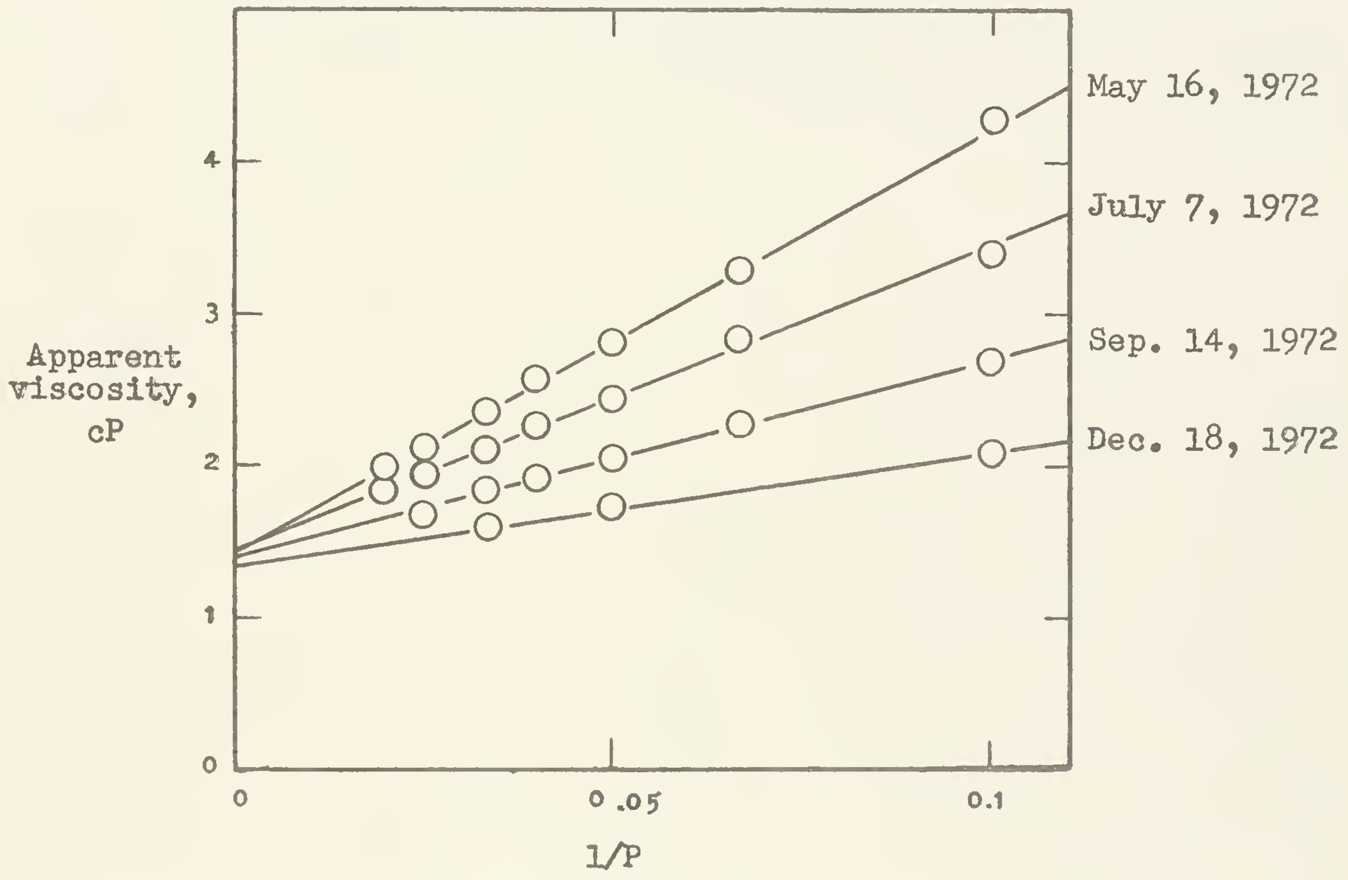

FIGURE H-1. Variation in apparent viscosity with time (T = 21.8° C).

APPENDIX I

VARIATION IN MILLING YELLOW APPARENT VISCOSITY WITH CONCENTRATION AND TEMPERATURE

When measured with the Höppler Rheo-Viscometer using the manufacturer's instructions, the apparent viscosity of Milling Yellow varies considerably with the concentration of the fluid, with the temperature, and with the average shear stress. Prior to the inception of the testing reported in Chapters Four and Five of this dissertation and before the analysis of the viscometer in the latter chapter was completed, a series of measurements were made to determine the temperature dependence of Milling Yellow solutions of different concentrations. These measurements are described in this appendix.

Apparatus

The instrument used was the Höppler Rheo-Viscometer which has been adequately described in Chapter Five and Appendix E; however, the calibration described in Appendix E had not been performed at the time these temperature studies were conducted and the apparent viscosities reported herein are based on an older calibration using the simple expression:

$$\mu_a = 0.00543 \text{ Pt}$$

where μ_a is the apparent viscosity in cP, P is the "average shear stress" (force on ball divided by cross-sectional area of ball) in gm/cm^2 [sic], and t is the time required for the ball to fall 30 mm.

With a single exception (run 103-20 at 19° C, P = 15) the apparent viscosity was measured at least three and oftener five times for each sample, each temperature, and each value of P indicated in the data which follow. The variations in the fall times during these runs were comparable to those in Tables XIX to XXVII, although the temperature variations in the earlier runs were somewhat larger. In run 103-20 at 16° C, for example, the measured temperature ranged from 15.70° to 15.88 ° C. This range may be regarded as typical for the earlier runs as may the departure of the actual temperatures from the nominal value. Toward the end of the testing period the temperature variations were no greater than those reported in Chapter Five. All of the tests were conducted in October, 1972. Run 1012, for instance, was prepared on October 12.

Preparation of Samples

With the exception of one sample taken from the original stock solution whose preparation has been detailed in Appendix B, all of the samples were prepared by weighing out a prescribed amount of Milling Yellow and adding it to a sufficient abundance of distilled water so that the initial concentration was less than 1.3 percent. The mixture was then boiled until the total volume was slightly greater than a predetermined value. At this time the solution was removed from the hot plate and placed on one scale of a triple beam balance previously set to the exact mass desired. When the mass was attained by evaporation, the solution was immediately bottled and capped. A check of the solid content of these samples was later made by evaporating to dryness as described in Appendix L. The value of the concentration cited in the data which follow is the value given in Appendix L.

Experimental Data

The variation in apparent viscosity with temperature is given in Figures I-1 through I-6. It will be noted that there are no data on certain of these plots above a certain temperature. This reflects a restriction on the use of the viscometer which is discussed at greater length in Appendix J.

Computation of Temperature Coefficients

The replication of the data from separately prepared samples is quite good at higher concentrations ($q > 2.3$ percent) as shown in Figures I-1 and I-2. At very low concentrations ($q \doteq 1.3$ percent) the agreement between samples 104-14 and 1016-14 was so close that the data coincide, and only the former are plotted in Figure I-5. At intermediate concentrations, which unluckily include

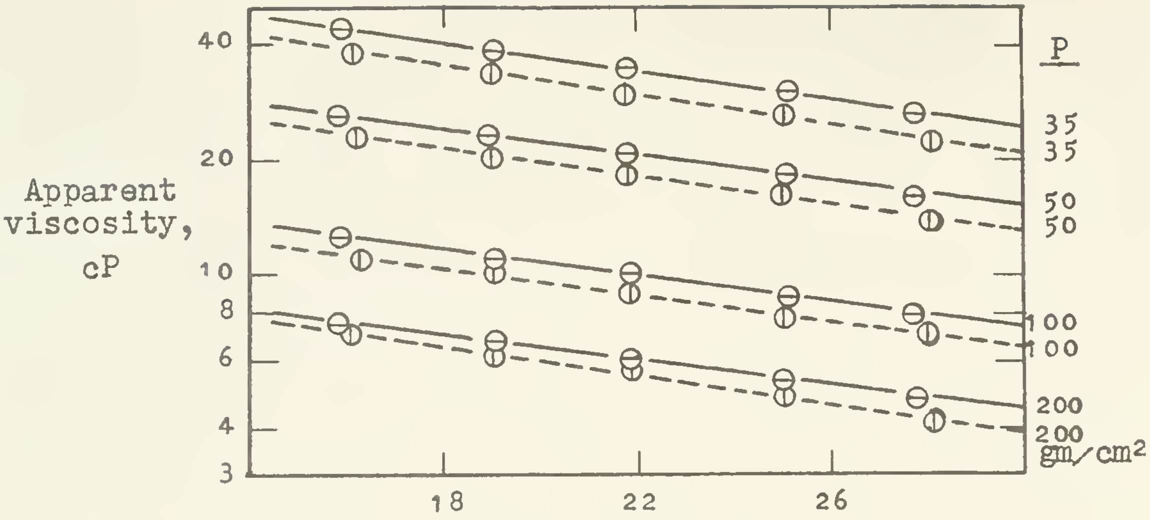

Temperature, °C

FIGURE I-1. Temperature variation of samples 103-30, concentration q = 2.94 (solid lines), and 1012-30, concentration q = 2.84 (dashed lines). The load on the ball is given in the right hand margin.

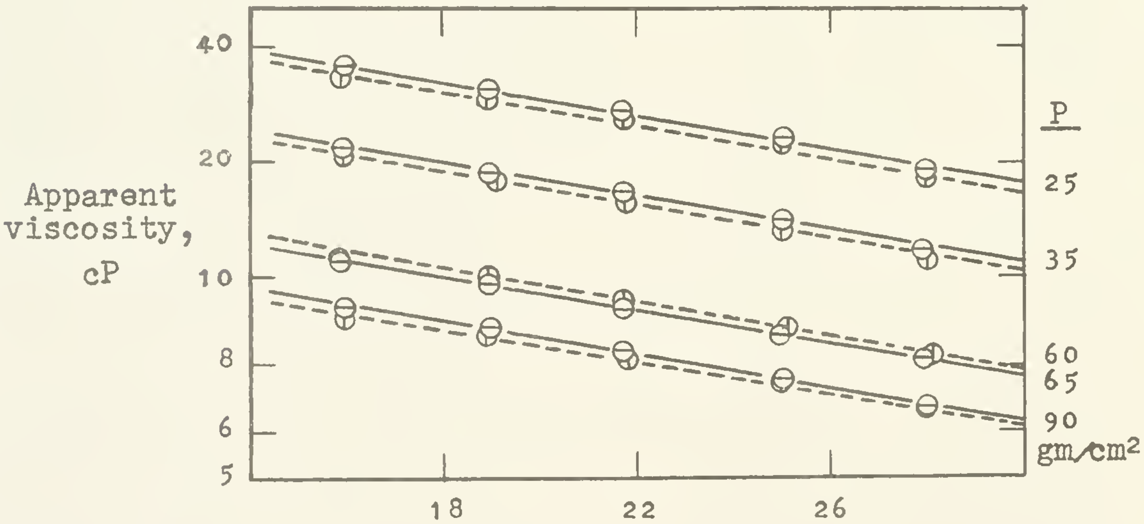

Temperature, °C

FIGURE I-2. Temperature variation of samples 107-25, concentration q = 2.33 (solid lines), and 1011-25, concentration q = 2.34 (dashed lines). The load on the ball is given in the margin. Note that for the third pair of lines the load on the ball differs in the two samples.

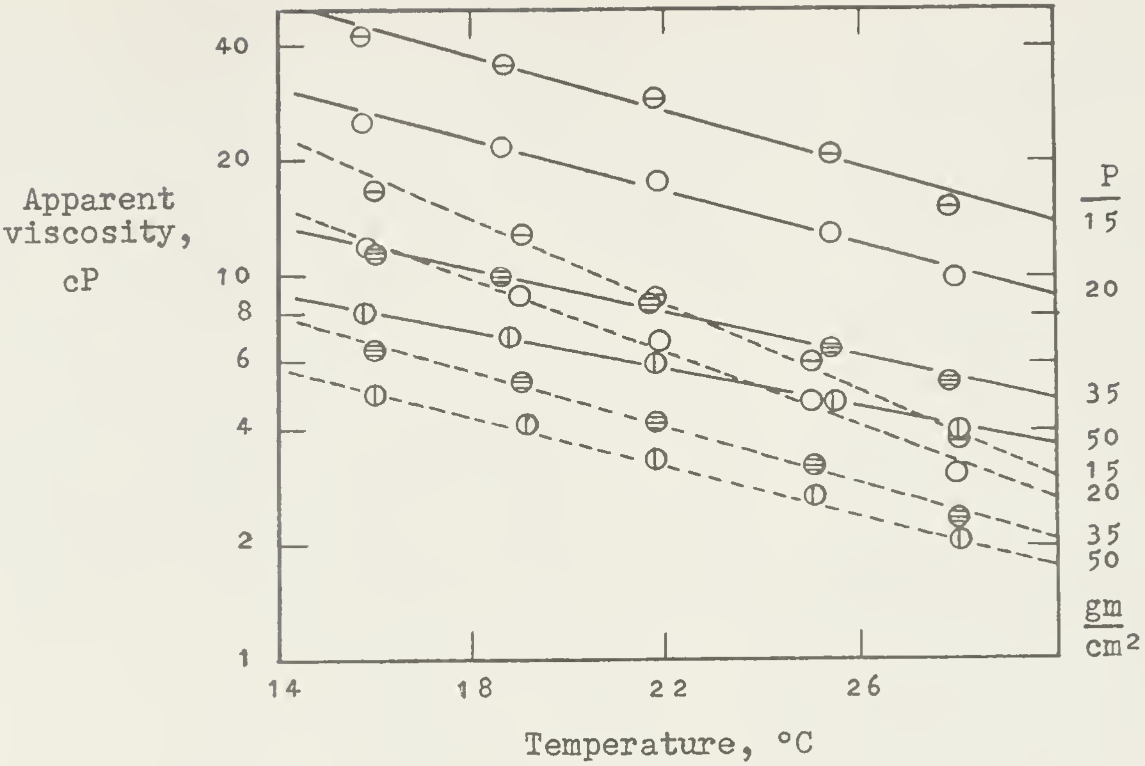

FIGURE I-3. Temperature variation of samples 103-20, concentration q = 1.89 (solid lines), and 109-20, concentration σ = 1.92 (dashed lines). The load on the ball is given in the right hand margin.

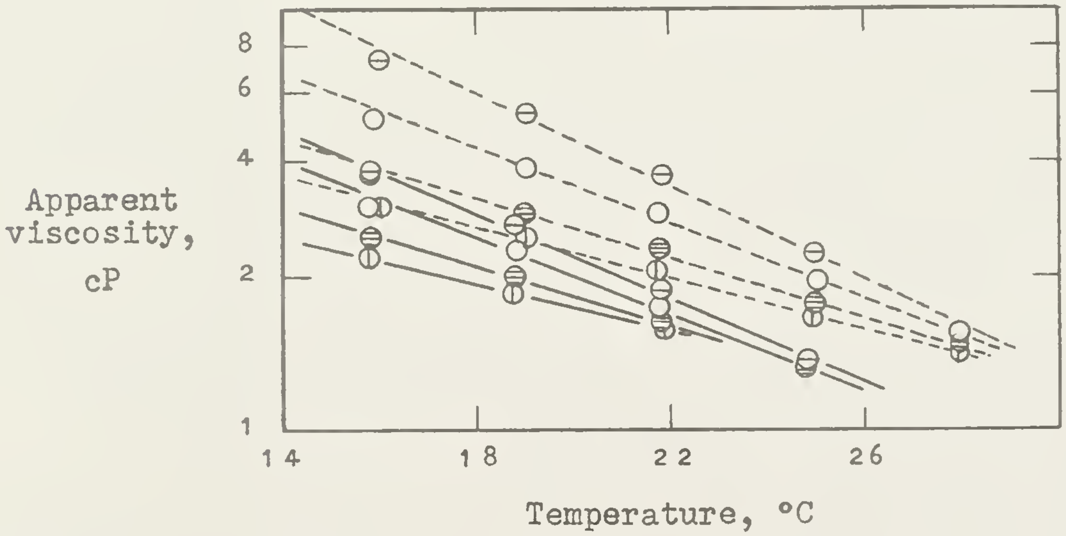

FIGURE I-4. Temperature variation of samples 104-17, concentration q = 1.59 (solid lines), and 1011-17, concentration q = 1.57 (dashed lines). Load on ball: ⊖ 10 gm/cm^2; ○ 15 gm/cm^2; ⊜ 25 gm/cm^2; ⦶ 35 gm/cm^2.

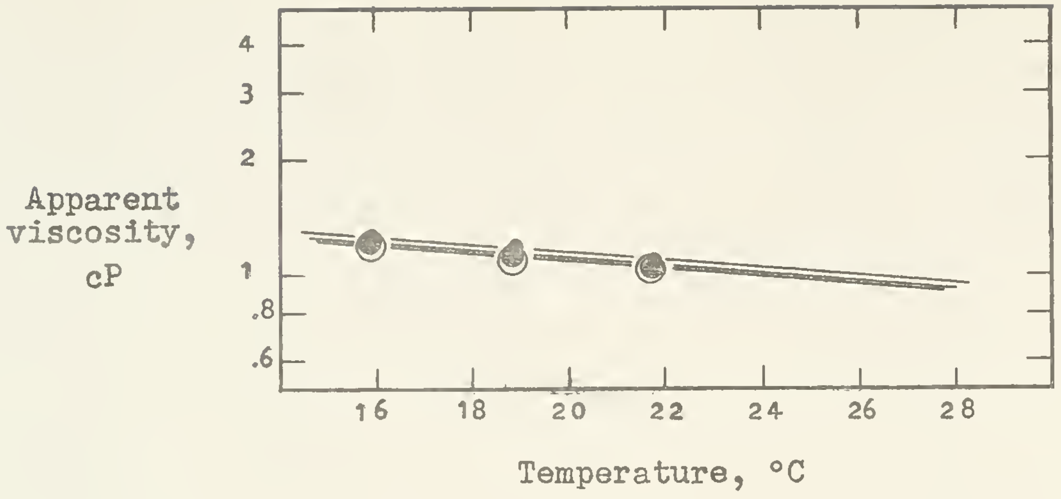

FIGURE I-5. Temperature variation of sample 104-14, concentration: q = 1.31. Load on ball, P: ● 5 gm/cm^2; ⊜ 10 gm/cm^2; ○ 15 gm/cm^2.

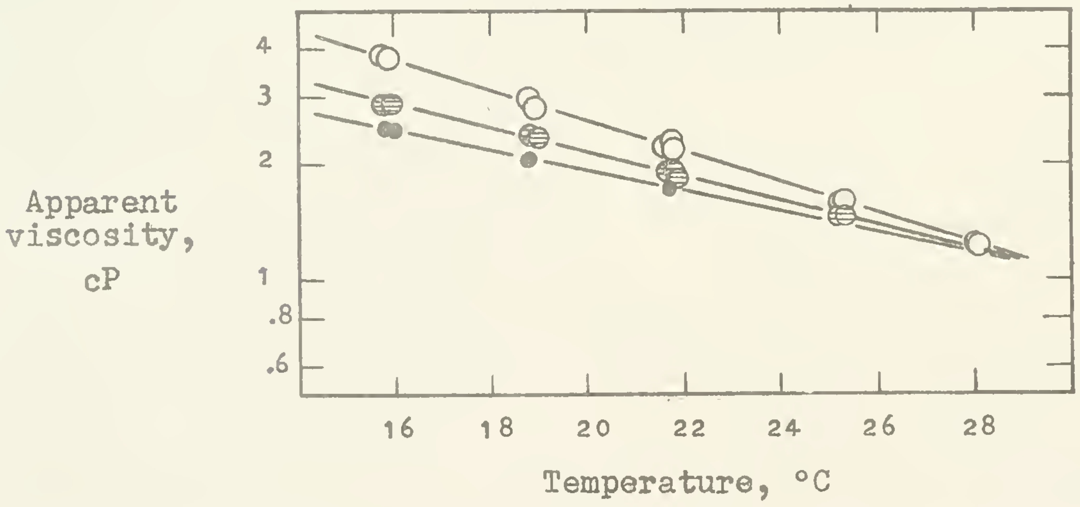

FIGURE I-6. Temperature variation of original stock solution, nominal concentration: q = 1.5. Load on ball, P: ○ 15 gm/cm^2; ⊜ 25 gm/cm^2; ● 40 gm/cm^2.

the range of concentrations studied in this dissertation, the results obtained from separately prepared samples were disparate, as shown in Figures I-3 and I-4. The disparity was also evident in the appearance of the sediment resulting when the samples were evaporated to dryness to determine their concentration. The data in Figures I-3 and I-4 form the principal basis for the decision not to attempt the preparation of standardized solutions of the commercial dye.

Besides a failure to replicate, there is evidence of an alternation in the character of the temperature dependence as the concentration decreases. At high concentrations the data plot as parallel lines indicating that the temperature dependence is independent of the shear stress. At intermediate concentrations the variations due to temperature increase in magnitude as the shearing stress decreases. Although straight lines have been drawn through the data in Figure I-2 to facilitate comparisons from figure to figure, close inspection indicates a distinct curvature is present. Since each value of the apparent viscosity reflects a wide range of local shear stresses, the curvature may be due to the integration of two characteristic responses, only one of which is dependent upon the shear stress. In Figure I-2 these shear rate dependencies are nearly negligible, but at the lower concentrations plotted in Figures I-3 and I-4 the shear-rate dependent terms dominate the relationship.

At the lowest concentration, plotted in Figure I-5, the shear-rate dependence is still present, but its magnitude is negligible.

The straight lines drawn in Figures I-1 through I-6 have the general form

$$\mu_a = \mu_{a_0} e^{-kT}$$

from which

$$\partial\mu_a/\partial T = -k\mu_a$$

where k has an empirical value which depends upon both the concentration and the average shear stress, P. Typical values of k are given in Table I-I.

The data for the original stock solution which are plotted in Figure I-6 are accurately represented by the empirical expression

$$\mu_a = \exp\left[0.252(30.3-T)P^{-.377}\right]$$

from which

$$k = -\frac{1}{\mu_a}\frac{\partial u_a}{\partial T} = 0.252\ P^{-.377}.$$

For comparison, run 104-17 yields by the method of least squares:

$$\mu_a = \exp\left[0.335(26.8-T)P^{-.429}\right]$$

and

$$k = 0.335\ P^{-.429}.$$

The temperatures in these empirical expressions are in degrees Celsius.

TABLE I-I

TEMPERATURE COEFFICIENTS

Run	Concentration, wt %	Average shearing stress, P, gm/cm^2	$k = \frac{1}{\mu_a} \frac{\partial u_a}{\partial T}$
103-30	2.94	200	0.040
		100	0.039
		50	0.040
		35	0.044
107-25	2.33	90	0.051
		65	0.050
		35	0.050
		25	0.050
103-20	1.89	50	0.058
		35	0.061
		20	0.076
		15	0.085
104-17	1.59	35	0.071
		25	0.086
		15	0.109
		10	0.121
104-14	1.31	15	0.026
		10	0.025
		5	0.024

It appears that at higher concentrations ($q > 2.3$ percent) and at low concentrations ($q \doteq 1.3$ percent) the variations in the apparent viscosity can be computed from the empirical constants in Table I-I. At intermediate concentrations the temperature dependence has the form

$$-\frac{1}{\mu_a}\frac{\partial \mu_a}{\partial T} = k_0 P^{-n}$$

but the constants k_0 and n must be obtained on a case by case basis.

APPENDIX J

RESTRICTION OF VISCOMETER TO LIQUIDS HAVING VISCOSITY ABOVE 4 CENTIPOISE

The instrument booklet furnished with the Höppler Rheo-Viscometer gives the useful range of the instrument as 4 to 280 centipoise for the ball and cylinder which were used in this dissertation. When queried about the use of the instrument at lower viscosities, the manufacturer replied:

> We are sorry to inform you that the extension of the application range of the Rheo-Viscometer to liquids with a viscosity below 4 cP is not possible in general. The measurement of such viscosities may be carried out only with Newtonian liquids.*

The difficulty which arises when the viscometer is used indiscriminately with liquids having viscosities less than 4 cP is shown in Figure J-1. Here the apparent viscosity of a Milling Yellow sample at 21.8° C has been plotted against the reciprocal of the so-called average shear stress, P. It is evident that the character of the flow undergoes an abrupt transition on or about P = 60 gm/cm². A similar transition is observed in water at about P = 15 gm/cm².

---

*Meyer, Commercial Director, VEB MLW Prüfgeräte-Werk, Medingen, Sitz Freital, D. D. R. Letter dated October 19, 1972

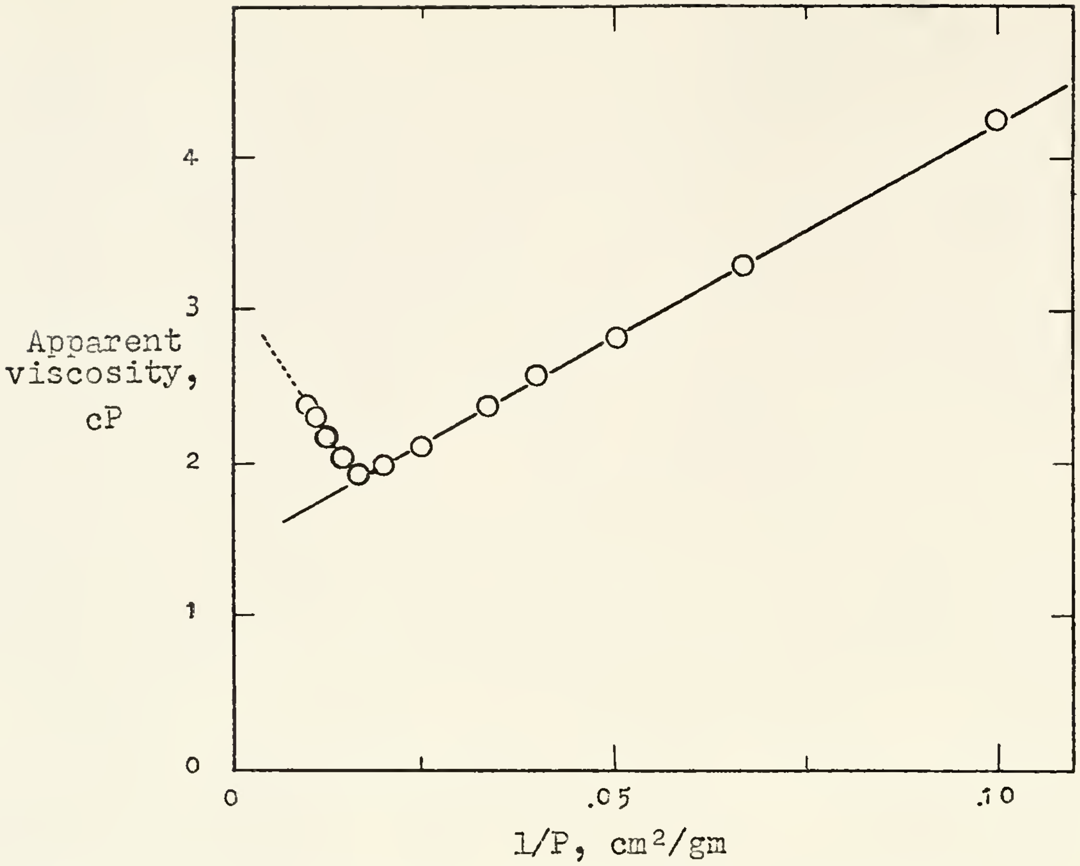

FIGURE J-1. Transition in measurement of apparent viscosity when P is too large. Fluid sampled from original stock solution in May, 1972. Temperature: 21.8° C.

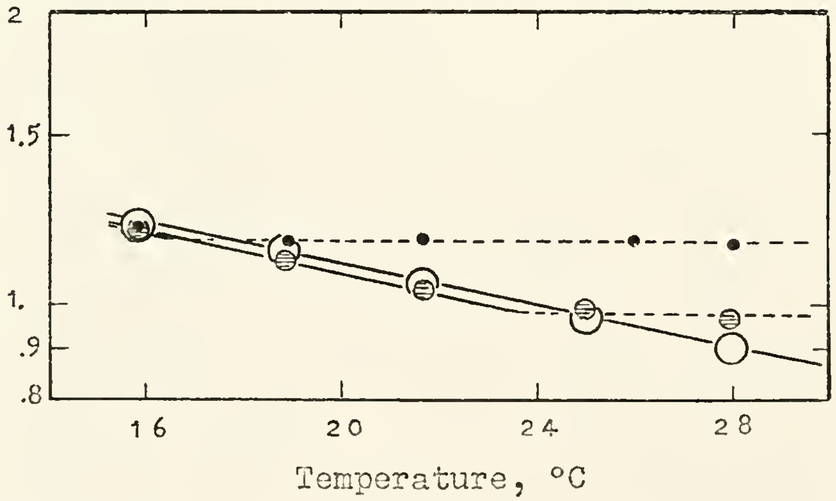

FIGURE J-2. Transition in measurement of apparent viscosity when temperature is too high, sample 104-14. Load on ball: ○ 10 gm/cm²; ⊜ 15 gm/cm²; • 20 gm/cm².

Similar transitions are observed if P is held constant and the temperature of the fluid is raised. As shown in Figure J-2, above a certain critical temperature the fall time of ball (and hence the apparent viscosity) remains nearly constant.

All of the data observed during the current study, for both Newtonian and non-Newtonian liquids, indicate that the transition in the viscometer occurs at about

$$P/\mu_a{}^2 \doteq 15.5 \text{ gm/cm}^2\text{-cP}^2.$$

If $P/\mu_a{}^2$ is significantly greater than 15.5, reliable results cannot be obtained with the Höppler instrument. Since the largest mass supplied by the manufacturer (i.e., the sum of the masses provided) corresponds to P = 200 gm/cm², the lowest viscosity which can be measured without concern for the transition is

$$\mu_a = \sqrt{200/15.5} = 3.6 \text{ cP},$$

a value in good agreement with the manufacturer's restriction; however, if only those masses less than $15.5\ \mu_a{}^2$ are used with the less viscous liquids, the difficulty with the transition is circumvented. An example is the use of distilled water, as described in Appendix E, to check the calibration of the instrument.

It is not certain what phenomenon is responsible for the change in the response of the viscometer at the transition point. Three possibilities are turbulence, flow separation, and movement of the ball away from the wall of the cylinder. Since no use of the viscometer has been made for values of $P/\mu a^2$ greater than 15.5, it is not necessary to discriminate between these alternatives; however, the question is not without interest and a brief discussion of each possibility follows.

Turbulence. – It is commonly known (e.g. Schlichting, 1968, pp. 15-19) that drag becomes substantially greater during the transition from laminar to turbulent flow. The Reynolds number for the viscometer ball is

$$Re = 2\rho \ell a/\mu t$$

where ρ is the density, ℓ/t is the velocity of the ball, a is the radius of the ball, and μ is the viscosity of the fluid. For water, $Re = 380$ when transition occurs in the viscometer. Calculation of the Reynolds number based upon the average width of the annulus and the average flow velocity in the annulus yields the value $Re = 95$. Both of these estimates are less than those usually associated with turbulence, although Eckert and Irvine (1956) have shown that in narrow channels of varying width, turbulence can occur in the wider portion even when flow in the narrower part of the cross-section remains laminar. Occurrence of the Eckert-Irvine phenomenon, however, would be expected to yield a gradual, rather than an abrupt transition, so this possibility appears unlikely.

A Reynolds-number dependence is evident in the transition whether turbulence is present or not. Since the apparent viscosity is defined by

$$\mu_a = KPt,$$

it follows that

$$t = \mu_a/KP.$$

Substituting this value for t into the expression given previously for the Reynolds number yields

$$Re = 2K\rho l P/a\mu_a{}^2$$

which differs only by a proportionality constant from the criterion for transition:

$$P/\mu_a{}^2 = \text{constant}.$$

Flow Separation. - Separation, if it occurs, must take place on the downstream side of the ball, that is, on its upper surface. An analysis of this possibility requires specification of flow around the sphere in the viscometer. In this dissertation the flow has been specified only along the "effective length" of the annulus, a narrow region in the vicinity of the point of closest clearance between ball and cylinder. If the flow along the effective length is compared with flow in a convergent-divergent channel, then the criterion for flow in the latter case may give some indication of the likelihood of flow separation in the viscometer.

Millsaps and Pohlhausen (1953) found that backflow occurs in divergent channels having 5° half-angles when the Reynolds number exceeds 684. In this case the Reynolds number was defined as:

$$Re = u_{max}\rho r_c/\mu$$

where u_{max} is the speed at the center of the divergent channel and r_c is the radial distance of the flow from the origin of the divergence. In the Höppler viscometer the maximum flow rate for a Newtonian fluid is about 2.4 times the average rate, so one can estimate

$$u_{max} = 2.4\ \bar{u} = 2.4\ (\ell/t)(a/\delta_m)$$

$$= 2.4 \frac{\ell a}{t\,\delta_m} .$$

Perhaps the least unreasonable estimate of r_c is that it is half the previously calculated effective length:

$$r_c = L/2.$$

With these very crude estimates the corresponding Reynolds number may be calculated. When the viscometer undergoes its transition with water (ρ = 1 gm/cm^3, μ = 0.01 poise, t = 12.7 sec) the corresponding Reynolds number is

$$Re \approx 500.$$

Since separation is more apt to occur at larger half-angles than at smaller ones, and since the half-angle* in the Rheo-Viscometer at the upper end of the effective length is about 2.5°, compared to the 5° for which Re = 684 implied separation, the present analogy, if valid, seems to indication that flow separation is not responsible for the transition point observed in the viscometer.

---

*In the Höppler Rheo-Viscometer the half-angle is defined as half the angle between the wall and a tangent to the ball.

Movement away from the wall. — Irving (1972) has shown that cylinders in inclined tubes fall as much as twice as fast as those in vertical tubes. This result leads to the expectation that movement of the ball away from the wall in the Höppler instrument would increase the fall time with a corresponding increase in the apparent viscosity. In the original design of the Rheo-Viscometer, Höppler (1942) insured that the ball would remain against the wall by inclining the cylinder to a significant angle from the vertical. In the modern design a counterweight attached to the side of the ball's shaft accomplishes the same objective. When the pressure drop in the eccentric annulus exceeds a certain value, the ball may be expected to swing away from the wall into the flow much as cylindrical shell viscometers center themselves as shown by Lindgren (1972). It is not unlikely that this is what is happening at the transition point in the Höppler viscometer, but it cannot be stated with certainty that this is the case.

APPENDIX K

VISCOMETER RESPONSE AT VERY SLOW FALL TIMES

Among the assumptions implicit in the analysis of the Höppler Rheo-Viscometer in Chapter Five was the presumption that the response of the viscometer was independent of the location of the ball in the axial direction. This assumption was tested by observing the descent of the ball at speeds sufficiently slow so that the fall time could be separately measured at each 1-mm interval along the path. As an additional check, the point at which the fall was initiated was also varied.

It was found that fall times for 1-mm increments vary from point to point along the cylinder axis. The speed appeared greater (times were smaller) during the first millimeter of travel. As a result, it appears that calibrations of the Höppler Rheo-Viscometer are valid only if the starting point and fall distance for each measurement are identical with those used for calibration of the instrument. Further details are provided in the paragraphs which follow.

Tests were conducted at 21.8° C using a 1.89 percent solution of Milling Yellow and an "average shearing stress" of P = 10 gm/cm². Under these conditions the total fall time is about 340 seconds, so that the average fall time for each of the 30 1-mm intervals along the axis exceeds 11 seconds, an ample time for sequential measurements.

The procedure was as follows. Starting points at 12 different locations within the cylinder were selected with the aid of a table of random numbers. The ball was positioned opposite the first starting point and the temperature was recorded. Simultaneously, the ball was released and a timer started. As the ball passed the first millimeter marking, easily observed on the Höppler instrument, the first timer was stopped and a second was started. The time on the first was read into a recorder, the timer was reset, and as the next millimeter marking was passed, restarted as the other timer was stopped. This process was repeated until the ball had fallen 3 mm below the terminal point of the calibration runs reported in Appendix E.

Individual fall times for each 1-mm interval are provided in Table K-I. Also tabulated are temperatures measured between runs and the average fall time for each location along the viscometer axis.

Inspection of the data indicates that the 1-mm fall times vary significantly along the viscometer cylinder and that the variations are roughly reproducible from one run to the next. An exception is the first millimeter of travel for each run. Times for this interval tend to

TABLE K-I

FALL TIMES FOR 1-MM INCREMENTS

Start point, mm	Run:	1-mm Fall times, seconds:											Average time, sec
	1	2	3	4	5	6	7	8	9	10	11	12	
0		12.3										11. 7*	11.70
1		12.0										11.3	11.65
2		11.3										11.1	11.20
3		10.5										10.3	10.40
4		12.1					10.2					11.6	11.85
5		11.1					11.0					11.0	11.07
6		10.8			12.8		10.4					10.7	10.63
7		10.9			10.6		10.9					10.6	10.75
8		11.5			**		11.7					11.5	11.57
9		10.6			11.2		10.9					10.8	10.88
10	9.5	9.9			10.5		9.9					9.5	9.95
11	11.5	11.5			10.9		11.3					***	11.30
12	11.4	11.1			11.0		10.9	9.7					11.10
13	10.8	10.8			10.8		10.8	10.5		9.7			10.74
14	10.8	10.4			10.2		10.3	10.0		10.3			10.33
15	11.7	11.8			11.6		11.5	11.4		11.0			11.50
16	11.0	10.6			10.6		10.5	10.1		10.4			10.53
17	10.0	10.1			10.4		9.7	10.1		9.7			10.00
18	11.4	11.3			11.0		11.3	11.4	10.4	10.9			11.22
19	11.3	11.4			11.1		11.2	11.0	10.8	11.1			11.13
20	11.2	10.8			11.1		11.2	10.7	10.9	11.0			10.98

---

*Run began at start point of -2 mm.
**Stop watch failed to start
***Run interrupted

TABLE K-I (Continued)

Start point, mm	Run:				1-mm Fall times, seconds:								Average time, sec
	1	2	3	4	5	6	7	8	9	10	11	12	
21	10.9	10.8			10.6		10.7	10.5	10.6	10.4	9.9		10.64
22	11.6	11.7			12.1		12.1	11.7	10.9	11.9	11.5		11.69
23	11.5	11.4			11.3		12.1	11.3	11.4	11.0	11.2		11.40
24	10.7	10.4			10.7		10.6	10.3	10.5	10.8	10.7		10.59
25	11.3	11.3		12.0	11.4		11.3	11.0	11.7	11.1	11.4		11.31
26	12.3	11.8		11.5	12.1	11.1	12.1	12.1	12.2	11.8	11.7		11.96
27	12.0	12.2		11.9	12.3	12.3	12.4	12.3	12.7	12.2	12.1		12.24
28	11.5	11.6		11.0	11.6	11.3	12.0	**	11.7	11.6	11.4		11.53
29	12.9	12.8		12.6	13.5	13.0	13.0	12.6	13.0	12.7	12.6		12.87
30	12.9	12.7	11.6	12.7	12.9	12.7	13.2	12.8	12.9	12.6	12.6		12.80
31	12.8	12.5	12.6	12.4	12.9	12.5	12.5	12.6	12.3	12.8	12.2		12.55
32	12.1	12.0	11.4	12.4	12.4	12.4	12.4	12.2	12.6	12.4	11.8		12.19
Temp:	21.80	21.74	21.74	21.84	21.80	21.72	21.8	21.76	21.8	21.84	21.86	21.88	°C

**Stop watch failed to start

be significantly lower than for the same location when the ball was started further up the axis. Because of this disparity, fall times for "first millimeters" are not included in the computation of average fall times for their respective locations.

An attempt to observe time-dependent properties of the fluid was made by correcting the fall time for each 1-mm interval by multiplying the measured fall time at each location by the average fall time for all measurements divided by the average fall time at the axial location in question. Corrected fall times are compared in Table K-II for the first 10 mm of travel, whatever the starting point. Those runs which terminate before the ball has fallen 10 mm are those which were begun at axial locations near the bottom of the range tested. No significant dependence upon time is apparent after the first millimeter of travel.

TABLE K-II

CORRECTED FALL TIMES FOR FIRST 10 MM OF FALL BY 1-MM INCREMENTS

Corrected 1-mm fall times, seconds:

Order of Increments	Run: 1	2	3	4	5	6	7	8	9	10	11	12
1st	10.9	12.0	10.4	12.1	13.8	10.6	9.8	10.0	10.6	10.3	10.6	—
2nd	11.6	11.8	11.5	11.0	11.3	11.5	11.5	11.2	11.1	11.4	11.2	—
3rd	11.8	11.5	10.7	11.1	—	11.2	11.2	11.1	11.3	10.9	11.2	—
4th	11.5	11.5	11.4	10.9	11.8	11.5	11.6	11.3	11.4	11.3	11.5	11.1
5th	11.95	11.7		11.2	12.1	11.3	11.55	10.95	10.65	11.95	11.5	11.3
6th	11.6	11.5		11.3	11.0	11.4	11.45	11.5	11.4	11.1	11.2	11.3
7th	11.9	11.6		11.3	11.3	11.6	11.4	11.6	11.3	11.4	11.3	11.2
8th	11.4	11.6		11.6	11.5		11.4	11.3	11.8	11.45	11.3	11.35
9th	11.6	11.35			11.3		11.2	11.1	11.7	11.2	11.2	11.5
10th	11.6	11.1			11.5		11.5	11.3	11.9	11.6	11.25	11.3

APPENDIX L

DETERMINATION OF SAMPLE CONCENTRATIONS

Because of the variations in concentration which occurred during testing, the solid content was determined for each of the samples taken for viscometric analysis. The value of these measurements is limited by the unknown inorganic salt content of commercial Milling Yellow which averages 30 percent of the total weight according to Swanson and Green (1969) and the supplier.

The samples used for concentration measurements averaged 50 ml and were weighed out to the nearest milligram on a chain-link balance. Following evaporation to dryness in a clean container maintained at about 42° C, the residue was again weighed, this time to ± 0.1 milligram, a variation easily within the calibrated precision of the instrument. A typical calculation follows, principally to indicate the relative magnitudes of the tare, the solution, and the residue.

Sample calculation, run 42. —

Sample & tare:	86.585 gm	Residue & tare:	34.1643 gm
- Tare:	-33.353 gm	- Tare:	-33.3526 gm
Sample mass:	53.232 gm	Residue mass:	0.8117 gm

Weight fraction = 0.8117/53.232 = 0.01525

The results of these calculations have been summarized in Table L-I. Two sets of data are tabulated. One set corresponds to the tests run in the rectangular conduit, the other to the study of temperature variability reported in Appendix I.

TABLE L-I

CONCENTRATIONS OF SAMPLES

Sample	Percentage solids	Sample	Percentage solids
42	1.525	104-14	1.309
44	1.534	1016-14	1.316
418	1.695	104-17	1.586
419	1.716	1011-17	1.572
420	1.753	103-20	1.886
420B	1.663	109-20	1.922
424	1.719	107-25	2.329
424B	1.717	1011-25	2.344
425	1.697	103-30	2.939
		1012-30	2.838

The dried samples showed a considerable variation in color and texture, two distinct constituents predominating: coarse, deeply tinted, orange crystals and a fine, nearly amorphous powder. The relative proportions of these varied widely. For example, the original stock solution, after a year's sedimentation of fine yellow powder, yielded dried residues in which the orange crystals heavily predominated, while samples from the fresh stock solution were as predominately yellow. Considering the difference in weight percentages cited in Table L-I and the fact that the optical and rheological properties are quite similar, one is drawn to the conclusion that there are two conditions present within Milling Yellow solutions: one, the deep orange which characterizes birefringent solutions, is active; the other, the light yellow of dilute solutions, is inactive. A further investigation of the nature of Milling Yellow's special properties may require the specialized attention of physical chemists.

BIBLIOGRAPHY

AMENEMHET 1540 B.C. Grave inscription, translated in Höppler, Kolloid-Z. 98, 1 (1942)

ARAI, T. & TOYODA, H. 1968 Fifth International Conference on Rheology, Kyoto, Japan

ARIMAN, T., TURK, M. A., & SYLVESTER, N. D. 1973 Inter. J. Eng. Sci. 11, 905

ASHARE, E., BIRD, R. B., & LESCARBOURA, J. A. 1965 A. I. Ch. E. J. 11, 910

ATKIN, R. J. & LESLIE, F. M. 1970 Quart. J. Mech. Appl. Math. 23, 2

BATCHELOR, G. K. 1971 J. Fluid Mech. 46, 813

BAUER, A. B. & DUPUIS, R. A. 1967 J. Appl. Mech. E 89, 538

BINNIE, A. M. 1945 Proc. Phys. Soc. (London) 57, 390

BIRD, R. B. & TURIAN, R. F. 1964 Ind. & Eng. Chem. Fund. 3, 87

BLAIR, G. W. S. 1949 A Survey of General and Applied Rheology. Sir Isaac Pitman & Sons

BOEDER, P. 1932 Z. Physik 75, 258

BOGUE, D. C. & PEEBLES, F. N. 1962 Trans. Soc. Rheol. 6, 317

BRETHERTON, F. P. 1962 J. Fluid Mech. 14, 284

BROERSMA, S. 1960 J. Chem. Phys. 32, 1626

BURGERS, J. M. 1938 Verh. Kon. Ned. Akad. Wet. 16, 113

CAULFIELD, H. J. & SOREF, R. A. 1971 Appl. Phys. Lett. 18, 5

CERF, R. & THURSTONE, G. B. 1964 J. Chim. Physiq. 61, 1457

CHEN, M. C. S., LESCARBOURA, J. A., & SWIFT, G. W. 1968 A. I. Ch. E. J. 14, 123

CHRISTIANSEN, E. B., RYAN, N. W., & STEVENS, W. E. 1955 A. I. Ch. E. J. 1, 544

CHRISTOPHERSON, D. G. & DOWSON, D. 1959 Proc. Roy. Soc. A 251, 550

COLEMAN, B. D., MARKOVITZ, H., & NOLL, W. 1966 Viscometric Flows of Non-Newtonian Liquids. Springer-Verlag

CORNISH, R. J. 1928 Proc. Roy. Soc. A 120, 691

DALLY, J. W. & RILEY, W. F. 1965 Experimental Stress Analysis. McGraw-Hill

DAVIES, S. J. & WHITE, C. M. 1928 Proc. Roy. Soc. A 119, 92

DEBYE, P. 1946 J. Chem. Phys. 14, 636

DEHAVEN, E. S. 1959a Ind. Eng. Chem. 51, 813

DEHAVEN, E. S. 1959b Ind. Eng. Chem. 51, 63A-7

DEMING, W. E. 1964 Statistical Adjustment of Data. Dover

DEWEY, D. R. 1941 Ph.D. Dissertation, Massachusetts Institute of Technology

DURELLI, A. J. & NORGARD, J. S. 1972 Exper. Mech. 12, 169

ECKERT, E. R. G. & IRVINE, T. F. 1956 Trans. ASME 78, 709

EINSTEIN, A. 1906 Ann. Physik 19, 289

EIRICH, F. R. 1956 *et seq.* Editor of Rheology, Vol. I *et seq.* Academic Press

ERICKSEN, J. L. 1956 Quart. Appl. Math. 14, 318

ERICKSEN, J. L. 1960a Kolloid-Z. 173, 117

ERICKSEN, J. L. 1960b Arch. Ratl. Mech. Anal. 4, 231

ERICKSEN, J. L. 1961 Trans. Soc. Rheol. 5, 23

ERICKSEN, J. L. 1962a Arch. Ratl. Mech. Anal. 9, 371

ERICKSEN, J. L. 1962b Arch. Ratl. Mech. Anal. 10, 189

ERICKSEN, J. L. 1966a *Arch. Matl. Mech. Anal.* *23*, 266

ERICKSEN, J. L. 1966b *Phys. Fluids* *9*, 1205

ERICKSEN, J. L. 1967 *Appl. Mech. Rev.* *20*, 1029

ERICKSEN, J. L. 1969 *Trans. Soc. Rheol.* *13*, 9

ERINGEN, A. C. 1964 *Inter. J. Eng. Sci.* *2*, 205

ERINGEN, A. C. 1966a *J. Math. & Mech.* *15*, 909

ERINGEN, A. C. 1966b *J. Math. & Mech.* *16*, 1

EWING, J. A. 1925 *Proc. Roy. Soc. (Edinburgh)* *45*, 308

FEYNMAN, R. P., LEIGHTON, R. B., & SANDS, M. 1963 *Feynman Lectures on Physics*, Vol. 1. Addison-Wesley

FIELDS, B. J. 1952 B.S. Thesis, University of Tennessee

FLOBERG, L. 1968 *Acta Polytech. Scand.*, *Mech. Eng. Ser.* *36*

FREDERICKSON, A. G. 1964 *Principles and Applications of Rheology*, Prentice-Hall

FROHLICH, H. & SACK, R. 1946 *Proc. Roy. Soc. A* *185*, 415

GAUTHIER, F., GOLDSMITH, H. L., & MASON, S. G. 1971 *Trans. Soc. Rheol.* *15*, 297

GIESEKUS, H. 1962 *Rheol. Acta* *2*, 50

GOLDSMITH, H. L. & MASON, S. G. 1961 *Nature* *190*, 1095

GOLDSMITH, H. L. & MASON, S. G. 1962 *J. Colloid Sci.* *17*, 448

GOLDSMITH, H. L. & MASON, S. G. 1964 *Proc. Roy. Soc. A* *282*, 569

GREENBERG, H. J., DORN, W. S., & WETHERELL, E. H. 1960 In *Plasticity*, *Proc. 2nd Sym. Naval Struct. Mech.* Pergamon

HAGEN, G. 1839 *Poggendorff Ann.*, Vol 2, *46*, 423

HAMEL, G. 1916 *Jahresber. Deut. Math.-Ver.* *25*, 34

HANZAWA, H. & ISHIKAWA, H. 1970 *Bull. Jap. Soc. Mech. Eng.* *13*, 509

HARGROVE, L. E. & THURSTONE, G. B. 1957 J. Acoust. Soc. Am. 29, 966

HARRIS, J. 1970 Rheol. Acta 9, 467

HARTSHORNE, N. H. & STUART, A. 1970 Crystals and the Polarising Microscope, 4th Ed. Edward Arnold Ltd.

HIRSCH, A. E. 1964 Ph.D. Dissertation, University of Tennessee

HONEYCUTT, E. H., Jr. & PEEBLES, F. N. 1955 Prog. Rpt. 3, Contract Nonr-811(04). Eng. Exper. Station & Dept. Chem. Eng., University of Tennessee

HÖPPLER, F. 1933 Z. tech. Physik 14, 165

HÖPPLER, F. 1941a Oel und Kohle 48, 995

HÖPPLER, F. 1941b Kolloid-Z. 97, 61

HÖPPLER, F. 1942 Kolloid-Z. 98, 348

HUBBARD, R. M. & BROWN, G. G. 1943a Ind. Eng. Chem., Anal. Ed. 15, 212

HUBBARD, R. M. & BROWN, G. G. 1943b Ind. Eng. Chem. 35, 1276

IRVING, J. B. 1972 J. Phys. D 5, 214

JEFFERY, G. B. 1915 Phil. Mag. 6, 455

JEFFERY, G. B. 1922 Proc. Roy. Soc. A 102, 161

JERRARD, H. G. 1959 Chem. Rev. 59, 345

JOHNSON, R. R. 1974 Ph.D. Dissertation, University of Florida

KIRKWOOD, J. G. & RISEMAN, J. 1948 J. Chem. Phys. 16, 565

KIRKWOOD, J. G. & RISEMAN, J. 1949 J. Chem. Phys. 17, 442

KISIEL, I. 1968 Appl. Mech. Rev. 21, 1043

KRIEGER, I. M. & MARON, S. H. 1952 J. Appl. Phys. 23, 147

KUHN, W. & KUHN, H. 1943 Helv. Chim. Acta 26, 1394

KUHN, W. & KUHN, H. 1945 Helv. Chim. Acta 28, 1533

LAMB, H. 1945 Hydrodynamics, 6th Ed. Dover

LAWACZECK, F. 1919 Z. Ver. deut. Ing. 63, 677

LEA, F. & TADROS, A. G. 1931 Phil. Mag. 11, 1235

LEAL, L. G. & HINCH, E. J. 1971 J. Fluid Mech. 46, 685

LESLIE, F. M. 1966 Quart. J. Mech. Appl. Math. 19, 357

LESLIE, F. M. 1968 Arch. Rat. Mech. Anal. 28, 265

LESLIE, F. M. 1971 Rheol. Acta 10, 91

LEWIS, H. W. 1953 Anal. Chem. 25, 507

LINDGREN, E. R. 1953 Arkiv Fysik 7, 293

LINDGREN, E. R. 1957 Arkiv Fysik 12, 1

LINDGREN, E. R. 1959 Arkiv Fysik 15, 97; ibid. 15, 503; ibid. 16, 101

LINDGREN, E. R. 1962 Arkiv Fysik 23, 403

LINDGREN, E. R. 1963 Arkiv Fysik 24, 269

LINDGREN, E. R. 1972 Rev. Sci. Instr. 43, 557

LITVINOV, V. G. 1968 Prikl. Mech. 4, 33

LIU, K.-C. & PEEBLES, F. N. 1963 Trans. Soc. Rheol. 7, 421

LODGE, A. S. 1956 Trans. Faraday Soc. 52, 120

LOHRENZ, J., SMITH, G. W., & KURATA, F. 1960 A. I. Ch. E. J. 6, 547; erratum, ibid. 7, 68

MACH, M. E. 1873 Optisch-Akustische Versuche. Calve, Prague

MAUDE, A. D. & WHITMORE, R. L. 1956 Brit. J. Appl. Phys. D 7, 98

MAXWELL, J. C. 1873 Proc. Roy. Soc. A 22, 46

MILLSAPS, K. & POHLHAUSEN, K. 1953 J. Aeron. Sci. 20, 187

MOODY, L. F. 1944 Trans. ASME 66, 671

MOONEY, M. J. 1931 *Rheol.* 2, 210

NIKURADSE, J. 1930 *Ing. Archiv.* 1, 306

NIKURADSE, J. 1933 *Ver. deut. Ing. Forsch.* 361

NOLL, W. 1958 *Arch. Ratl. Mech. Anal.* 2, 197

OLDROYD, J. G. 1950 *Proc. Roy. Soc. A* 200, 523

PEEBLES, F. N., GARBER, H. J., & JURY, S. H. 1953 *Proc. 3rd Midwest Conf. on Fluid Mech.* 441

PEEBLES, F. N. & LIU, K.-C. 1965 *Exper. Mech.* 5, 229

PEEBLES, F. N., PRADOS, J. W., & HONEYCUTT, E. H., JR. 1965 *J. Polymer Sci. C*, 5, 37

PETERLIN, A. 1938 *Z. Physik* 111, 232

PETERLIN, A. 1956 Chapter 15 of *Rheology, Theory and Applications*, Vol. 1, ed. Eirich, F. R. Academic Press

PETERLIN, A. & STUART, H. A. 1939 *Z. Physik* 112, 129

POINCARÉ, H. 1889 *Theorie Mathematique de la Lumiere*, Vol. II, 282

POISEUILLE, J. L. M. 1840 *Compt. rend.* 11, 961

POWELL, R. E. & EYRING, H. 1942 *Adv. Colloid.Sci.* 1, 183

PRADOS, J. W. 1957 Ph.D. Dissertation, University of Tennessee. Pub. as Prados, J. W. & Peebles, F. N., *Analysis of Two-Dimensional Laminar Flow Utilizing a Doubly Refracting Liquid*, Final Report, Contract Nonr-811(04), Office of Naval Research

PRADOS, J. W. & PEEBLES, F. N. 1959 *A. I. Ch. E. J.* 5, 225

PURDAY, H. F. P. 1949 *An Introduction to Mechanics of Viscous Flow*. Dover

RABINOWITSCH, B. 1929 *Z. Physik. Chem. A* 145, 1

ROSENBERG, B. 1952 *Taylor Model Basin Report 617*. Navy Department

RÖTHEMEYER, F. 1970 *Rheol. Acta* 9, 259

SAITO, N. 1951 *J. Phys. Soc. Japan* 6, 302

SCHECHTER, R. S. 1961 A. I. Ch. E. J. 7, 445

SCHERAGA, H. A. 1955 J. Chem. Phys. 23, 1526

SCHERAGA, H. A., EDSALL, J. T., & GADD, J. O., JR. 1951 J. Chem. Phys. 19, 1101

SCHLICHTING, H. 1968 Boundary-Layer Theory, 6th Ed. McGraw-Hill

ŠESTÁK, J. & AMBROS, F. 1973 Rheol. Acta 12, 70

SHURCLIFF, W. A. & BALLARD, S. C. 1964 Polarized Light. D. Van Nostrand

SIMHA, R. 1950 J. Colloid. Sci. 5, 386

SKELLAND, A. H. P. 1967 Non-Newtonian Flow and Heat Transfer. John Wiley & Sons

SNELLMAN, O. & BJORNSTAHL, Y. 1941 Kolloid. Beih. 52, 403

SOCIETY OF DYERS AND COLOURISTS/AMERICAN ASSOCIATION OF TEXTILE CHEMISTS AND COLORISTS 1971 Colour Index, Vol. 4

SOKOLOVSKII, V. V. 1966 Quart. J. Mech. Appl. Math. 19, 41

SOMMERFELD, A. 1964 Optics. Academic Press

STEVENSON, A. C. 1948 Phil. Mag. 39, 297

SWANSON, W. M. & GREEN, R. L. 1969 J. Colloid Interface Sci. 29, 161

SWANSON, W. M. & OUSTERHOUT, D. S. 1965 Proc. ASME Rheol. Symposium, 37

SWANSON, W. M., SCHEUNER, J. R., & OUSTERHOUT, D. S. 1965 Proc. ASME Rheol. Symposium, 21

SWINDELLS, J. R. COE, JR., & GODFREY, T. B. 1966 In Handbook of Chemistry and Physics, 47th Ed. Chemical Rubber Company, F31

TANNER, R. I. 1970 Trans. Soc. Rheol. 14, 483

TAYLOR, G. I. 1934 Proc. Roy. Soc. A 146, 501

TAYLOR, G. I. 1969 Festschrift for L. I. Sedov in Problems of Hydrodynamics and Continuum Mechanics, Soc. Ind. & Appl. Mech.

THURSTONE, G. B. 1961 *J. Acoust. Soc. Am.* **33**, 1091

THURSTONE, G. B. & SCHRAG, J. L. 1962 *Trans. Soc. Rheol.* **6**, 325

THURSTONE, G. B. & SCHRAG, J. L. 1964 *J. Appl. Phys.* **35**, 144

TIEDT, W. 1969 *Appl. Mech. Rev.* **22**, 900

TRICOMI, F. G. 1957 *Integral Equations*. Interscience

TRUESDELL, C. 1965 *Proc. 4th Inter. Congress Rheol.*, Vol. II, 3. Interscience

TRUESDELL, C. & NOLL, W. 1965 "The Non-Linear Field Theories of Mechanics," *Encyclopedia of Physics*, ed. Flugge, S., Vol III, 3. Springer-Verlag

TSENG, H. C., SILVER, D. L., & FINLAYSON, B. A. 1972 *Phys. Fluids* **15**, 1213

TSVETKOV, V. N. 1951 *Dokl. Akad. Nauk. SSSR* **78**, 465

VAN DAELE-DOSSCHE & VAN GEEN, R. 1969 *Seminar on Stress Analysis*, 8. Free University of Brussels

VINOGRADOV, G. V. 1950 *Dokl. Akad. Nauk. SSSR* **71**, 505

VOLK, W. 1969 *Applied Statistics for Engineers*, 2nd Ed. McGraw-Hill

WALES, J. L. S. 1969 *Rheol. Acta* **8**, 38

WAYLAND, J. H. 1955 *J. Phys. Radium* **16**, 27S

WELLER, R. 1947 *J. Appl. Mech.* **14**, 103

WHEELER, J. A. & WISSLER, E. H. 1965 *A. I. Ch. E. J.* **11**, 207

WHEELER, J. A. & WISSLER, E. H. 1966 *Trans. Soc. Rheol.* **10**, 353

ZIEGEL, K. D. 1970 *J. Colloid Interface Sci.* **34**, 185

BIOGRAPHICAL SKETCH

Eric Schonblom was born in the oil fields of Pennsylvania in December, 1934. He attended Culver Military Academy, graduating cum laude in 1952, and went on to M.I.T. where he recieved his S.B. (1956) and S.M. (1957) in Chemical Engineering. After a further year of course work, he left M.I.T. for a year of applied research at Birdwell, Inc., an oil-well service company in Bradford, Pennsylvania.

He served in the U. S. Army from June, 1959 to December, 1963. Following a two-year tour as an artillery officer, he was assigned to the Army Munitions Command in Dover, N. J., where he was action officer for a $13,000,000 development program and secretary for the joint AEC-DOD (Army) coordinating committees for nuclear warheads.

Resigning his regular army commission in 1963, he began work as an explosive physicist for the research division of the Martin-Marietta Corporation in Orlando, Florida. Here he investigated momentum transfer at the interface between an explosive and the plastically deforming metal upon which it acts, developing improved techniques for the high-speed instrumentation of the interaction.

In 1967 he accepted an Assistant Professorship at the University of Pittsburgh Bradford Campus where he taught physics, mathematics, and interdisciplinary studies.

He took leave, subsequently resigning, from his faculty position to re-enter graduate school in 1970, this time at the University of Florida. He expects to receive his Ph.D. in Engineering Mechanics in March, 1974 with a minor in psychology.

Mr. Schonblom is unmarried. He is interested in chess, sleight-of-hand magic, and classical music. Since 1970 he has been spending his summers working with disadvantaged and emotionally disturbed children under the auspices of the Presbyterian Church.

I certify that I have read this study and that in my opinion it conforms to acceptable standards of scholarly presentation and is fully adequate, in scope and quality, as a dissertation for the degree of Doctor of Philosophy.

E. Rune Lindgren, Chairman
Professor of Engineering
Mechanics

I certify that I have read this study and that in my opinion it conforms to acceptable standards of scholarly presentation and is fully adequate, in scope and quality, as a dissertation for the degree of Doctor of Philosophy.

Martin A. Eisenberg

Martin A. Eisenberg
Associate Professor of
Engineering Mechanics

I certify that I have read this study and that in my opinion it conforms to acceptable standards of scholarly presentation and is fully adequate, in scope and quality, as a dissertation for the degree of Doctor of Philosophy.

U. H. Kurzweg

Ulrich H. Kurzweg
Associate Professor of
Engineering Mechanics

I certify that I have read this study and that in my opinion it conforms to acceptable standards of scholarly presentation and is fully adequate, in scope and quality, as a dissertation for the degree of Doctor of Philosophy.

Robert L. Sierakowski

Robert L. Sierakowski
Associate Professor of
Engineering Mechanics

I certify that I have read this study and that in my opinion it conforms to acceptable standards of scholarly presentation and is fully adequate, in scope and quality, as a dissertation for the degree of Doctor of Philosophy.

C. Michael Levy, Jr.
Associate Professor of
Psychology

This dissertation was submitted to the Dean of the College of Engineering and to the Graduate Council, and was accepted in partial fulfillment of the requirements for the degree of Doctor of Philosophy.

March, 1974

Dean, College of Engineering

Dean, Graduate School

1853

UNIVERSITY OF FLORIDA
3 1262 08553 8048